minerals

MDPI

Article

Transforming LCT Pegmatite Targeting Models into AI-Powered Predictive Maps of Lithium Potential for Western Australia and Ontario: Approach, Results and Implications

Oliver P. Kreuzer [1,2,*] and Bijan Roshanravan [3,4]

[1] Corporate Geoscience Group (CGSG), P.O. Box 5128, Rockingham Beach, WA 6969, Australia
[2] Economic Geology Research Centre (EGRU), College of Science & Engineering, James Cook University, Townsville, QLD 4811, Australia
[3] Department of Mining Engineering, Faculty of Engineering, University of Birjand, Birjand P.O. Box 97174-34765, Iran; bijan.roshanravan@gmail.com
[4] Department of Mining Engineering, Birjand University of Technology, Birjand P.O. Box 97198-66981, Iran
* Correspondence: opkreuzer@gmail.com

Abstract: Here, we present holistic targeting models for lithium–cesium–tantalum (LCT) pegmatites in Western Australia, the world's largest supplier of hardrock lithium ores, and Ontario, an emerging hardrock lithium mining jurisdiction. In this study, the LCT pegmatite targeting models, informed by a review of this deposit type and framed in the context of a mineral system approach, served to identify a set of targeting criteria that are mappable in the publicly available exploration data for Western Australia and Ontario. This approach, which formed the basis for artificial intelligence (AI)-powered mineral potential modeling (MPM), using multiple, complimentary modeling techniques, not only delivered the first published regional-scale views of lithium potential across the Archean to Proterozoic terrains of Western Australia and Ontario, but it also delivered an effective framework for exploration and revealed hidden trends. For example, we identified a statistically verifiable proximity relationship between lithium, gold, and nickel occurrences and confirmed a significant size differential between LCT pegmatites in Western Australia and Ontario, with the former typically containing much larger resources than the latter. Overall, this regional-scale targeting study served to demonstrate the power of precompetitive, high-quality geoscience data, not only for regional-scale targeting but also for the development of camp-scale targets that have the resolution to be investigated using conventional prospecting techniques. Importantly, MPM does not generate 'treasure maps'. Rather, MPM provides another tool in the 'exploration toolbox', and its output should be taken as the starting point for further investigations.

Keywords: exploration targeting; LCT pegmatites; lithium; artificial intelligence (AI); mineral potential modeling (MPM); mineral systems approach; Western Australia; Ontario

check for updates

Academic Editors: Pei Ni, Ruoshi Jin, Yinhang Cheng, Yitao Cai, Mincheng Xu, Tiangang Wang and Junyi Pan

Received: 11 February 2025
Revised: 5 April 2025
Accepted: 7 April 2025
Published: 9 April 2025

Citation: Kreuzer, O.P.; Roshanravan, B. Transforming LCT Pegmatite Targeting Models into AI-Powered Predictive Maps of Lithium Potential for Western Australia and Ontario: Approach, Results and Implications. *Minerals* **2025**, *15*, 397. https://doi.org/10.3390/min15040397

Copyright: © 2025 by the authors. Licensee MDPI, Basel, Switzerland. This article is an open access article distributed under the terms and conditions of the Creative Commons Attribution (CC BY) license (https://creativecommons.org/licenses/by/4.0/).

1. Introduction

Lithium deposits can be grouped into the following three principal types: Brine-, clay-, and hardrock-hosted. Lithium–cesium–tantalum (LCT) pegmatites, which fall into the hardrock category, are products of extreme crystal-melt fractionation, whereby the fractional crystallization of a parental granitic melt leads to enrichment in lithium, cesium, and tantalum ± boron, beryllium, fluorine, gallium, hafnium, manganese, niobium, phosphorous, rubidium, and tin in the residual pegmatitic facies. From a commercial perspective, the most important lithium mineral in LCT pegmatites is spodumene [1–4].

LCT pegmatites constitute a major economic resource of lithium. For example, in 2022, this deposit type accounted for almost 30% of global lithium resources and 60% of global lithium production [5]. LCT pegmatites in the Precambrian terrains of Western Australia (Australia) and Ontario (Canada), the subject of this study, are very well endowed regarding lithium. Western Australia ranks fourth in terms of global lithium resource endowment and is the world's largest lithium supplier. Total resources amount to ~2000 Mt of ore for 26 Mt of contained lithium oxide (Li_2O), or lithia, contained in 19 LCT pegmatite deposit clusters (Figure 1; Table 1) [6]. The lithium mined in Western Australia to date has come entirely from LCT pegmatites of the Archean Pilbara and Yilgarn cratons. These two cratons host almost the entire Western Australian lithium endowment except for the Malinda lithium resource, which is hosted in LCT pegmatites of the Proterozoic Gascoyne Orogen. Greenbushes, located in the southwestern Yilgarn Craton, is not only the largest LCT pegmatite deposit in Western Australia, but it is also the largest operating hardrock lithium mine in the world [6,7]. Ontario, on the other hand, does not have any producing lithium mines; although, it is host to a number of advanced projects [8,9], some of which are moving towards production. Total resources are estimated at just under 120 Mt of ore for ~1.5 Mt Li_2O contained in seven LCT pegmatite deposit clusters (Figure 2; Table 2), which are all located in the Archean Superior Craton.

Table 1. LCT pegmatite lithium resources, Western Australia.

Project	Province	Ore (Mt)	Grade (% Li_2O)	Li_2O (kt)	Status	Owner
Greenbushes	YC	445.5	1.48	6547	Operating	Albemarle/Tianqi/IGO
Pilgangoora	PC	413.9	1.16	4802	Operating	Pilbara Minerals
Andover	PC	240.0	1.50	3600	Exploration	SQM/Hancock Prospecting)
Mt Holland	YC	186.0	1.53	2846	Operating	SQM/Wesfarmers
Wodgina	PC	217.4	1.16	2517	Operating	Albemarle/Mineral Resources
Kathleen Valley	YC	156.0	1.35	2100	Operating	Liontown Resources
Mt Marion	YC	64.8	1.43	924	Operating	Ganfeng/Mineral Resources
Tabba Tabba	PC	74.1	1.00	740	Pre-feasibility	Wildcat Resources
Manna	YC	51.6	1.00	515	Pre-feasibility	Global Lithium Resources
Bald Hill	YC	26.5	0.97	256	Operating	Lithco No. 2
Malinda	GO	24.7	0.98	243	Exploration	Delta Lithium
Marble Bar	PC	18.0	1.00	180	Exploration	Global Lithium Resources
Mt Ida	YC	14.6	1.22	178	Exploration	Delta Lithium
Mt Cattlin	YC	13.3	1.29	172	Operating	Arcadium Lithium
Buldania	YC	15.0	0.97	145	Exploration	Liontown Resources
Dome North	YC	11.1	1.15	128	Scoping	Develop Global
Split Rocks	YC	11.9	0.72	86	Exploration	Zenith Minerals
Mt Edwards	YC	2.0	0.69	13	Exploration	WIN Metals
Niobe	YC	4.6	0.07	3	Exploration	Aldoro Resources
King Tamba	YC	5.0	0.05	3	Exploration	Krakatoa Resources
Totals		1996		25,998		

All figures are rounded. All projects are LCT pegmatite-hosted. All resources are compliant with JORC 2012 (https://jorc.org/), except for Mt Holland, which is compliant with CRIRSCO (https://crirsco.com/). Tabba Tabba resource was compiled from [10]. Manna resource was compiled from [11]. Andover is a pre-resource stage discovery with a JORC 2012-compliant exploration target range from 100 to 240 Mt @ 1.0 to 1.5% Li_2O for 1000 to 3600 kt Li_2O [12] that was included here given its very significant size potential and exploration upside. All other resource figures were compiled from [6]. Key to abbreviations: GO = Gascoyne Orogen (Proterozoic); PC = Pilbara Craton (Archean); YC = Yilgarn Craton (Archean).

Table 2. LCT pegmatite lithium resources, Ontario.

Project	Province	Ore (Mt)	Grade (% Li_2O)	Li_2O (kt)	Status	Owner
PAK	SC	58.5	1.49	871	Feasibility	Frontier Lithium/Mitsubishi
Separation Rapids	SC	12.9	1.36	175	Exploration	Avalon/SCR-Sibelco
Georgia Lake	SC	14.8	0.91	93	Pre-Feasibility	RockTech Lithium
Root Bay	SC	10.1	1.29	130	Exploration	Green Technology Metals
Seymour Lake	SC	10.3	1.03	106	Feasibility	Green Technology Metals
Mavis Lake	SC	8.0	1.07	86	Exploration	Critical Resources
McCombe	SC	4.5	1.01	45	Exploration	Green Technology Metals
Totals		119		1549		

All figures are rounded. All resources are LCT pegmatite-hosted and are compliant with either JORC 2012 or NI 43-101. Mineral resources were compiled from [13] for PAK, [14] for Separation Rapids, [15] for Root Bay, Seymour Lake, and McCombe, [16] for Georgie Lake, and [17] for Mavis Lake. Key to abbreviations: Avalon = Avalon Advanced Materials; SC = Superior Craton (Archean).

In addition to their existing lithium resource endowments, both Western Australia and Ontario have excellent potential for future discoveries given that they host large areas of favorable geology, which, by and large, have recorded only limited historic lithium exploration activity, and keep attracting significant lithium exploration expenditure. In the last couple of years alone, lithium exploration has resulted in a series of demonstrably and potentially significant (re-)discoveries such as Andover (Azure Minerals, Perth, WA, Australia) and Tabba Tabba (Wildcat Resources, Perth, WA, Australia) in Western Australia, as well as Case Lake (Power Metals, Vancouver, BC, Canada) and Falcon Lake (Battery Age Minerals, Perth, WA, Australia) in Ontario. Recent, more speculative, and yet-to-be drilled, or more comprehensively drill tested, prospects include, for example, Big Red (Future Battery Metals, Perth, WA, Australia), Kobe (Greentech Metals, Perth, WA, Australia), Farson (WIN Metals, Perth, WA, Australia), Andover South (Raiden Resources, Perth, WA, Australia), and Andover West (Errawarra Resources, Perth, WA, Australia) in Western Australia, as well as Despard (Green Technology Metals, Perth, WA, Australia), Victory (Beyond Lithium, Winnipeg, MB, Canada), Gorman (Patriot Lithium, Perth, WA, Australia), Livyatan (Blaze Minerals, Perth, WA, Australia), and SBC (Libra Lithium, Toronto, ON, Canada) in Ontario.

Whilst the LCT pegmatite systems of Western Australia and Ontario have been featured in several government reports and journal publications, e.g., [18–25], no mineral prospectivity modeling (MPM) studies exist in the public domain for these important jurisdictions, both of which have significant lithium endowment and undiscovered resource potential and, thus, are vital in meeting future lithium demands. This study set out to generate artificial intelligence (AI)-driven mineral potential models, mapping the prospectivity for LCT pegmatite-hosted lithium mineralization across the entire state of Western Australia and the province of Ontario. The study results, which include the first published lithium prospectivity maps for both jurisdictions, were developed to (i) capture the current understanding of the genesis of and controls on LCT pegmatite mineralizing systems as well as their mappable expressions; (ii) delineate both the known and the new areas of lithium prospectivity, including extensions to known lithium occurrence clusters and greenfield areas not previously explored for lithium; (iii) identify the publicly available datasets that lend themselves to MPM and important datasets that are missing; (iv) compare geological, data, and exploration aspects unique to Western Australia and Ontario; (v) determine the most effective spatial proxies for targeting LCT pegmatite mineralizing systems; and (vi) compare the results obtained from continuous, knowledge-driven, and data-driven MPM.

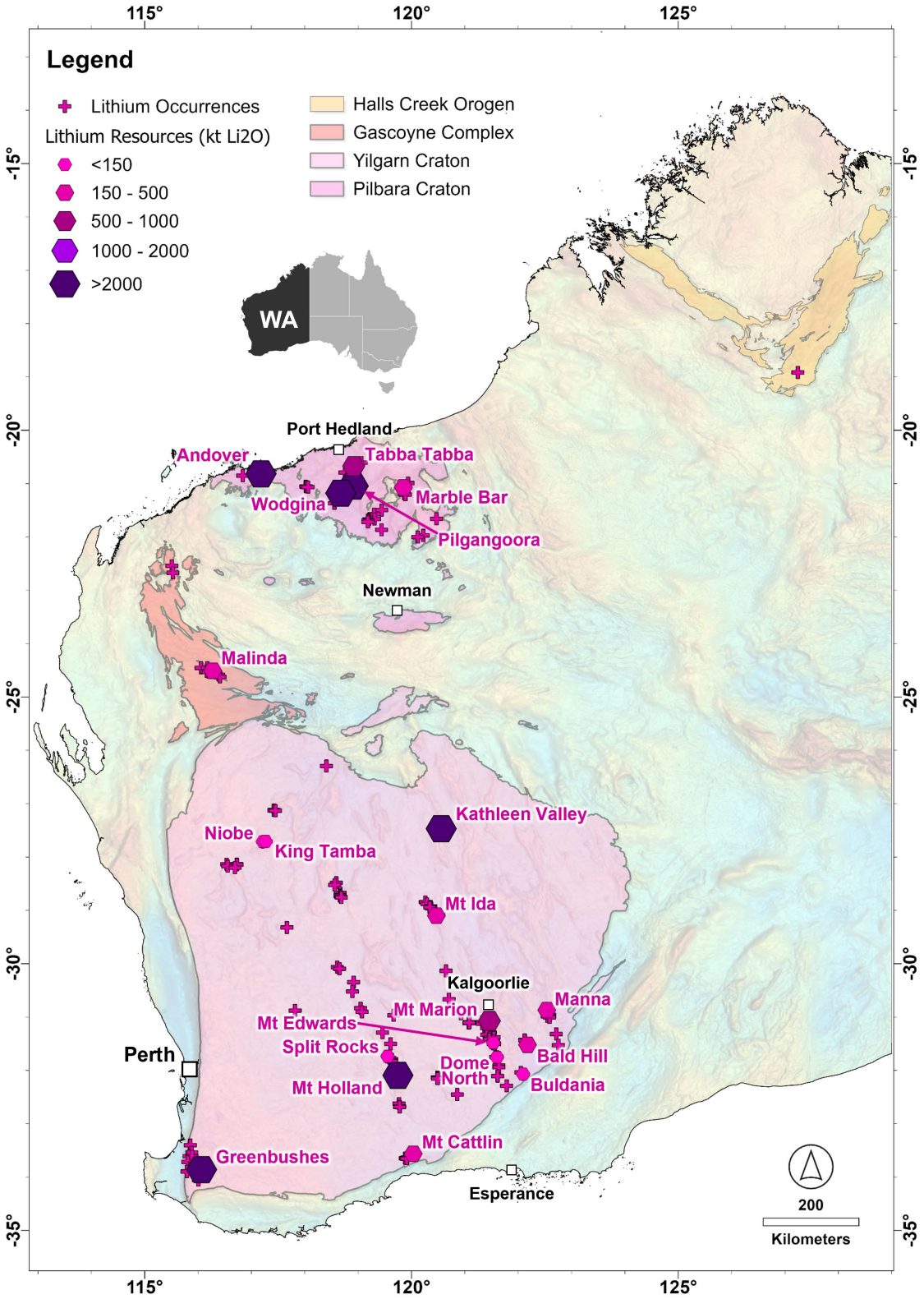

Figure 1. Map of LCT pegmatite-hosted lithium occurrences and deposits of Western Australia. See Table 1 for grade-tonnage estimates. The map also shows the outlines of the geological regions that host these lithium pegmatites, including the Archean Yilgarn and Pilbara cratons and the Proterozoic Gascoyne Complex and Halls Creek Orogen. The data sources used in the drafting of this map are listed in Table 3. Background image: Bouguer gravity of Western Australia [26] with gravity highs shown in red and gravity lows in blue colors. Coordinate system: Geocentric Datum of Australia (GDA) 2020.

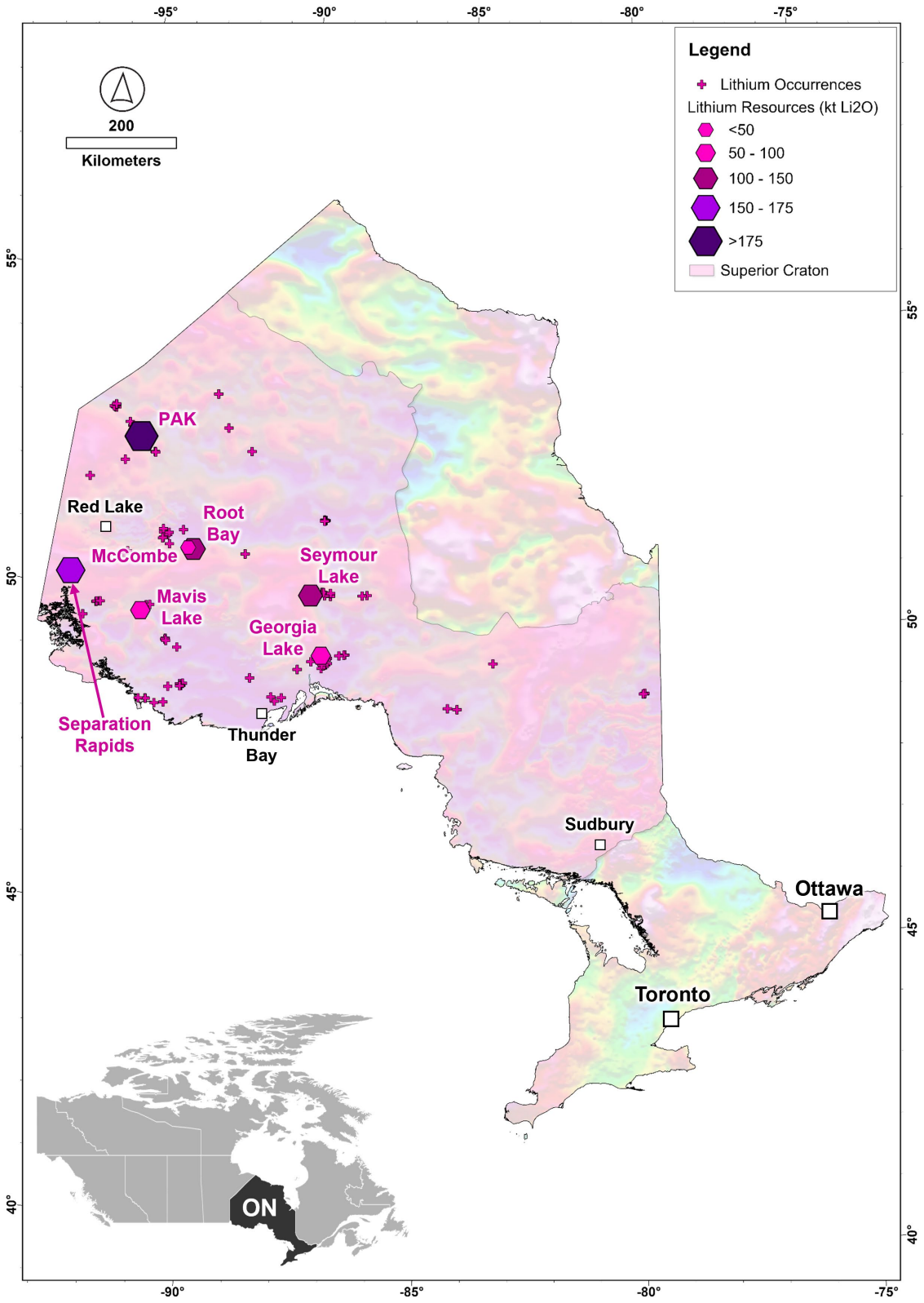

Figure 2. Map of LCT pegmatite-hosted lithium occurrences and deposits of Ontario. See Table 2 for grade-tonnage estimates. The map also shows the outline of the Superior Craton, the geological region that hosts these lithium pegmatites. The data sources used in the drafting of this map are listed in Table 3. Background image: Bouguer gravity of Ontario [27] with gravity highs shown in red and gravity lows in blue colors. Coordinate system: World Geodetic System (WGS) 1984 Universal Transverse Mercator (UTM) Zone 17N.

2. Materials and Methods

The approach taken in this targeting study was broadly similar to that employed by [28,29] and entailed the following key steps:

- A review was undertaken of the LCT pegmatite lithium deposit model with a focus on the deposits of this type in Western Australia and Ontario.
- The mineral systems approach [30–32] was used to guide the preparation of a targeting model with an emphasis on the critical processes of LCT pegmatite genesis and their mappable expressions.
- The supporting spatial input data were compiled and prepared, and the best-performing predictor maps were selected based on the results of spatial statistical assessments.
- A multi-technique approach to mineral potential modeling (MPM) was adopted, using continuous as well as data- and knowledge-driven mathematical techniques, thereby facilitating the cross-validation and comparison of the resulting prospectivity maps.

2.1. Data Sources

The geoscience and exploration data used in this study were almost entirely sourced from open-access repositories maintained by the Geological Survey of Western Australia (GSWA) and the Ontario Geological Survey (OGS) (Table 3).

In addition to their proven lithium endowment and potential, it was the excellent quality and broad coverage of the publicly available geoscience data provided by the state of Western Australia and the province of Ontario that made these jurisdictions highly attractive and amenable to an MPM study, such as that presented in this paper.

2.2. Mineral Occurrence Data

For the purpose of MPM, the GSWA and OGS lithium occurrence data (Figures 1 and 2) had to be 'cleaned up' with any 'non-substantial' lithium occurrences omitted from the database and modeling process. More specifically, for the MPM, we only used the lithium occurrences that met one or more of the following criteria: the occurrence (i) is, or was, an operating mine with lithium as the principal product or a by-product; (ii) contains a lithium resource; (iii) has returned one or more lithium mineralized drillhole intersections; (iv) is characterized by significant lithium anomalism in sawn channel, trench, or bulk samples; and/or (v) is marked by lithium-in-rock chip $\pm$ lithium-in-soil anomalism of significant grade and along a significant trend. Occurrences marked only by sporadic lithium-in-rock chip or lithium-in-soil anomalism or those defined solely by petrographic evidence (e.g., visual recognition of spodumene or lepidolite crystals) were rejected. Regarding Western Australia, 73 lithium occurrences out of a total of 208 lithium occurrences were rejected, with 135 used for MPM. Regarding Ontario, 44 lithium occurrences out of a total of 135 lithium occurrences were rejected, with 78 used for MPM. Summary tables of the Western Australian and Ontarian lithium occurrence data used in this study are provided in the Supplementary Materials (Tables S1 and S2).

Table 3. Data sources.

Data Repository	Datasets and Types	Website URL
	Geological Survey of Western Australia (GSWA)	
Data and Software Center	Mines and mineral deposits (MINEDEX) (GIS point data) [1] Mineral exploration reports (WAMEX) (GIS polygon data) Mineral systems atlas: Rare-element pegmatite systems (GIS point, line, and polygon data) Open-file mineral exploration drillholes (GIS point data) Geochronology (GIS point data) Surface geochemistry (GIS point data) Field observations (WAROX) (GIS point data) Regolith, surface, and interpreted bedrock geology (GIS polygon data) Tectonic units (GIS polygon data) Airborne geophysics (gravity, magnetics, and radiometrics) (GIS raster and/or image data) Multiscale edges from gravity and magnetics (GIS line data) Tenements (GIS polygon data)	[33]
eBookshop	Digital books, reports, and maps (PDF data)	[34]
	Ontario Geological Survey (OGS)	
OGSEarth	Mines and mineral deposits (OMI) (GIS point data) [1] Mineral exploration activity reports (OAFD) (GIS polygon data) Open-file mineral exploration drillholes (ODHD) (GIS point data) Geochronology (GIS point data) Surface geochemistry (GIS point data) Surface and interpreted bedrock geology (GIS polygon data) Airborne geophysics (gravity, magnetics) (GIS raster and/or image data) Tenements (GIS polygon data) Digital books, reports, and maps (PDF data)	[35]

[1] Summary tables of the Western Australian and Ontarian lithium occurrence data used in this study are provided in the Supplementary Materials.

2.3. Mineral Systems Concept

The targeting model developed in this study was generated in the framework of a mineral system approach [30–32,36,37] and in a manner described in more detail by [38–41]. Briefly, the mineral system concept views mineral deposits as small-scale expressions of a series of geological processes operating at different temporal and spatial scales:

- Source processes extract the essential mineral deposit components (i.e., melts and/or fluids, metals, and ligands) from their crustal or mantle sources;
- Transport processes drive the transfer of the essential components from source to trap regions via melts and/or fluids;
- Trap processes focus melt and/or fluid flow into physically and/or chemically responsive, deposit-scale sites;
- Deposition processes drive the efficient extraction of metals from melts and/or fluids passing through the traps;
- Preservation processes act to preserve the accumulated metals through time.

By definition, in situations where one or more of these processes fail to operate, a mineral deposit cannot form or will not be preserved. The probabilistic principle at the core of this concept is one of the key strengths of the mineral system approach, and one that lends itself well to MPM [38,39,41]. An additional key strength of the mineral system approach is that it provides a robust yet flexible framework for formulating a holistic, process-based targeting model and for observing, mapping, and/or querying in the available geoscience data the expressions of the critical processes of mineral deposit formation [36,42].

2.4. Mineral Potential Modeling (MPM)

MPM, first developed and applied in the late 1980s in conjunction with the arrival of geographic information systems (GIS) [43,44], has since evolved into a powerful, time- and cost-effective targeting tool capable of big data analytics. More specifically, MPM is capable of simultaneously handling, integrating, processing, and modeling the typically diverse and often very substantial geological, geochemical, geophysical, remote sensing, and drilling data generated and used in mineral exploration. It is also a tool that is well-suited for efficient screening and target generation within large search areas, be it a particular mineral district or belt or an entire country or continent. On the whole, MPM includes the following steps [32,42,45–48]:

- Genetic model stage: Identification of the geological processes that are essential in the formation of the targeted deposit type to build a conceptual deposit model.
- Targeting model stage: Translation of the genetic model into a targeting model in which the essential processes are reflected by mappable targeting criteria (also referred to as targeting elements, predictors, predictor maps, or spatial proxies).
- Mathematical model stage: Allocation of weights to combine the various spatial proxies using mathematical algorithms.
- Target identification and prioritized stage: Mapping and prioritization of the most prospective areas.

The mathematical modeling can be broadly subdivided into data-driven, knowledge-driven, hybrid knowledge- and data-driven, and continuous approaches that employ logistic functions [45,49,50]. The selection of weighting technique is strongly guided by data availability, specifically the number of known mineral occurrences in support of the targeting model, commonly referred to as prospect locations. For example, un- or underexplored 'greenfields', 'grassroots' or 'frontier' regions are typically data poor and may contain only few, if any, mineral occurrences of the target type. In such search spaces, a knowledge-driven approach is often required, with MPM reliant on expert opinion. 'Brownfields' regions, on the other hand, are typically well explored and, thus, more data-rich, especially in the vicinity of known mineral deposits. For such regions, the weighting is commonly data-driven [45,49]. In contrast, continuous weighting methods require neither expert opinion nor prospect locations, with continuous spatial evidence offering superior predictive capability compared to discretized evidence [50].

In this study, we adopted a multi-technique approach to MPM [29] comprised of continuous (data-driven index overlay [51], fuzzy gamma [52], geometric average [53]), knowledge-driven Best Worst Method Measurement of Alternatives and Ranking according to COmpromise Solution (BWM-MARCOS) [48] and data-driven random forest (RF) [54] approaches.

3. Lithium–Cesium–Tantalum (LCT) Pegmatites

3.1. Descriptive LCT Pegmatite Deposit Model

Only ~0.1% of all granitic pegmatites on Earth are classified as rare-element pegmatites, distinguishable from common pegmatites by their typically more complex mineralogy and compositional zoning and variably anomalous contents of beryllium, cesium, lithium, niobium, rare earth elements, rubidium, tantalum, tin, and uranium, yttrium, and zirconium [55]. The class of rare-element granitic pegmatites has the following two end-members: LCT and niobium-yttrium-fluorine (NYF) pegmatites [1,55] (Figure 3). In contrast to LCT pegmatites, which can host significant deposits of beryllium, cesium, lithium, tantalum, and/or tin, NYF pegmatites are of little importance economically [55].

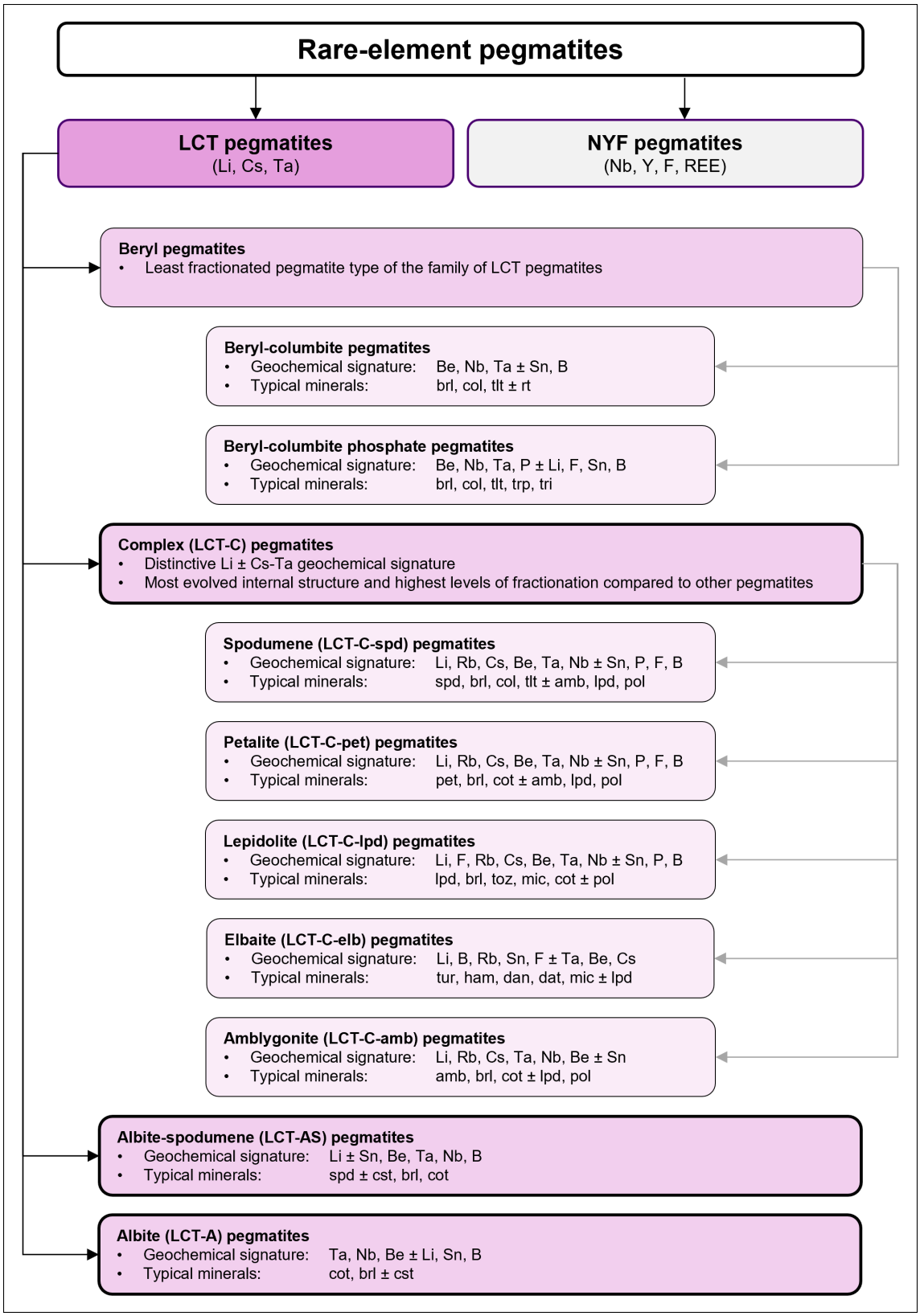

Figure 3. Summary of the classification of rare-element pegmatites compiled from [1,24]. Key to abbreviations: *Pegmatite families*: LCT = lithium–cesium–tantalum. NYF = niobium–yttrium–fluorine. *Minerals*: amb = amblygonite; brl = beryl; col = columbite; cot = columbite-tantalite; cst = cassiterite; dan = danburite; dat = datolite; elb = elbaite; ham = hambergite; lpd = lepidolite; mic = microlite; pet = petalite; pol = pollucite; rt = rutile; spd = spodumene; tlt = tantalite; toz = topaz; tri = triphylite; trp = triplite; tur = tourmaline.

LCT pegmatites can be found on all continents and range in age from Meso-Archean (Pilgangoora, Western Australia: ~2879 Ma) to Cenozoic (Fonte del Prete, Italy: ~7 Ma). Most pegmatites are hosted by belts of sedimentary and igneous rocks that have been deformed and metamorphosed to upper greenschist to amphibolite facies grades. While it is common to observe LCT pegmatites that lack any apparent source granite, there are many belts worldwide where a continuum can be observed from 'parental' granites to their pegmatite 'offspring' (Figure 4), or a genetic link can be inferred between the two based on textural, mineralogical, geochemical, isotopic, and geochronological evidence. The interpreted source intrusions are commonly relatively small, chemically and texturally evolved, and spatially and genetically associated with the waning stages of much more voluminous felsic magmatism. In addition, in many cases, the pegmatite offspring shows a district-scale zoning pattern with respect to the parental granite, with the greatest enrichment in incompatible elements characteristically recorded in the more distal pegmatites [3,56,57]. Overall, the geological features and spatial and temporal distribution of LCT pegmatites, at least those of Proterozoic and Phanerozoic age, are consistent with their genesis in zones of crustal thickening along convergent plate boundaries, triggered by subduction or continental collision but most likely contemporaneous with post-tectonic crustal relaxation of the thickened crust [3,22,58]. The relevance of these tectonic patterns to Archean LCT pegmatites remains disputed, as do the models for the tectonic evolution of Archean cratons [59–61]. According to [58], LCT pegmatites can theoretically form in any setting in which the crust contains previously un-melted, mica-rich metamorphic source rocks, regardless of tectonic regime.

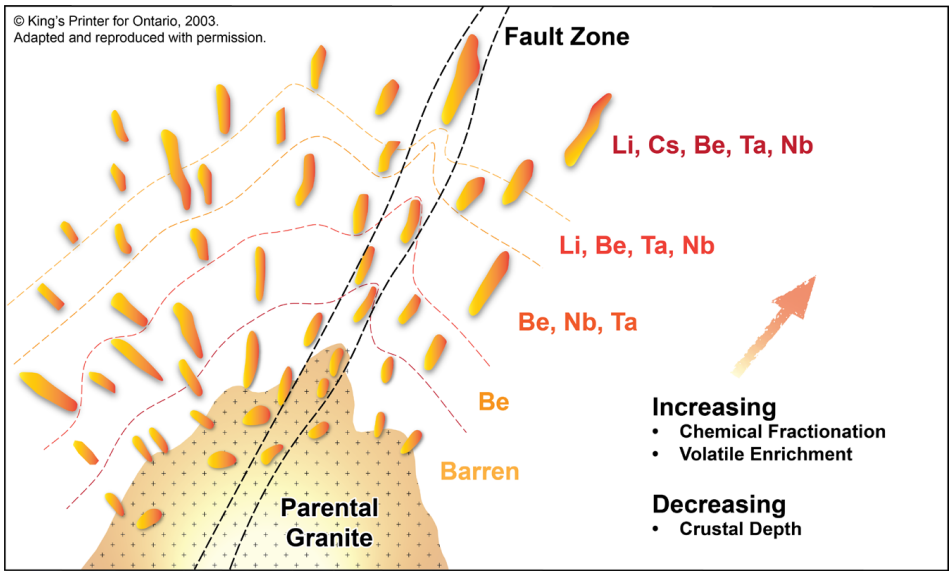

Figure 4. Schematic representation of regional zoning in a cogenetic granite–pegmatite system with the pegmatites increasingly fractionated with increasing distance from the parent granite. Modified from [19] and with the permission of the Ontario Ministry of Mines.

LCT pegmatites can be very large in size (Figure 5), as exemplified by Western Australia's Greenbushes lithium–tantalum–tin deposit, which is centered upon a group of pegmatites that are traceable along the strike for up to 3500 m, have maximum widths of up to 300 m, and are interpreted to persist to vertical depths of at least 600 m [62]. In terms of their geometries, LCT pegmatites can take the form of flat-lying tabular sills, variably dipping tabular dykes, lenticular bodies, or oddly shaped masses that commonly occur in groups (i.e., pegmatite swarms, fields, or districts). Dykes are often vertically stacked [3].

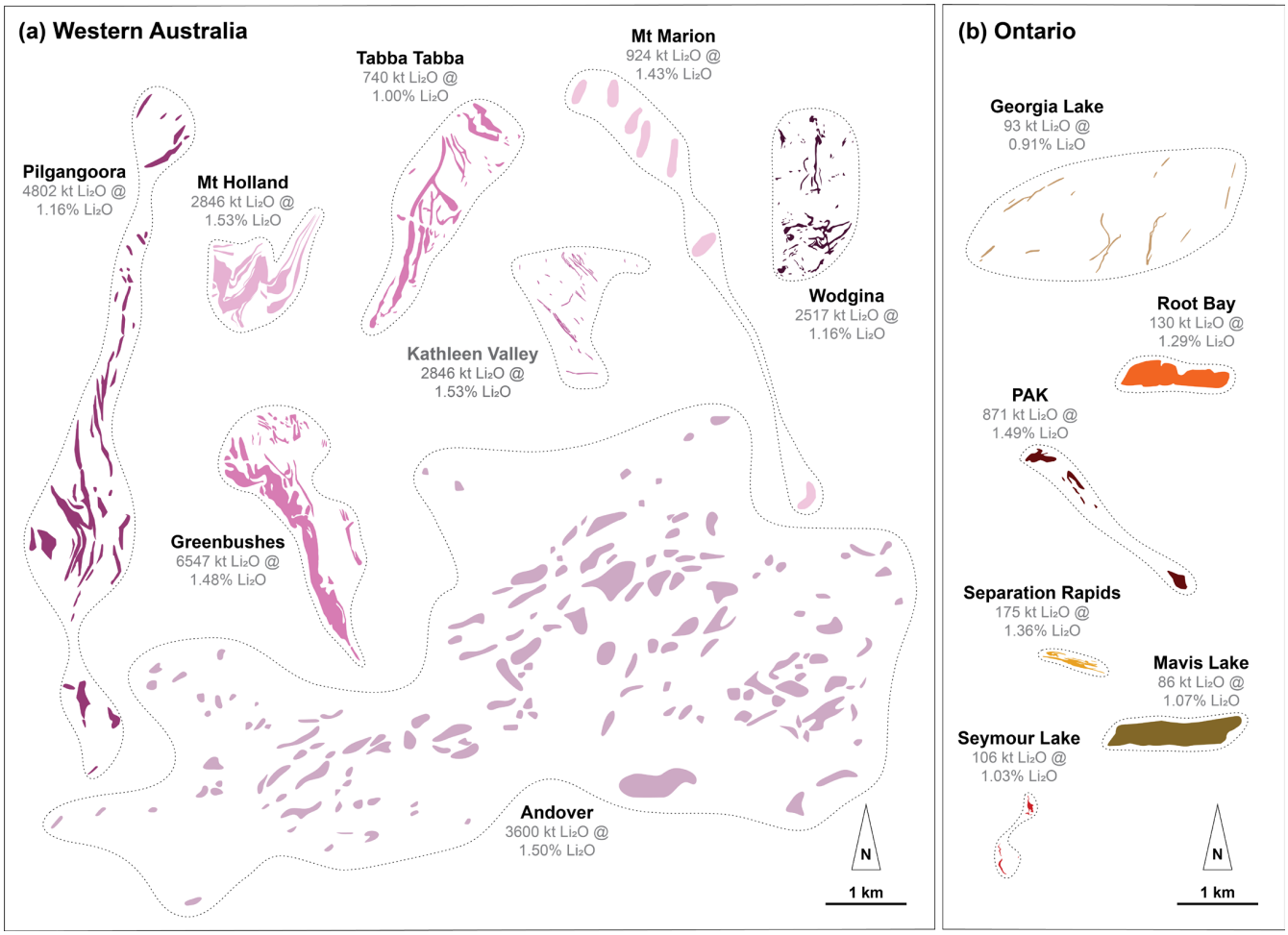

Figure 5. Comparison of individual LCT pegmatite system 'footprints' for the best-endowed hardrock lithium deposits in (**a**) Western Australia and (**b**) Ontario, in plan view. All 'footprint' maps, which represent mapped pegmatite outcrop (i.e., Andover, Mt Marion, Separation Rapids, Georgia Lake) and/or vertical projections of geological models to surface, are shown at the same scale and are orientated according to geographic north. Stippled lines provide approximate camp boundaries; although, in many cases, the true extent of the LCT pegmatite systems is yet to be defined. While none of these LCT pegmatite systems are mineralized throughout, the various systems are at different stages of exploration and/or mining, and considering differences in data quantity and quality, the 'footprint' maps serve to illustrate the wide variety of pegmatite shapes and sizes in 2D. They also provide a general sense of scale for the targeted deposit type. For example, while the stacked, gentle- to moderate-dipping Andover system is marked by numerous pegmatite outcrops over an area of >35 km^2, the (sub-)vertical PAK system, albeit highly significant, has a relatively small surface footprint of <0.5 km^2 with individual pegmatite outcrops no larger than ~30,000 m^2. Grade-tonnage and geological information as well as source references are provided in Tables 1, 2, 4 and 5.

The degree of internal compositional zoning in LCT pegmatites ranges from relatively homogeneous types with relatively simple mineral assemblages (e.g., Pilgangoora, Western Australia) to distinctly zoned types with complex mineralogical assemblages (e.g., Greenbushes, Western Australia) (Figure 3), likely reflecting different expressions of anisotropies [63]. Mineralogically, LCT pegmatites are comprised mostly of quartz, potassium feldspar, albite, and muscovite. Biotite, garnet, tourmaline, and apatite are typical accessories. The principal components of economic interest are the lithium-bearing minerals spodumene, petalite, and/or lepidolite (a member of the polylithionite–trilithionite series), the cesium-bearing mineral pollucite, the tantalum-bearing columbite-tantalite

group of minerals, the tin-bearing mineral cassiterite, and the beryllium-bearing mineral beryl [3].

Global examples of prominent LCT pegmatite systems are Greenbushes (Australia), Tanco (Canada), King's Mountain (USA), Manono-Kitotolo (DRC), and Jiajika (China) [3].

3.2. LCT Pegmatites of Western Australia

3.2.1. Geological Background and Distribution of Endowment

Western Australia records a great four-billion-year history of the assembly and breakup of cratonic elements, tied to global supercontinent cycles, that shaped the Australian continent and its mineral resources [64].

The oldest crustal elements of Western Australia, the Archean-age Yilgarn (~3730 to 2660 Ma) and Pilbara (~3530 to 2930 Ma) cratons (Figures 1, 6 and 7), comprised of extensive granite–greenstone and high-grade metamorphic gneiss terrains, are thought to have been formed by either crustal overturn, sagduction, or tectonic processes more analogous to modern plate tectonics. During early Proterozoic times, these Archean nuclei were amalgamated and incorporated into the broader Western Australian Craton, driven by a series of orogenies between ~2215 and 1950 Ma. The subsequent collision of the West Australian Craton with the North Australian Craton, a previously formed amalgamation of several Archean-to-Paleoproterozoic (pre-1840 Ma) tectonic elements, led to a complex series of tectono-thermal events concurrent with the final assembly of the Columbia/Nuna Supercontinent between 1950 and 1770 Ma [65–68].

The entire Western Australian lithium endowment and all but one of the known lithium occurrences are contained within the West Australian Craton, particularly its Archean nuclei, the Yilgarn and Pilbara cratons (Figures 1, 6 and 7). The Paleoproterozoic Gascoyne Block (Figures 1 and 6), also located in the West Australian Craton, represents an emerging lithium province. The only known lithium occurrence outside of the West Australian Craton is found in the Paleoproterozoic Halls Creek Orogen (Figure 1) of the North Australian Craton. No lithium occurrences have been identified thus far in any of the other Proterozoic orogenic belts of Western Australia. Many of the Phanerozoic geological regions in the state are composed of unmetamorphosed basin sequences that have little to no LCT pegmatite potential (cf. [3]).

3.2.2. LCT Pegmatites of the Archean Yilgarn Craton

Eastern Yilgarn Craton LCT pegmatites are hosted in greenstone belts close to granite–greenstone contacts. They typically occur no more than 10 km from major faults or lineaments, which are often substantial structures marking domain or terrane boundaries, and they generally have a preference for mafic or ultramafic host rocks metamorphosed at greenschist to amphibolite grade [69] (Figure 6; Table 4). While the LCT pegmatites in the Eastern Goldfields Superterrane tend to cluster along first-order faults that separate individual terranes or lithostructural domains, those in the Murchison and Southern Cross terranes tend to be associated with less substantial second- or third-order faults. They also tend to be smaller in size compared to those in the Eastern Goldfields Superterrane.

Age-wise, the eastern Yilgarn Craton LCT pegmatites fall within a relatively narrow bracket from ~2650 to 2600 Ma, contemporaneous with a major period of global pegmatite emplacement [3,59,69]. No S-type granites exist in the Yilgarn Craton that would indicate the melting of sedimentary crustal sources [70], a key ingredient in the widely accepted LCT pegmatite deposit model (cf. [3]). However, in the Yilgarn Craton, the interval from 2650 to 2600 Ma correlates with the formation of voluminous low-Ca granite melts of I-type affinity and with chemistries indicative of crustal melting. Granites of this igneous suite are potassic in composition, with high LILE and HFSE contents, and illustrate features

indicative of late-magmatic fluid movements, such as miarolitic cavities and common pegmatites [59,69,71–74]. A plausible genetic link between some low-Ca granites and LCT pegmatites in the Kalgoorlie Terrane of the eastern Yilgarn Craton was documented by [75]. More specifically, [75] demonstrated that the geochemical and petrographic characteristics of the inferred parental granites are comparable to those of demonstrated lithium source granites in pegmatite provinces elsewhere on Earth. Recent work by [70] and [76] demonstrated that the low-Ca granites are progressively more radiogenic and enriched in lithium close to granite–greenstone contacts, typically marked by fault systems. The enrichment was interpreted as the signature of a preconditioned crust, which, at the time, was primed for biotite-dehydration melting at relatively shallow greenstone-root levels [70,76].

Compositionally and mineralogically, most eastern Yilgarn Craton LCT pegmatites classify as albite–spodumene pegmatites (Figure 3; Table 4), a category that is reserved for homogenous, un-zoned LCT pegmatites that are predominantly comprised of spodumene crystals in a quartz–albite matrix. If present, other lithium minerals, such as petalite, amblygonite, eucryptite, lepidolite, or zinnwaldite, are not abundant enough in these pegmatites to be of economic interest. Albite–spodumene LCT pegmatites commonly take a form from subhorizontal to gently-dipping, sheet-like bodies [24,69], which, in the eastern Yilgarn Craton, can have strike lengths of >3 km (Manna) and maximum thicknesses of up to 100 m (Mt Holland). With proven distances of >2 km (Mt Holland), down-dip extents can be equally significant.

The giant Greenbushes LCT pegmatite in the southwestern Yilgarn Craton (Figure 6; Table 1) does not fit the general mold. Rather, it is dated at ~2527 Ma and, therefore, postdates the period of eastern Yilgarn Craton LCT pegmatite emplacement by about 75 to 100 m.y. Moreover, Greenbushes lacks an apparent causative parental intrusion, was emplaced syntectonically into a 150 km-long regional-scale shear zone, and is extensively deformed. It crystallized at upper amphibolite facies temperature and pressure conditions, which are higher than those recorded for its eastern Yilgarn Craton counterparts, and it displays an atypical, complex mineralogical zonation pattern [69,77–80] (Table 4).

3.2.3. LCT Pegmatites of the Archean Pilbara Craton

Pilbara Craton LCT pegmatites (Figure 7) are in many respects like those found in the eastern Yilgarn, including their preference for mafic–ultramafic, greenschist to amphibolite facies grade host rocks, their proximity to granite–greenstone contacts and major faults and lineaments, and the prevalence of albite-spodumene LCT pegmatites. Yet, the Pilbara Craton LCT pegmatites are older (~2880 to 2830 Ma) and, by and large, illustrate stronger spatial, geochemical, geochronological, and, thus, genetic links to their inferred source intrusions, which are highly fractionated, high silica monzogranites, with high LILE and HFSE contents and low K/Rb ratios, of the ~2850–2830 Ma post-tectonic Split Rock Supersuite (Figure 7; Table 4) [69].

3.2.4. LCT Pegmatites in Proterozoic Terrain

Little information exists in the public domain about LCT pegmatites in the Proterozoic terrains of Western Australia, and discoveries of lithium deposits in these terrains are rare to date. The largest known system occurs at Malinda in the Yinnetharra LCT pegmatite district of the Paleoproterozoic Gascoyne Complex (Figure 6; Table 4). Here, multiple gently south- and north-dipping pegmatites cut a Paleoproterozoic basement of folded amphibolite and sedimentary schist, metamorphosed at upper greenschist to lower amphibolite facies conditions. The pegmatites are located along a greater 200 km-long mantle tapping fault system and are immediately adjacent to a composite intrusive body

dominated by porphyritic monzogranite and leucocratic tourmaline-bearing granite of the Neoproterozoic (995 to 939 Ma) Thirty-Three Supersuite. This igneous suite, which was emplaced during and immediately after the Edmundian Orogeny (1030 to 955 Ma), is interpreted as a possible causative intrusion [81,82]. The Malinda LCT pegmatites are sheet-like bodies that pinch and swell, with the thicker parts of the pegmatites mineralized. Over 5 km of combined strike length of pegmatites has been defined to date. Individual pegmatites are up to 1.8 km long and have maximum widths up to >100 m and down-dip extents of >400 m. Lithium minerals within the pegmatites are predominantly spodumene, with subordinate lepidolite. Gangue minerals are mainly quartz and albite, with some microcline and muscovite [82].

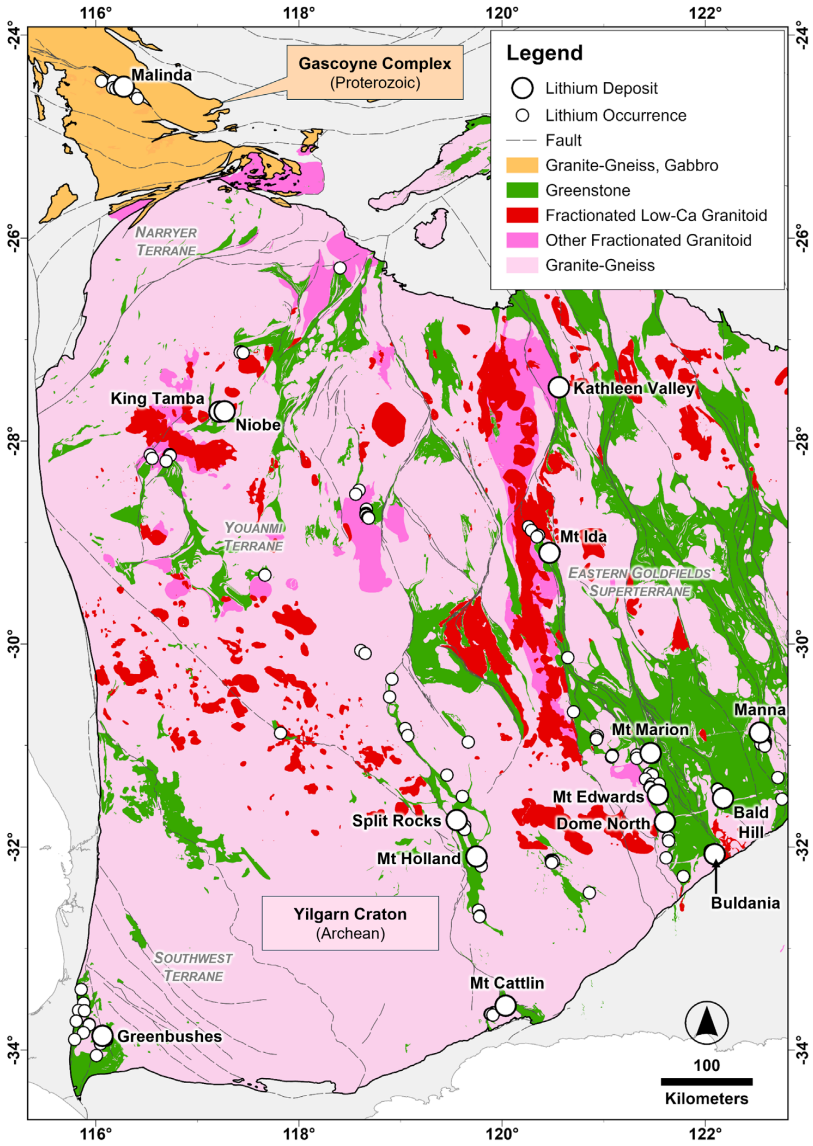

Figure 6. Map of lithium deposits and occurrences in the western and central Archean Yilgarn Craton and southern Proterozoic Gascoyne Complex, Western Australia. The map also shows the spatial distribution of potentially lithium-fertile fractionated felsic intrusions and greenstone host sequences. Most LCT pegmatites in the Yilgarn Craton were emplaced from ~2650 to 2600 Ma, contemporaneous with the low-Ca granites [59,69]. The giant Greenbushes LCT pegmatite in the Southwest Terrane is dated at ~2527 Ma and, therefore, postdates the low-Ca felsic igneous event. It lacks an apparent causative parental intrusion, was emplaced syntectonically into a regional-scale shear zone, and is extensively deformed [69,77–80]. The data sources used in the drafting of this map are listed in Table 3. Coordinate system: GDA 2020.

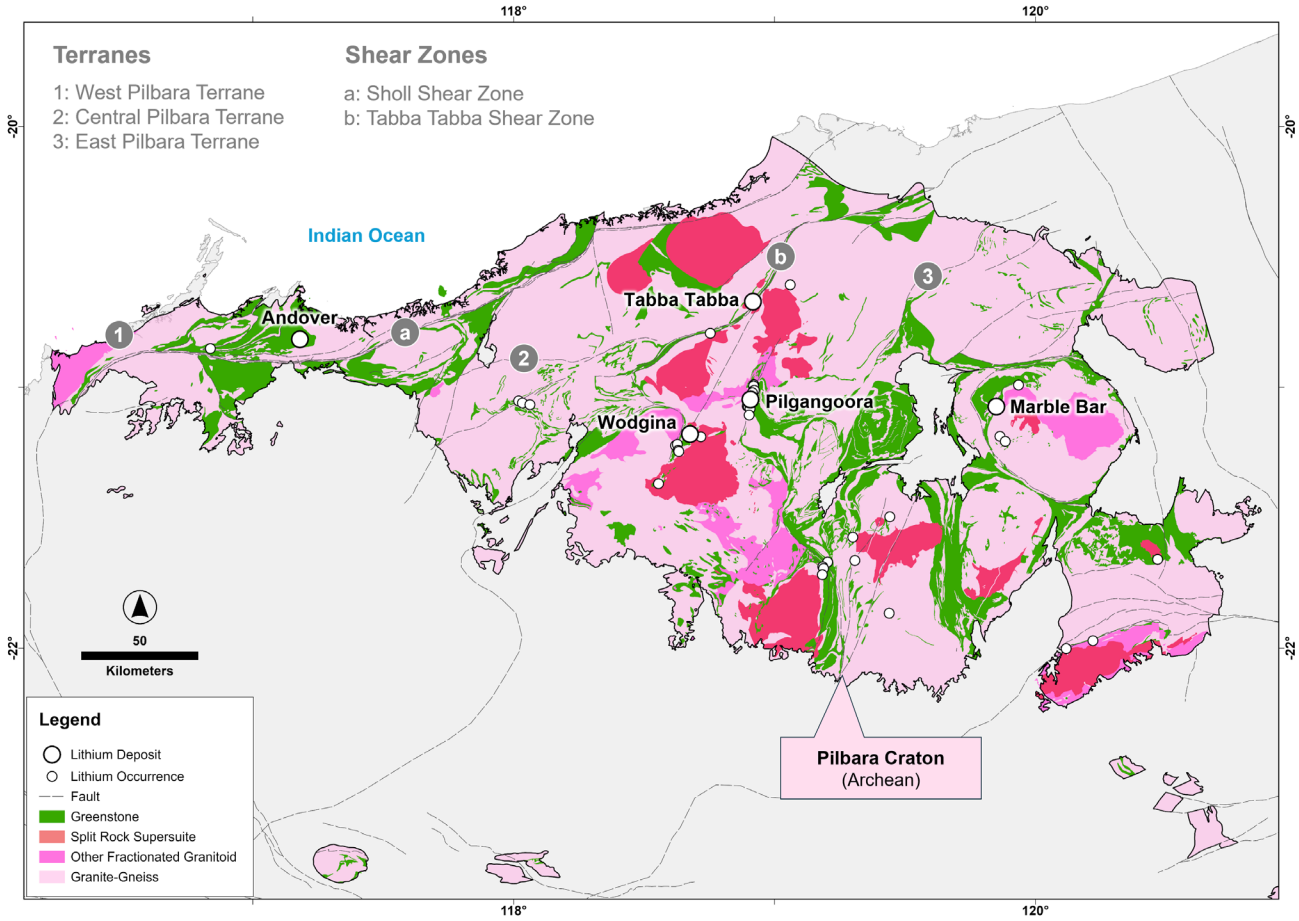

Figure 7. Map of lithium deposits and occurrences in the Archean Pilbara Craton, Western Australia. The map also shows the spatial distribution of potentially lithium-fertile, fractionated felsic intrusions and greenstone host sequences. Most of the fractionated intrusions form part of the ~2850–2830 Ma Split Rock Supersuite, which aligns along a broad north-northwest trend. Split Rock Supersuite intrusive rocks are believed to be genetically associated with the ~2880–2830 Ma LCT pegmatites at Wodgina, Pilgangoora, and Tabba Tabba, as well as other LCT pegmatite occurrences [69]. No fractionated intrusions are known within a radius of 55 km from the Andover deposit, a highly significant, relatively recent discovery. However, Andover is located proximal to the Sholl Shear Zone, a regionally extensive, terrane-bounding fault zone. The data sources used in the drafting of this map are listed in Table 3. Coordinate system: GDA 2020.

Table 4. Basic characteristics of LCT pegmatite systems, Western Australia.

System	Sub-Type	Province	Age	Geology and Structure	Key Minerals	References
Pilgangoora	LCT-AS	PC	Mesoarchean (~2879 Ma)	HR: basalt, dolerite, undifferentiated ultramafic rock; SC: shear zone corridor; SR: Kadgewarrina and Poocatche Monzogranite, Split Rock Supersuite; MG: upper greenschist to lower amphibolite facies	spd, lpd, cot, cst, tlt, tap, brl	[25,83]
Andover	LCT-AS	PC	Mesoarchean	HR: peridotite, dunite; SC: poorly defined and/or described but proximal to shear zone corridor; SR: no obvious causative intrusion; MG: upper greenschist to lower amphibolite facies	spd, lpd, brl, cot, cst	[12]
Wodgina	LCT-A + LCT-AS	PC	Mesoarchean (~2829 Ma)	HR: komatiite (Wodgina), metasedimentary sequence (Mt Cassiterite); SC: shear zone corridor; SR: Numbana Monzogranite, Split Rock Supersuite; MG: upper greenschist to lower amphibolite facies	spd, cot, wod, Cs-brl, Li-mic, lit	[25,59]

Table 4. *Cont.*

System	Sub-Type	Province	Age	Geology and Structure	Key Minerals	References
Tabba Tabba	LCT-AS	PC	Mesoarchean (~2877 Ma)	HR: dolerite sill, siliciclastic rocks; SC: shear zone corridor, schistosity; SR: Split Rock Supersuite; MG: upper greenschist to lower amphibolite facies(?)	spd, pet, Li-mic, brl, cot, cst, tlt	[10,84]
Marble Bar	LCT-AS (?)	PC	Mesoarchean	HR: amphibolite, dolerite, basalt; SC: shear zone corridor; SR: Moolyella Monzogranite–Mt Edgar Batholith (Split Rock Supersuite); MG: upper greenschist to lower amphibolite facies(?)	spd, cst	[85,86]
Greenbushes	LCT-C-spd	YC	Neoarchean (~2527 Ma)	HR: amphibolite, ultramafic schist, granofels; SC: shear zone corridor; SR: no obvious causative intrusion; MG: upper amphibolite facies	spd, brl, cot, cst, wod	[25,62,78–80]
Mt Holland	LCT-AS	YC	Neoarchean	HR: komatiite, dolerite, basalt, andesite; SC: shear zone corridor, folding; SR: post-tectonic, low-Ca granite; MG: upper greenschist to lower amphibolite facies	spd, pet	[87]
Kathleen Valley	LCT-C-spd	YC	Neoarchean	HR: gabbro, basalt, conglomerate; SC: shear zone corridor; SR: post-tectonic, low-Ca granite(?); MG: upper greenschist to lower amphibolite facies	spd, tlt, lpd	[88,89]
Mt Marion	LCT-AS + LCT-C-spd	YC	Neoarchean	HR: amphibolite, serpentinite, ultramafic schist, basalt, carbonaceous black shale; SC: folding, shear zone corridor; SR: Depot Granodiorite; MG: lower amphibolite facies	spd, cot, cst, brl, lpd	[90,91]
Manna	LCT-AS(?)	YC	Neoarchean	HR: gabbro, basalt; SC: shear zone corridor; SR: Cardunia Granite; MG: lower to middle amphibolite facies(?)	spd, lpd	[92,93]
Bald Hill	LCT-AS	YC	Neoarchean	HR: schist, greywacke, granite; SC: schistosity, shear zone corridor; SR: post-tectonic, low-Ca granite(?); MG: upper greenschist to lower amphibolite facies	spd, lpd, tlt	[24]
Mt Ida	LCT-AS(?)	YC	Neoarchean	HR: anorthosite-leucogabbro; SC: shear zone corridor, folding; SR: post-tectonic, low-Ca Oberwyl Granite; MG: upper greenschist to lower amphibolite facies	spd, lpd	[94]
Mt Cattlin	LCT–AS	YC	Neoarchean (~2625 Ma)	HR: intermediate to mafic volcanic rocks, dolerite, tonalite; SC: shear zone corridor; SR: post-tectonic, fractionated, low-Ca granite; MG: greenschist to amphibolite facies	spd, cot, lpd, tlt, cst, tap, brl	[24,95]
Buldania	LCT-C-spd(?)	YC	Neoarchean	HR: komatiite, basalt, dolerite, carbonaceous shale; SC: shear zone corridor; SR: post-tectonic, fractionated, low-Ca granite; MG: upper greenschist to middle amphibolite facies	spd	[96]
Dome North	LCT-C-pet	YC	Neoarchean	HR: komatiite, basalt, sedimentary rock sequence; SC: shear zone corridor; SR: Pioneer Monzogranite; MG: upper greenschist to lower amphibolite facies	pol, pet, lpd, spd, lpd	[97]
Split Rocks	LCT-C-pet(?)	YC	Neoarchean	HR: undifferentiated mafic rock; SC: shear zone corridor; SR: post-tectonic, fractionated, low-Ca granite(?); MG: lower amphibolite facies(?)	euc, spd, pet, lpd	[98]
Mt Edwards	LCT-AS(?)	YC	Neoarchean	HR: komatiite, basalt; SC: shear zone corridor; SR: post-tectonic, fractionated, low-Ca granite(?); MG: middle to upper amphibolite facies	spd	[99]
Niobe	LCT-C-lpd(?)	YC	Neoarchean	HR: gabbro; SC: poorly defined and/or described; SR: post-tectonic, fractionated, low-Ca Walganna Suite granite(?); MG: greenschist to amphibolite facies	lpd, zwd, mic, brl, spd(?)	[100]

Table 4. *Cont.*

System	Sub-Type	Province	Age	Geology and Structure	Key Minerals	References
King Tamba	LCT-C-lpd(?)	YC	Neoarchean	HR: dolerite, sedimentary schist; SC: shear zone corridor, folding; SR: post-tectonic, fractionated low-Ca Walganna Suite granite(?); MG: greenschist to amphibolite facies	tap, tlt, cst, lpd, mic, zwd, brl	[101]
Malinda	LCT-AS(?)	GO	Neoproterozoic	HR: volcano (mafic)-sedimentary sequence; SC: shear zone corridor, folding; SR: Thirty-Three Supersuite granite; MG: upper greenschist to lower amphibolite facies	spd, lpd, pet, tlt, cst	[82]

Key to abbreviations. *Sub-Types*: LCT-A = LCT albite pegmatite, LCT-AS = LCT albite–spodumene–pegmatite, LCT-C-lpd = LCT complex pegmatite, lepidolite-type, LCT-C-pet = LCT complex pegmatite, petalite-type, LCT-C-spd = LCT complex pegmatite, spodumene-type. *Province*: GO = Gascoyne Orogen, PC = Pilbara Craton, YC = Yilgarn Craton. *Geology and Structure*: HR = host rock, MG = metamorphic grade, SC = structural control, SR = source rock. *Key Minerals*: brl = beryl; cot = columbite-tantalite; Cs = cesium; cst = cassiterite; euc = eucryptite; Li-mic = lithium mica (undifferentiated); lit = lithiophilite; lpd = lepidolite; mic = microlite; pet = petalite; pol = pollucite; spd = spodumene; tap = tapiolite; tlt = tantalite; wod = wodginite; zwd = zinnwaldite.

3.3. LCT Pegmatite Systems of Ontario

3.3.1. Geological Background and Distribution of Endowment

The Superior Craton of eastern Canada and the north-central United States consists of extensive granite–greenstone clastic sediment-dominated and high-grade metamorphic gneiss terrains. It represents the world's largest preserved piece of Archean crust, which forms the core of the much larger Canadian Shield. The craton was assembled between 2720 and 2680 Ma by the amalgamation of continental blocks with rocks as old as ~3800 Ma and intervening tracts of oceanic crust, most likely by tectonic processes analogous to modern plate tectonics. By and large, the Superior Craton has been tectonically stable since 2600 Ma, following progressive north-to-south assembly of its terranes into a coherent craton during the Kenoran Orogeny [102–105].

Ontario's entire lithium endowment, including all known lithium occurrences, is contained within the Archean Superior Craton (Figure 8; Tables 1 and 5). No lithium occurrences have been identified thus far in the Proterozoic orogenic belts of Ontario (i.e., 2200 to 1850 Ma Penokean and 1300 to 1000 Ma Grenville orogens); although, discovery potential may exist. Widespread Paleozoic to Mesozoic basin sequences in northern and southern Ontario are unmetamorphosed [106,107] and, theoretically, should have little to no LCT pegmatite potential [3].

3.3.2. LCT Pegmatites of the Archean Superior Craton

Like in the Western Australian Yilgarn and Pilbara cratons, LCT pegmatites in the Superior Craton are hosted in greenstone belts close to granite–greenstone contacts and typically occur no more than 10 km from prominent faults or lineaments. These are often substantial structures that mark domain or terrane boundaries. They also display a similar preference for mafic or ultramafic host rocks metamorphosed at greenschist to amphibolite grade and fall into a broadly similar Neoarchean age bracket as the eastern Yilgarn LCT pegmatites, from ~2670 to 2640 Ma [19,20] (Figure 8; Table 5). Where most of the Archean LCT pegmatite systems in Ontario differ from those in Western Australia is in the following aspects:

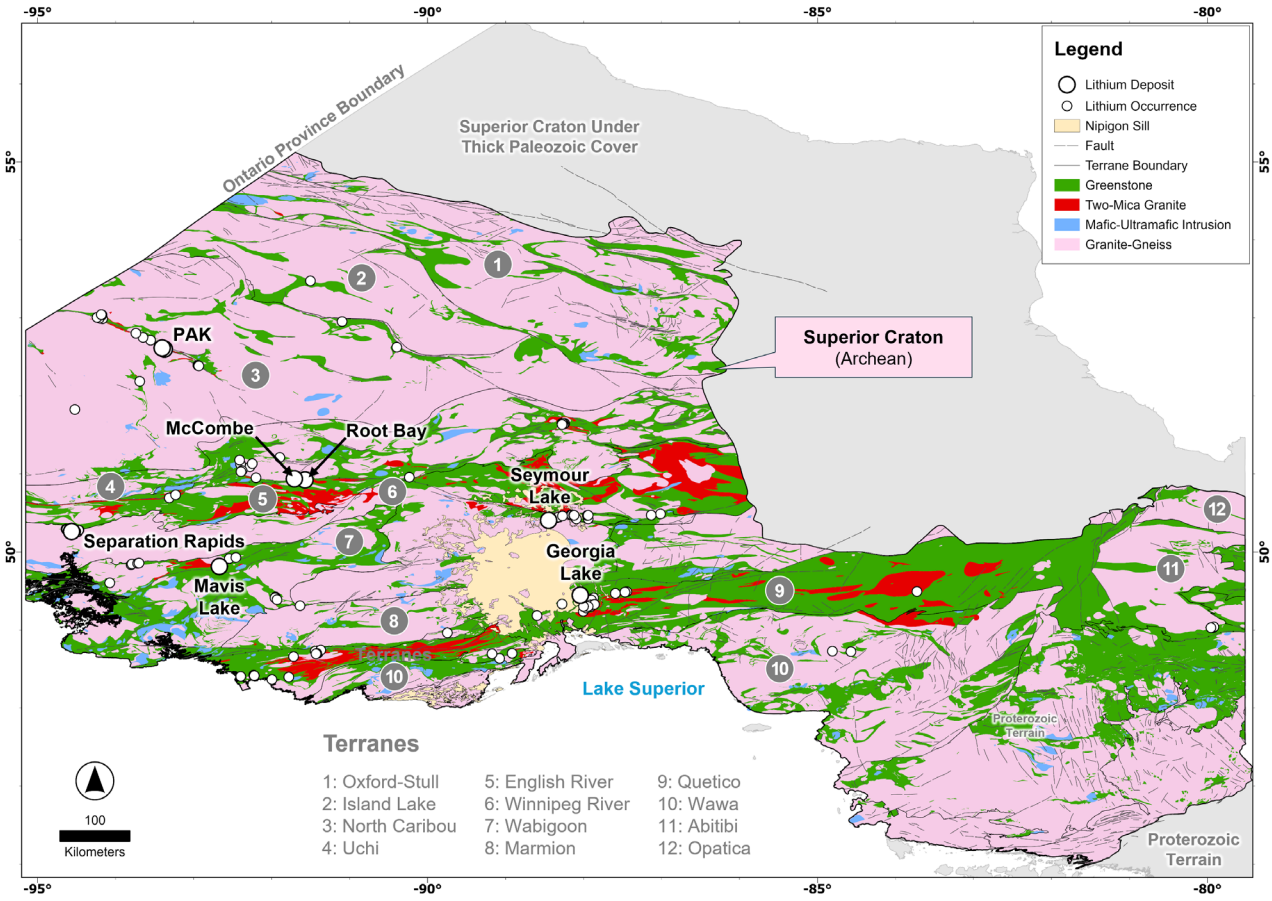

Figure 8. Map of lithium deposits and occurrences in the Archean Superior Craton of Ontario. There is good evidence in this part of the Superior Craton of a strong genetic link between peraluminous S-type magmas, represented by a suite of 2680 to 2640 Ma two-mica granites, and LCT pegmatite formation between ~2670 and 2640 Ma [19,20]. Spatially, both two-mica granites and associated LCT pegmatites are concentrated within two approximately east–west-trending lithostructural zones, the metasediment-dominant English River and Quetico terranes. Lesser concentrations of two-mica granites and LCT pegmatites are known from the North Caribou, Uchi, and Western Wabigoon terranes. Nevertheless, these terranes host important lithium deposits, such as PAK and Mavis Lake. The data sources used in the drafting of this map are listed in Table 3. Coordinate system: North American Datum (NAD) 1983 Canadian Spatial Reference System (CSRS).

- There is good evidence in the Superior Craton of Ontario of a genetic link between fertile parental granites and spatially associated LCT pegmatites. The fertile, peraluminous, Neoarchean-age (2680 to 2640 Ma) S-type granites, derived from the partial melting of a thickened sedimentary crustal source, are most abundant in the metasediment-dominant English River and Quetico terranes. Well-documented examples of lithium source granites and their related pegmatites are the Ghost Lake Batholith and Mavis Lake pegmatites and the Separation Rapids Pluton and Separation Rapids pegmatites, which typically occur no more than 15 km from the margins of their parental intrusions [19,20,108,109]. Terranes that lack these S-type granites are largely devoid of LCT pegmatites (Figure 8).
- Most LCT pegmatites in the Superior Craton of Ontario are classified as complex pegmatites, whereas this subtype is less common in the Archean cratons of Western Australia. Interestingly, the two largest lithium resources in Ontario, hosted by the PAK and Separation Rapids LCT pegmatite systems, both classify as complex petalite types, a category of LCT pegmatite that is rare in Western Australia. On the other hand, Ontario has few known LCT pegmatites of the albite–spodumene type, which is a

common type in Western Australia, where pegmatites of this type can host substantial lithium resources.

- As defined from drilling at this time, LCT pegmatites in Ontario have a preponderance for steep to subvertical dip angles (e.g., PAK, Separation Rapids), while their Western Australian counterparts are typically gently dipping to subhorizontal in nature. There also appear to be more examples of LCT pegmatites in Ontario that (i) are tectonically deformed or strongly deformed (e.g., PAK is schistose [110], Separation rapids is complexly folded, strongly schistose, and locally mylonitized [111]), and (ii) have lenticular or prolate (e.g., PAK, Separation Rapids) rather than sheet-like geometries, which is more common in Western Australia. Pegmatite footprints are commonly more modest than in Western Australia, with the larger Ontarian systems (i.e., PAK, Separations Rapids) characterized by strike lengths between 1.5 and 2.3 km, maximum widths between 70 and 125 m, and proven down-dip extents between 275 and 400 m. The smaller systems have strike lengths in the range from 0.2 to 1.3 km, maximum thicknesses from 10 to 25 m, and proven down-dip extents from 300 to 950 m. As in Western Australia, stacked pegmatite systems are commonly observed.
- Ontario's known LCT pegmatites have a combined lithium resource endowment of 1549 kt Li_2O, which amounts to only 6% of the combined Western Australian lithium resource endowment of 25,998 kt Li_2O (Table 1). Even at the craton level, the Superior Craton in Ontario hosts significantly less lithium than the Yilgarn (13,916 kt Li_2O) or Pilbara (11,839 kt Li_2O) cratons of Western Australia, despite its size of ~595,000 km^2 (the entire Superior Craton has a size of 1 572 000 km^2, comprising almost a quarter of the Earth's exposed Archean crust [102]), which is comparable to that of the Yilgarn Craton (~609,000 km^2) and several times larger than that of the Pilbara Craton (~57,000 km^2). Looking at individual deposits, PAK, the largest lithium resource in Ontario, would only rank at number eight amongst the Western Australian lithium resources. To a certain degree, this discrepancy may be a function of exploration maturity, but the latter is unlikely to account for the large variability. Rather, it is more likely that the specific conjunction of critical geological factors, including some of those mentioned above, had an important role to play.

Table 5. Basic characteristics of LCT pegmatite systems, Ontario.

System	Sub-Type	Province	Age	Geology and Structure	Key Minerals	References
PAK	LCT-C-pet	SC	Neoarchean (~2670 Ma)	HR: felsic to ultramafic volcano-sedimentary rocks, granite; SC: shear zone corridor; SR: peraluminous two-mica granite; MG: amphibolite facies	pet, spd, cot, wod, cst	[25,110,112]
Separation Rapids	LCT-C-pet	SC	Neoarchean (~2644 Ma)	HR: basalt (± pillowed); SC: shear zone corridor; SR: Separation Rapids Pluton; MG: lower to middle amphibolite facies	pet, spd, euc, cot, wod, lpd, cst, brl	[25,111]
Root Bay	LCT-C-spd	SC	Neoarchean	HR: basalt (± pillowed); SC: shear zone corridor; SR: genetic linkage not well established, possible linkage with Allison Lake Batholith; MG: upper greenschist to lower amphibolite facies(?)	spd	[113]
Seymour Lake	LCT-C-spd	SC	Neoarchean (~2666 Ma)	HR: pillow basalt ± amphibolite, dolerite, gabbro; SC: poorly defined and described; SR: no obvious causative intrusion; MG: upper greenschist to lower amphibolite facies(?)	spd, pol, lpd, Cs-brl, cot	[25,113]
Georgia Lake	LCT-AS	SC	Neoarchean	HR: sedimentary rocks, granite; SC: poorly defined and described; SR: Glacier Lake and Barbara Lake batholiths; MG: upper greenschist to lower amphibolite facies(?)	spd, brl, cot, cst	[16]

Table 5. *Cont.*

System	Sub-Type	Province	Age	Geology and Structure	Key Minerals	References
Mavis Lake	LCT-AS	SC	Neoarchean (~2665 Ma)	HR: mafic volcanic rock; SC: shear zone corridor; SR: Ghost Lake Batholith; MG: upper greenschist to lower amphibolite facies(?)	spd, tri, cot	[17,25]
McCombe	LCT-C-spd	SC	Neoarchean	HR: basalt (± pillowed); SC: shear zone corridor; SR: peraluminous two-mica granite; MG: upper greenschist to lower amphibolite facies(?)	spd, lpd, tlt, col, pet, mic, brl	[113]

Key to abbreviations: *Sub-Types*: LCT-AS = LCT albite–spodumene pegmatite, LCT-C-pet = LCT complex pegmatite, petalite-type, LCT-C-spd = LCT complex pegmatite, spodumene-type. *Province*: SC = Superior Craton. *Geology and Structure*: HR = host rock, MG = metamorphic grade, SC = structural control, SR = source rock. *Key Minerals*: brl = beryl; col = columbite; cot = columbite-tantalite; Cs = cesium; cst = cassiterite; euc = eucryptite; lpd = lepidolite; mic = microlite; pet = petalite; pol = pollucite; spd = spodumene; tlt = tantalite; tri = triphylite; wod = wodginite.

3.4. LCT Pegmatite Targeting Model

Table 6 provides a summary of the processes deemed critical in the genesis of the LCT pegmatite-hosted lithium deposits using the information summarized above and succinctly presented in [2,3,21,22].

Table 6. LCT pegmatite targeting model adopted and predictor maps used in this study.

Critical Processes	Constituent Processes	Targeting Criteria	Targeting Elements and Signatures (Predictor Maps/Spatial Proxies)
Source	LCT pegmatites are products of the extreme fractionation of granitic magmas and acquire most of their compositional attributes at source. Their genesis requires a high degree of crustal melting to form fertile granitic magmas as a source for fluids, metals, and energy to drive the mineral system. The genetic link between LCT pegmatites and S-type or evolved I-type granitic magmas and their tectonic settings is relatively well established; although, Archean tectonic processes are subject to ongoing dispute (i.e., subduction versus sagduction and/or drip tectonics).	Convergent plate margin settings (Phanerozoic, Proterozoic ± Archean) or continental rift zones marked by greenstone belts (Archean). Granite stocks, plutons, or batholiths of S-type or evolved I-type affinity.	Proximity to fractionated granitic rock units. [1,2] Proximity to pegmatitic or pegmatite-bearing rock units.
Transport	Granitic melts ascent into the upper crust along zones of structural weakness. Upper crustal fault-fracture systems act as conduits for focusing large volumes of melts and fluids over short periods of time	First- and second-order fault systems. High degree of crustal permeability.	Domains of greater density of Bouguer gravity breaks. Proximity to Bouguer gravity breaks. Domains of greater density of RTP magnetic breaks. Domains of greater density of major crustal boundaries. Proximity to faults and lineaments.
Trap	Given their affinity with convergent plate margin settings (Phanerozoic, Proterozoic ± Archean) or continental rift zones (Archean) and emplacement of source granites at mid-crustal levels, LCT pegmatites cut and solidify in metamorphosed supra-crustal rocks.	Metamorphosed terrains of greenschist to amphibolite facies grade.	Proximity to metamorphic rocks.
	LCT pegmatites have a distinct preference for mafic or ultramafic host rocks; this is likely a function of favorable physico-chemical parameters that serve to enhance trap and depositional processes. Competency contrasts may give rise to local zones of dilation and permeability, focusing fluid flow at or close to lithological contacts.	Mafic and ultramafic rock sequences. Domains of favorable host rheology (competency contrast).	Proximity to mafic–ultramafic rocks.
	LCT pegmatites have statistically valid abundance and proximity relationships with gold and nickel occurrences; this is likely a function of loosely comparable transport and trap processes (this study).	Clusters of gold and/or nickel occurrences.	Proximity to Au occurrences. Proximity to Ni occurrences.

Table 6. *Cont.*

Critical Processes	Constituent Processes	Targeting Criteria	Targeting Elements and Signatures (Predictor Maps/Spatial Proxies)
Deposition	Concentration of incompatible rare elements and volatiles in residual LCT pegmatite melts. LCT pegmatite melt solidification, magmatic–hydrothermal transition, and rare metals mineralization.	Confirmed LCT pegmatites. Presence of indicator minerals (e.g., tourmaline or garnet in pegmatites or holmquistite in country rocks). Litho-geochemical dispersion halos (e.g., Li, Rb, Cs) in country rocks. Geochemical anomalism (e.g., Li, Cs, Ta). Fractionation indicators (e.g., very low K/Rb, K/Cs, or Nb/Ta ratios as revealed by rock chip geochemistry or portable XRF spot readings).	Proximity to mapped pegmatites. Proximity to LCT pegmatite indicator minerals. [3]
Preservation	Metasomatic alteration processes can result in the selective to complete replacement of primary minerals (e.g., spodumene, petalite) by secondary minerals (e.g., albite, cookeite, or kaolinite) and the removal of deleterious elements. Tectonic and/or climatic and erosional forces can have positive (e.g., LCT pegmatite exhumation) or negative (e.g., complete destruction of LCT pegmatites) effects.	Sub-solidus hydrothermal alteration. Post-magmatic hydrothermal activity. For example, topographic highs formed by outcropping, weathering-resistant LCT pegmatites.	Not mappable at the scale of this investigation.

[1] Fractionated granitic rock units, Western Australia: Archean Split Rock Supersuite and Archean low-Ca, leuco-, two-mica, and pegmatite-bearing granitoids; Proterozoic Thirty-Three Supersuite, Durlacher Supersuite, Yarlarweelor Gneiss Complex, Scrubber Granite, Eddy Suite, Slatey Creek Granite, Lewis Granite, Balwina Granite, and Mount Joseph Migmatite. [2] Fractionated granitic rock units, Ontario: Archean muscovite–biotite and cordierite–biotite granitoids. [3] Pegmatite indicator minerals [22]: Spodumene, lepidolite, cassiterite, tantalite, columbite, beryl, and tourmaline.

Here, we followed the approach of [32], according to which the critical processes of a mineral system are translated into targeting criteria. In essence, this is performed by (i) breaking down the critical processes into their constituent processes, (ii) gathering the geological evidence that reflects the constituent processes, and (iii) developing targeting criteria that can be used to detect the targeting elements, either directly or by proxy.

Importantly, any expressions of a mineral system that cannot be mapped in the obtainable exploration geoscience data cannot be honored in MPM, and, ideally, the datasets that reflect the predictors should have relatively uniform, unbiased coverage of the target area [114].

4. Mineral Potential Modeling (MPM)

4.1. Statistical Assesment of Spatial Proxies

Data-driven predictive models must be trained. The training is typically conducted using the known occurrences of the targeted deposit type, referred to here as prospect locations (PL), and an equal amount of non-prospect locations (NPL) that are devoid of any mineralization of the targeted type. In this study, the PL data represent the known lithium deposits and occurrences. The NPL data were selected according to the following rules: the NPL must (i) be located outside of the lithium permissive tracts (i.e., they must be located within areas where the geological probability of LCT pegmatite occurrence is negligible); (ii) not be located close to any PL; and (iii) have a random spatial distribution, as they must not be representative of any particular geological units or processes [115]. The Western Australian training data comprised 208 PL (i.e., all known lithium-bearing LCT pegmatites within the state) and 208 NPL, while the Ontarian training data comprised 122 PL (i.e., all known lithium-bearing LCT pegmatites within the province) and 122 NPL.

Once prepared, the predictive capacity of each predictor map (or spatial proxy) was statistically assessed against the PL and NPL training data. Two procedures were used in this statistical assessment, namely the area under the receiver operating characteristic curve (*AUC*) (Figures S1 and S2) [116–118] and the index of normalized density (N_d) [119]. Prediction-area (P-A) plots (Figures S3 and S4) served to determine the best-performing spatial proxies for targeting lithium mineralized systems in Western Australia and Ontario. Any spatial proxies that fulfilled the statistical minimum requirements of $AUC > 0.50$ [116] and $N_d > 1.00$ [119] were considered adequate for use in the MPM (Tables 7 and 8).

Table 7. Statistical parameters of the spatial proxies used in the Western Australian lithium MPM.

Spatial Proxy	P_r (%)	O_a (%)	N_d	*AUC*	$ln(N_d)$
Proximity to mapped pegmatites	86	14	6.14	0.95	1.82
Proximity to LCT pegmatite indicator minerals	84	16	5.25	0.92	1.66
Proximity to mafic–ultramafic rocks	78	22	3.55	0.94	1.27
Proximity to Au occurrences	76	24	3.17	0.84	1.15
Proximity to Ni occurrences	74	26	2.85	0.86	1.05
Proximity to fractionated granitic rock units	70	30	2.33	0.81	0.85
Proximity to pegmatitic or pegmatite-bearing rock units	69	31	2.23	0.84	0.80
Proximity to faults and lineaments	67	33	2.03	0.67	0.71
Domains of greater density of RTP magnetic breaks	65	35	1.86	0.66	0.62
Domains of greater density of Bouguer gravity breaks	63	37	1.70	0.66	0.53
Domains of greater density of major crustal boundaries	58	42	1.38	0.59	0.32
Proximity to metamorphic rocks	57	43	1.33	0.55	0.28

Key to abbreviations: P_r = prediction rate, O_a = prediction area, $N_d = Pr/Oa$, *AUC* = area under the receiver operating characteristic curve, $ln(N_d)$ = weight.

Table 8. Statistical parameters of the spatial proxies used in the Ontarian lithium MPM.

Spatial Proxy	P_r (%)	O_a (%)	N_d	*AUC*	$ln(N_d)$
Proximity to LCT pegmatite indicator minerals	89	11	8.09	0.96	2.09
Proximity to mapped pegmatites	87	13	6.69	0.94	1.90
Proximity to fractionated granitic rock units	86	14	6.14	0.94	1.82
Proximity to Au occurrences	69	31	2.23	0.76	0.80
Domains of greater density of major crustal boundaries	68	32	2.13	0.73	0.75
Proximity to mafic–ultramafic rocks	65	35	1.86	0.90	0.62
Proximity to Ni occurrences	68	32	2.13	0.78	0.75
Proximity to Bouguer gravity breaks	51	49	1.04	0.54	0.04

Key to abbreviations: See Table 7.

4.2. Continuous Data-Driven Index Overlay, Continuous Fuzzy Gamma, Geometric Average Approaches

Three continuous modeling functions, data-driven index overlay (DDIO: [51]), fuzzy gamma (FG: [52]), and geometric average (GA: [53]), were used to model the lithium potential of Western Australia and Ontario. Large and small fuzzification functions [120,121] were utilized to assign weights to the spatial proxies, with the resulting fuzzy scores of the evidential values in the range [0, 1] (Figures S5–S24).

The MPM results for Western Australia and Ontario, as computed by these modeling functions, are provided in Figures 9a–c and 10a–c.

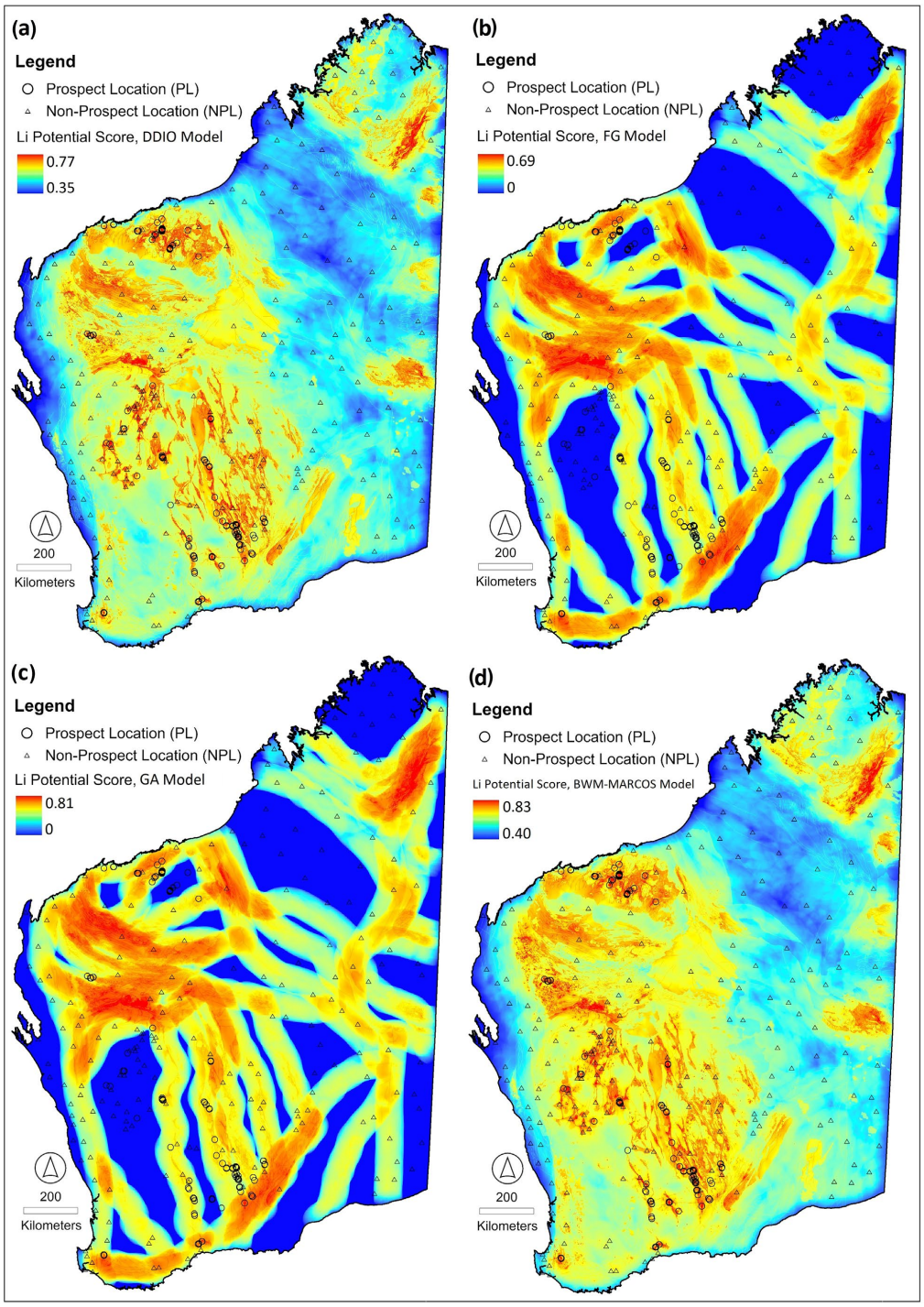

Figure 9. *Cont.*

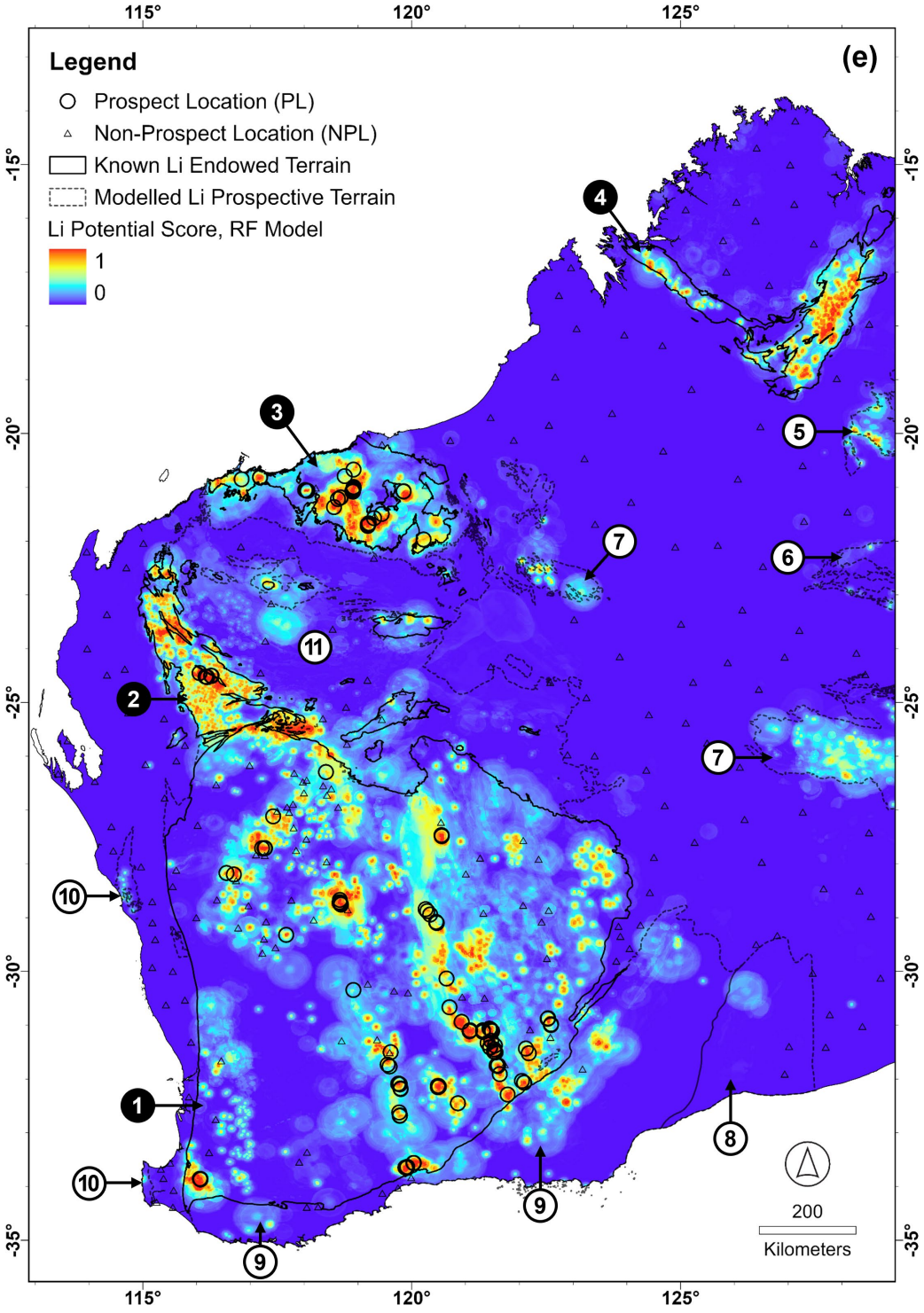

Figure 9. Lithium potential maps of Western Australia, as obtained with multiple continuous and knowledge-driven MPM techniques: (**a**) data-driven index overlay (DDIO), (**b**) fuzzy gamma (FG), (**c**) geometric average (GA), (**d**) BWM-MARCOS, and (**e**) random forest (RF). The maps only show the lithium occurrences (i.e., prospect locations) used for MPM, a summary of which is provided in Table S1 in the Supplementary Materials. The lithium potential map relating to the best-performing RF model (Figure 9e) also shows the outlines of the lithium-endowed terrains (numbered black circles: 1 = Yilgarn Craton, 2 = Gascoyne Orogen, 3 = Pilbara Craton, 4 = Halls Creek Orogen) and those modeled as lithium-prospective (numbered white circles; 5 = Granites-Tanami Orogen, 6 = Arunta Orogen, 7 = Paterson Orogen, 8 = Madura Province, 9 = Albany-Fraser Orogen, 10 = Pinjarra Orogen, 11 = Capricorn Orogen). Coordinate system: GDA 2020.

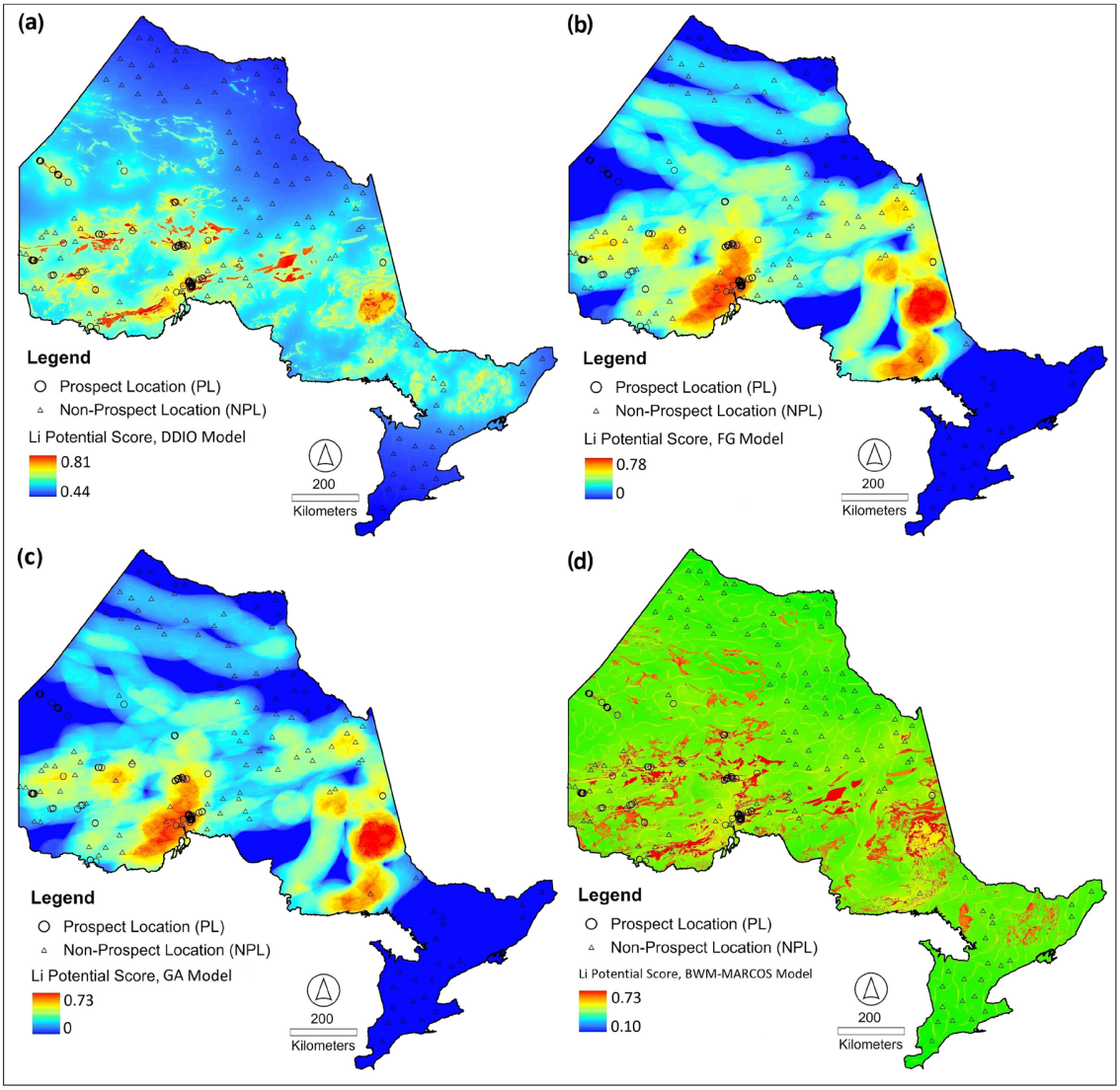

Figure 10. *Cont.*

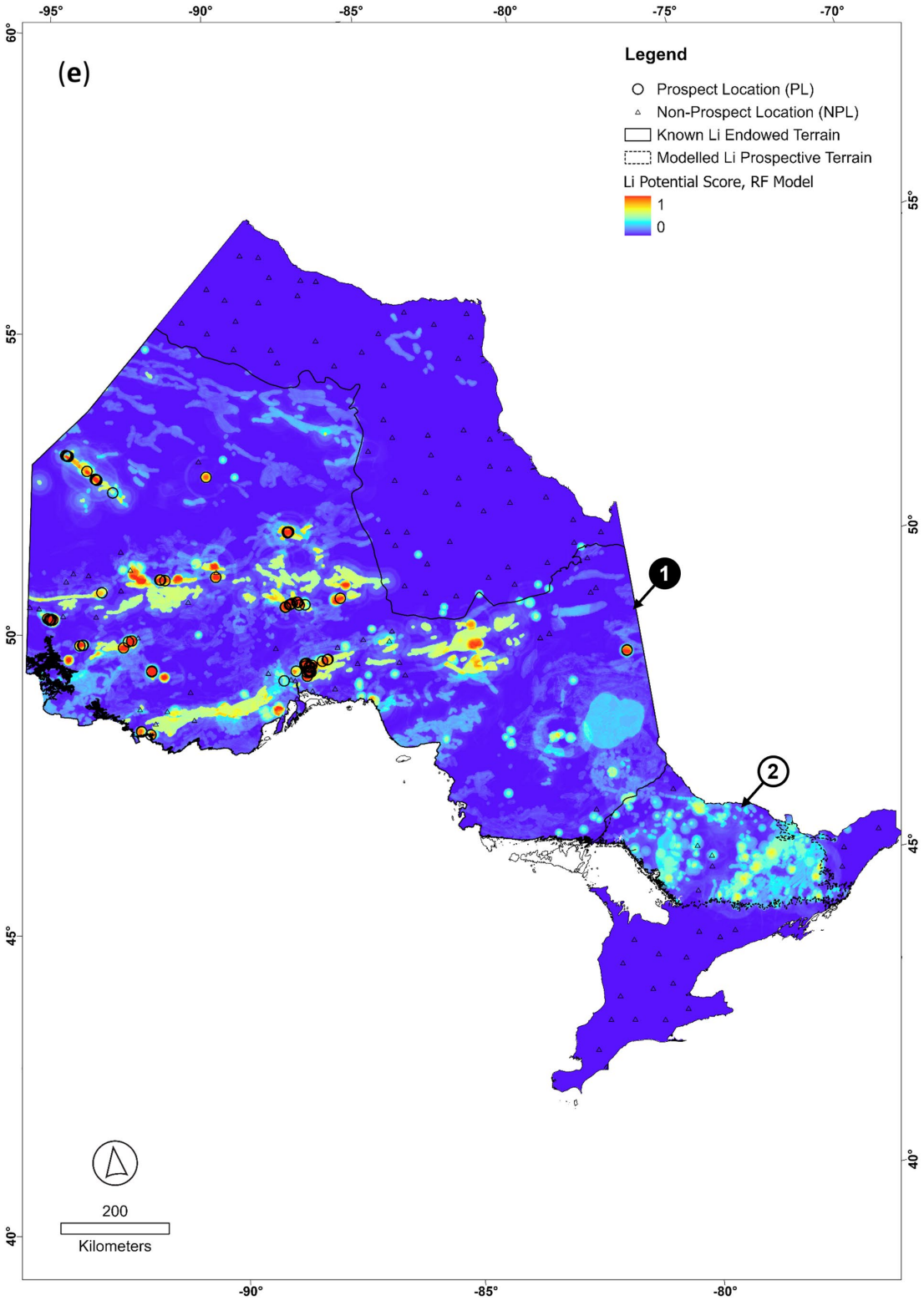

Figure 10. Lithium potential maps of Ontario, as obtained with multiple continuous and knowledge-driven MPM techniques: (**a**) data-driven index overlay (DDIO), (**b**) fuzzy gamma (FG), (**c**) geometric average (GA), (**d**) BWM-MARCOS, and (**e**) random forest (RF). The maps only show the lithium occurrences (i.e., prospect locations) used for MPM, a summary of which is provided in Table S2 in the Supplementary Materials. The lithium potential map relating to the best-performing RF model (Figure 10e) also shows the outlines of the lithium-endowed terrain (numbered black circle: 1 = Superior Craton) and that modeled as lithium-prospective (numbered white circle; 2 = Grenville Orogen). Coordinate system: NAD 1983 Lambert.

4.2.1. Data-Driven Index Overlay

Mathematically, the data-driven index overlay approach can be expressed as follows [51]:

$$D_{IO} = \frac{\sum_i^n W_{vi} W_i}{\sum_i^n W_i} \quad (1)$$

where, for individual cells, W_i is the weight of the ith individual spatial proxy computed utilizing P-A plots, and D_{IO} is the resulting score from the data-driven index overlay procedure. In the same equation, W_{vi} indicates the cell value of the ith spatial proxy assigned continuously through a fuzzification function. For the purpose of this study, Equation (1) was rewritten for Western Australia (WA) as Equation (2) and for Ontario (ON) as Equation (3):

$$D_{IO(\mathrm{WA})} = \frac{WV_1W_1 + WV_2W_2 + \ldots + WV_{12}W_{12}}{W_1 + W_2 + \ldots + W_{12}} \quad (2)$$

$$D_{IO(\mathrm{ON})} = \frac{WV_1W_1 + WV_2W_2 + \ldots + WV_8W_8}{W_1 + W_2 + \ldots + W_8} \quad (3)$$

where W_1, W_2, …, W_{12} and W_1, W_2, …, W_8 represent the weights of the spatial proxies assigned pursuant to corresponding P-A plots (Figures S3 and S4). The parameters WV_1, WV_2, …, WV_{12} and WV_1, WV_2, …, WV_8 are the continuously assigned weights of evidential values of cells in the corresponding individual spatial proxies.

Statistically, proximity to mapped pegmatites is the most important predictor for targeting LCT pegmatites in both Western Australia and Ontario, while proximity to metamorphic rocks (Western Australia) and domains of greater density of Bouguer gravity breaks (Ontario) present the least significant predictors (Tables 7 and 8).

4.2.2. Continuous Fuzzy Gamma Approach

Continuously weighted fuzzy spatial proxies can be synthesized utilizing fuzzy operators [49]. In this study, we utilized a fuzzy gamma operator that uses the *PRODUCT* and *SUM* operators, which provide the delicate adjustment of the diverse input components, as follows [46]:

$$\mu_C = \left[1 - \prod_{i=1}^n (1 - \mu_i)\right]^{\gamma} \times \left[\prod_{i=1}^n \mu_i\right]^{1-\gamma} \quad (4)$$

where, for each cell, μ_i is the ith input spatial proxy's fuzzy score, μ_C is the potential score resulting from the combination process, and $(0 \leq \gamma <= 1)$. Here, we used a gamma value of 0.9.

4.2.3. Geometric Average

Geometric average is a multiple-criteria decision-making technique for synthesizing weighted spatial proxies in MPM. Pursuant to Equation (5), the geometric average, G_A, is calculated for each cell as the nth root of the value products [53]:

$$G_A(F_1, F_2, \ldots, F_n) = \sqrt[n]{\prod_{i=1}^n F_i} = \sqrt[n]{F_1 F_2 \ldots F_n} \quad (5)$$

where, for each cell, n is the number of spatial proxies, and F_i is the fuzzy weight assigned for the ith spatial proxy. Here, Equation (5) was rewritten for Western Australia (WA) as Equation (6) and for Ontario (ON) as Equation (7):

$$G_{Lithium(WA)}(F_1, F_2, \ldots, F_{12}) = \sqrt[12]{\prod_{i=1}^{12} F_i} = \sqrt[12]{F_1 F_2 \ldots F_{12}} \quad (6)$$

$$G_{Lithium(ON)}(F_1, F_2, \ldots, F_8) = \sqrt[8]{\prod_{i=1}^{10} F_i} = \sqrt[8]{F_1 F_2 \ldots F_8} \quad (7)$$

where F_1, F_2, …, F_{12} and F_1, F_2, …, F_8 are fuzzy scores of evidential values in the corresponding spatial proxies. After computing the $G_{Lithium(WA)}$ and $G_{Lithium(ON)}$ values for each unit cell of the study areas, the cells were mapped to develop geometric average lithium potential models.

4.3. Knowledge-Driven BWM-MARCOS Approach

Among the various knowledge-driven approaches to MPM, multi-criteria decision-making (MCDM) techniques are highly regarded due to their effectiveness [122–125]. In the MCDM approach, the weighting of spatial proxies is either comparison- or matrix-based. While this is novel, the Best Worth method (BWM: [126]) and Measurement of Alternatives and Ranking according to COmpromise Solution (MARCOS: [127]) comparison- and matrix-based MCDM techniques have been successfully applied in MPM [48,122–125]. Here, we used a hybrid MCDM approach known as BWM-MARCOS [48] in combination with the overall performance (O_p) index [128,129]. The latter is computed via an improved P-A plot incorporating the following three principal criteria: (i) PL prediction rate curve, (ii) occupied area curve, and (iii) NPL prediction rate curve [128].

4.3.1. Western Australian BWM-MARCOS Model

Here, the BWM technique was applied to objectively delineate the weights of the decision criteria embodied by the spatial proxies (Table 7). The O_p index served to determine spatial proxy weights as well as the worst and best spatial proxies (Figure S25, Table 9). Following this initial step, others-to-worst (OW) and best-to-others (BO) vectors were defined (Tables S3 and S4) according to the O_p values given in Table 9. According to these parameters, problem 3 of [48] can be formulated as shown in the following Equation (8):

$$\begin{gathered} min\xi \\ \text{s.t.} \\ |W_8 - 7W_1| \le \xi, \text{forall} j \\ |W_8 - 8W_2| \le \xi, \text{forall} j \\ |W_8 - 9W_3| \le \xi, \text{forall} j \\ \vdots \\ |W_8 - 5W_{12}| \le \xi, \text{forall} j \\ |W_1 - 3W_3| \le \xi, \text{forall} j \\ |W_2 - 2W_3| \le \xi, \text{forall} j \\ |W_4 - 2W_3| \le \xi, \text{forall} j \\ \vdots \\ |W_{12} - 5W_3| \le \xi, \text{forall} j \\ \sum_j W_j = 1 \\ W_j \ge 0, \text{forall } j \end{gathered} \tag{8}$$

Next, optimal weights $\left(W_B^*, W_1^*, \ldots, W_W^*\right)$ and ξ^* were specified by solving Equation (8) (Table S5). For $a_{BW} = a_{83} = 9$, the obtained consistency index was 5.23 [48], while the consistency ratio was 0.062/5.23 = 0.011, showing appropriate consistency. After allocating weights to the spatial proxies, the MARCOS technique was applied to rank the alternatives. To achieve this, an initial decision matrix $B_{1758143\times12}$ was generated that contains 1758,143 decision alternatives, each linked to an individual cell with a particular coordinate in the corresponding spatial proxies, and 12 decision criteria. The alternatives were then ranked via the MARCOS step-by-step process, previously described by [48].

The BWM-MARCOS lithium potential model for Western Australia is shown in Figure 9d.

Table 9. BWM-MARCOS efficiency statistics for competent spatial proxies, Western Australia MPM.

Competent Spatial Proxies	Parameters						
	P_m	P_n	100-P_m	100-P_n	TP_r	FP_r	O_p
Proximity to mapped pegmatites (DC_8)	86	49	14	51	0.86	0.49	0.37
Proximity to LCT pegmatite indicator minerals (DC_{10})	84	52	16	48	0.84	0.52	0.32
Proximity to mafic–ultramafic rocks (DC_9)	78	50	22	50	0.78	0.50	0.28
Proximity to Au occurrences (DC_{11})	76	52	24	48	0.76	0.52	0.24
Proximity to Ni occurrences (DC_{12})	74	50	26	50	0.74	0.50	0.24
Proximity to pegmatitic or pegmatite-bearing rock units (DC_7)	69	52	31	48	0.69	0.52	0.17
Proximity to fractionated granitic rock units (DC_1)	70	53	30	47	0.70	0.53	0.17
Domains of greater density of RTP magnetic breaks (DC_6)	65	50	35	50	0.65	0.50	0.15
Domains of greater density of Bouguer gravity breaks (DC_5)	63	50	37	50	0.63	0.50	0.13
Proximity to faults and lineaments (DC_4)	67	55	33	45	0.67	0.55	0.12
Proximity to metamorphic rocks (DC_2)	57	47	43	53	0.57	0.47	0.10
Domains of greater density of major crustal boundaries (DC_3)	58	49	42	51	0.58	0.49	0.09

Key to abbreviations: P_m = hits, P_n = false alarms, 100-P_m = misses, 100-P_n = correct rejections, TP_r = true positive rate, FP_r = false positive rate, O_p = overall performance, DC = decision criterion.

4.3.2. Ontarian BWM-MARCOS Model

For Ontario, the same approach was followed as for Western Australia, with the relevant modeling information provided in Figure S26 and Tables 8 and 10, Tables S6 and S7. As for Western Australia, problem 3 of [48] can be formulated as per the following Equation (9):

$$\begin{aligned} & min\xi \\ & \text{s.t.} \\ & |W_8 - 2W_1| \le \xi, \text{forall} j \\ & |W_8 - 9W_2| \le \xi, \text{forall} j \\ & |W_8 - 4W_3| \le \xi, \text{forall} j \\ & \vdots \\ & |W_8 - 5W_7| \le \xi, \text{forall} j \\ & |W_1 - 8W_2| \le \xi, \text{forall} j \\ & |W_3 - 6W_2| \le \xi, \text{forall} j \\ & |W_4 - 8W_2| \le \xi, \text{forall} j \\ & \vdots \\ & |W_7 - 5W_2| \le \xi, \text{forall} j \\ & \sum_j W_j = 1 \\ W_j \ge 0, & \text{ forall } j \end{aligned} \tag{9}$$

Subsequently, the optimal weights $\left(W_B^*, W_1^*, \ldots, W_W^*\right)$ and ξ^* were defined by solving Equation (9) (Table S8). For $a_{BW} = a_{83} = 9$, the obtained consistency index was 5.23 [48], while the consistency ratio was 0.062/5.23 = 0.011, showing suitable consistency. As for Western Australia, the MARCOS technique was applied to rank the alternatives using an initial decision matrix $B_{1526806\times8}$ with 1526,806 decision alternatives linked to eight decision criteria. The alternatives were again ranked by the MARCOS step-by-step process.

The BWM-MARCOS lithium potential model for Ontario is illustrated in Figure 10d.

Table 10. BWM-MARCOS efficiency statistics for competent spatial proxies, Ontario MPM.

Competent Spatial Proxies	Parameters						
	P_m	P_n	100-P_m	100-P_n	TP_r	FP_r	O_p
Proximity to mapped pegmatites (DC8)	87	44	13	56	0.87	0.44	0.43
Proximity to LCT pegmatite indicator minerals (DC4)	89	47	11	53	0.89	0.47	0.42
Proximity to fractionated granitic rock units (DC1)	86	47	14	53	0.86	0.47	0.39
Proximity to mafic–ultramafic rocks (DC3)	65	38	35	62	0.65	0.38	0.27
Proximity to Au occurrences (DC5)	69	43	31	57	0.69	0.43	0.26
Proximity to Ni occurrences (DC6)	68	43	32	57	0.68	0.43	0.25
Domains of greater density of major crustal boundaries (DC7)	68	48	32	52	0.68	0.48	0.20
Proximity to Bouguer gravity breaks (DC2)	51	50	49	50	0.51	0.50	0.01

Key to abbreviations: See Table 9.

4.4. Data-Driven Random Forest (RF) Approach

A growing body of evidence, e.g., [29,41,130–135], has demonstrated that RF is more effective than and consistently outperforms other supervised machine learning algorithms applied to MPM. This is because the RF algorithm mitigates the problem of overfitting and improves model efficiency by way of a bagging procedure [54]. As an ensemble-based machine learning method, RF adopts a resampling strategy that generates each set of random training samples of an unpruned decision tree [54]. For MPM, a bootstrapping procedure is applied that collects sub-samples by resampling, with replacement, the spatial proxies for PL and NPL, referred to as labeled data. Decision trees are trained using in-bag samples, which include two-thirds of the labeled data. Decision tree impurity, termed out-of-bag (OOB) error, is measured by the remaining labeled data, termed OOB samples. As such, RF presents an aggregation of unpruned decision trees, each of which is developed in accordance with a distinct set of so-called existent patterns.

Executing RF requires (i) the number of trees (n) to be grown and (ii) the number of predictor variables (m) to be entered at each node [54]. These parameters should be tuned so that decision tree impurity is minimized. The mean decrease in the Gini impurity index (M_G) and accuracy (M_a) can be employed to assess the relative importance of the predictor variables. M_G is a measure of how each variable contributes to the homogeneity of the nodes and the final RF model, while M_a is defined by the computation of the OOB error. According to [54], the higher the values of M_a and M_G, the more important a predictor map is. Prospect locations (PL) were selected as outlined in Section 3.2., and they comprised 135 PL for Western Australia and 78 PL for Ontario.

4.4.1. Western Australian RF Model

As a first step, the original (non-transformed) spatial proxies (Figures S5a–S12a and S14a–S16a) were normalized via the following equation [136]:

$$X_i = \frac{x_i - x_{min}}{xmin_{max}} \quad (10)$$

where X_i per cell is the normalized score of the indicator value, x_i is the indicator value for the cell of the ith spatial proxy, and $x_{\max}$ and $x_{\min}$ are the largest and smallest indicator values pertaining to the ith spatial proxy. Hence, spatial proxy indicator values fall within a range of [0, 1]. Next, an n value of 1000 and m value of 4 were opted in accordance with the procedure provided by [131]. Figure S27 illustrates the significance of the predictor variables in the RF modeling according to the mean decrease in the accuracy and Gini impurity index. Pursuant to this figure, the proximity to metamorphic rocks is the least

significant spatial proxy in the RF MPM of Western Australia's lithium potential, while the proximity to mapped pegmatites is the most significant one.

Figure 9e is the RF lithium potential model for Western Australia, which was developed with normalized spatial proxies and a training error curve, as indicated in Figure S28. Pursuant to the latter, the error rate of modeling is progressively alleviated as the number of decision trees rises, with a mean squared error rate of ~0.15 for the first decision tree and 0.042 for the 1000th iteration.

4.4.2. Ontarian RF Model

After normalizing the original spatial proxies (Figures S17a–S21a, S23a and S24a) by Equation (10), an m value of 3 and n value of 1000 were chosen in accordance with [131]. Figure S29 illustrates the significance of the predictor variables in RF modeling according to the mean decrease in the accuracy and Gini impurity index, with proximity to mapped pegmatites the most significant spatial proxy and proximity to Bouguer gravity breaks the least significant one.

Figure 10e shows the RF lithium potential model for Ontario, which was developed with normalized spatial proxies and a training error curve, as indicated in Figure S30. Pursuant to the latter, the error rate of modeling is progressively alleviated as the number of decision trees rises, with a mean squared error rate of ~0.054 for the first decision tree and 0.028 for the 1000th iteration.

5. Discussion

5.1. Mineral Potential Mapping (MPM)

5.1.1. Criticisms, Limitations, and Opportunities

Mineral exploration is fundamentally a search and information problem associated with significant stochastic and systemic uncertainty in that our decision making is influenced by heuristics and biases and is reliant on inferences, extrapolations, and predictions revolving around sparse or heavily clustered data points. This is particularly true for mineral exploration targeting [137,138]. In other words, in mineral exploration targeting, geoscientists' interpretations and decisions will always be based on sparse information, invariably carrying an element of error and uncertainty. Additionally, data interpretation and decision-making under uncertainty will always be subject to prejudice, driven by a set of well-understood mental shortcuts, preferences, and unique personal experiences.

Modern computer systems, paired with AI approaches, are ideally suited to improve the outputs from mineral exploration targeting. MPM offers such an approach [139,140]. While often criticized for being biased toward mature, well-explored areas and tending toward the generation of excessively large areas of high prospectivity, these issues are not regarded as limitations in the MPM algorithms but shortcomings in the input data and targeting models that, in many cases, could be easily avoided [114].

It would be unwise to treat MPM output as 'treasure maps' given that MPM typically identifies more than a few areas of high potential. Rather, the output should be taken as the starting point for a 'treasure hunt' and regarded as just another tool in the 'exploration toolbox'. That is to say, MPM results (i) should be regarded as decision-support tools for delineating, ranking, and prioritizing exploration targets based on the underlying modeled prospectivity, (ii) present a snapshot in time of the conceptual understanding of the targeted mineral deposit type in combination with the quality, quantity, and variety of the data available to map the deposit footprints, and (iii) form the starting point for additional analyses, such as those of previously unrecognized areas of modeled high potential [42,141]. It is also important to understand that neither MPM nor any alternative targeting approach

can discriminate between targets that may host a small mineral occurrence and those that may host a world-class mineral deposit [142].

Given the current limitations, the most effective way of harnessing the power of advanced computer systems and AI in mineral exploration may be intelligence amplification (IA) rather than a sole reliance on AI. In other words, the best approach may be a hybrid of subjective human input and objective machine-based analysis that inform and balance each other [114]. In a practical sense, and where targeting projects are industry-funded, this could be achieved by addressing shortcomings in the predictor maps through geological interpretation and/or manual targeting by individuals or teams to augment GIS-driven MPM [143]. In such a two-pronged IA approach, multiple scenarios can be investigated, and a range of decision aids can be generated in support of the final targeting decisions [46,138].

5.1.2. Spatial Proxy Performance

Stochastic and systemic errors present significant sources of uncertainty affecting MPM. The former is typically linked to the nature and quality of the input data and can manifest in inappropriate targeting criteria. The latter primarily pertains to spatial proxies and how they are integrated for MPM. Hence, appropriate, well-performing spatial proxies and robust, fit-for-purpose modeling tools are critical aids in minimizing systemic uncertainty in MPM [114].

We also believe that utilizing only one statistical approach to help develop predictor maps is insufficient for a comprehensive analysis of their performance. Here, we used a combination of the *AUC* and N_d techniques to analyze and categorize the predictor maps and measure their performance. One of the key advantages of using a combination of statistical analysis tools is that such an approach provides a means for comparing predictor maps according to various performance metrics (Tables 7 and 8). For instance, while both the "proximity to LCT pegmatite indicator minerals" (spatial proxy E1) and "proximity to pegmatitic or pegmatite-bearing rock units" (spatial proxy E2) predictor maps achieved high *AUC* scores of 0.84, their N_d scores set them apart, in that proxy E1 scored an N_d value that is ~1.4 times higher than that of spatial proxy E2. Moreover, proxy E1 demonstrated superior statistical efficacy compared to E2, in that it achieved a greater prediction rate over a smaller area.

5.1.3. Comparative Model Performance

As demonstrated by the body of literature, modelers typically only use one modeling technique for the MPM of their study areas. In contrast, examples of studies that used two or more different modeling techniques are rare [29]. However, there are several benefits to a multi-technique approach to MPM, such as the ability to (i) better constrain exploration targets by integrating the results from different numerical models; (ii) compare, contrast, and cross-validate MPM results; (iii) ensure optimal use of the available empirical and conceptual information; and (iv) recognize and reduce stochastic and systemic uncertainties [29,114]. As clearly illustrated in [29,41,48,144], a multi-technique approach to MPM can (i) generate more robust targets, (ii) deliver insights that cannot be derived from a single modeling technique, and even (iii) aid in the development and calibration of new tools and techniques.

In addition to the above benefits, employing a multi-technique approach and developing a variety of lithium potential models (Figures 9 and 10) also support the assessment of model performance. For this, we used the improved P-A plot procedure of [128]. As illustrated by the improved prediction-area plots in Figures S31 and S32 and the performance statistics listed in Tables 11 and 12, the RF approach to MPM delivered the best-performing

lithium potential models for both Western Australia (overall performance, O_p = 0.52) and Ontario (O_p = 0.61) (Figures 9d and 10d). As the top ranked modeling technique, and given the relatively high O_p values of the RF models, it is clear that RF-driven MPM presents the tool of choice for targeting new lithium discoveries in these jurisdictions and likely elsewhere.

Table 11. Improved prediction-area (P-A) plot parameters for the Western Australian lithium potential models.

	Fuzzy Gamma	Geometric Average	Index Overlay	BWM-MARCOS	RF
P_m (Hits)	66	65	91	93	98
P_n (False Alarms)	48	48	50	48	46
100-P_m (Misses)	34	35	9	7	2
100-P_n (Correct Rejection)	52	52	50	52	54
True Positive Rate (TP_r)	0.66	0.65	0.91	0.93	0.98
False Positive Rate (FP_r)	0.48	0.48	0.50	0.48	0.46
Overall Performance (O_p)	0.18	0.17	0.41	0.45	0.52

Table 12. Improved prediction-area (P-A) plot parameters for the Ontarian lithium potential models.

	Fuzzy Gamma	Geometric Average	Index Overlay	BWM-MARCOS	RF
P_m (Hits)	75	75	92	88	98
P_n (False Alarms)	49	49	43	49	37
100-P_m (Misses)	25	25	8	12	2
100-P_n (Correct Rejection)	51	51	57	51	63
True Positive Rate (TP_r)	0.75	0.75	0.92	0.88	0.98
False Positive Rate (FP_r)	0.49	0.49	0.43	0.49	0.37
Overall Performance (O_p)	0.26	0.26	0.49	0.39	0.61

It is striking that the top-performing RF method produced a lithium prospectivity pattern that is unlike those generated by the other techniques (Figures 9 and 10). The reason for this characteristic and distinctive result is likely due to the specific mechanics of RF, a robust ensemble machine-learning algorithm that is ideally suited to model complex, multistage nonlinear systems, such as mineral systems.

5.2. Geological Validity and Insights

The lithium potential models generated in this study delivered new regional views of the lithium prospectivity of Western Australia and Ontario, two of the world's best endowed jurisdictions with regards to LCT pegmatite-hosted lithium deposits. The validity of the models, in particular the best-performing RF model (TP_r for both Western Australia and Ontario: 98%), is demonstrated by the fact that most known lithium deposits, camps, and districts plot within areas of elevated to very high lithium favorability. In addition, the models identified several areas that contain all ingredients for LCT pegmatite-hosted lithium mineralization that are mappable at the regional scale of our investigation but which may have been overlooked by previous explorers.

Our study, which included a comprehensive review of LCT pegmatite systems in Western Australia and Ontario, also delivered insights worthy of further analysis, in particular the statistically verifiable proximity relationship between lithium, gold, and nickel occurrences (Figure 11; Tables 7 and 8). At this stage, the underlying reason for this relationship is speculative in nature, but it seems plausible that the clustering of lithium, gold, and nickel occurrences is linked to common ingredients of the respective mineral system models, such as the presence of deep-seated faults and mafic–ultramafic

rock sequences. Interestingly, [145] postulated a genetic link between the Goulamina LCT pegmatite system, a globally significant hardrock lithium deposit located in Mali, and gold mineralization. The authors argued that albitization, elevated arsenic, and magmatic loellingite in the Goulamina pegmatites are also prominent features of gold deposits in the region, such as Morila (8 Moz Au), both of which formed during a period of felsic magmatism at ~2100 Ma.

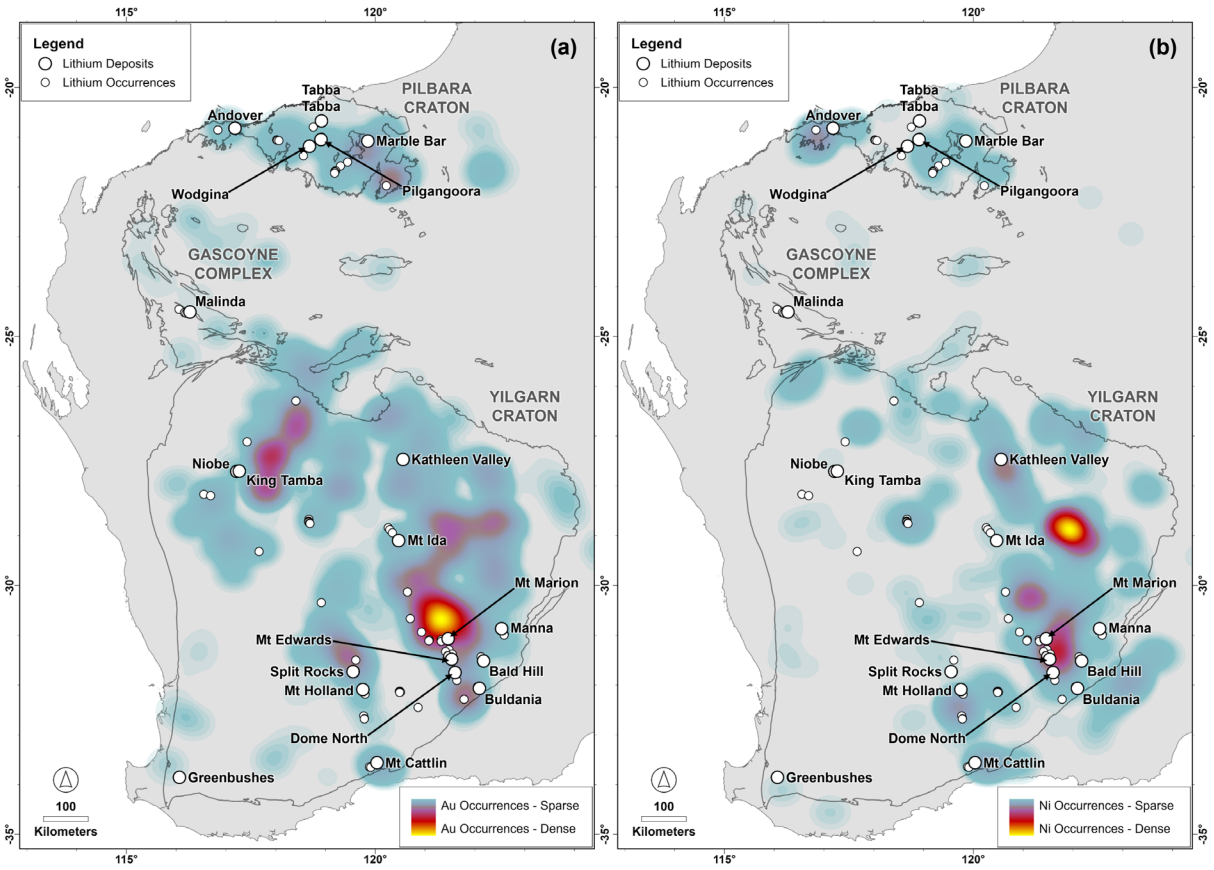

Figure 11. Maps illustrating the statistically verifiable proximity relationship between lithium and (**a**) gold and (**b**) nickel occurrences (Tables 7 and 8). Coordinate system: GDA 2020.

Also worthy of closer investigation may be some of the geological regions that have few LCT pegmatite lithium occurrences, or none, but were identified by MPM as having moderate to very high lithium potential. In Western Australia, these include, for example, the Proterozoic-age Halls Creek, southern Capricorn and Paterson orogens, as well as the eastern Archean-age Yilgarn Craton (Figure 12). Ontarian examples include the Kasabonika Lake-Ekwan River, Savant Lake-Crow Lake, Stull-Edmound Lake, Swayze, Abitibi, and Michipicoten greenstone belts of the Archean-age Superior Craton and the pegmatite belts of the Proterozoic Grenville Orogen in southern Ontario (Figure 13). Rather than the presence of demonstrably favorable lithium source intrusions, the modeled lithium prospectivity of these geological regions is typically linked to the presence of metamorphosed mafic–ultramafic rocks, structure, mapped pegmatites, and indicator minerals. The next step in any follow-up investigation of this as-of-yet theoretical lithium prospectivity would be desktop and field reviews of the geology of these regions, in particular the known granitoid intrusions and pegmatites.

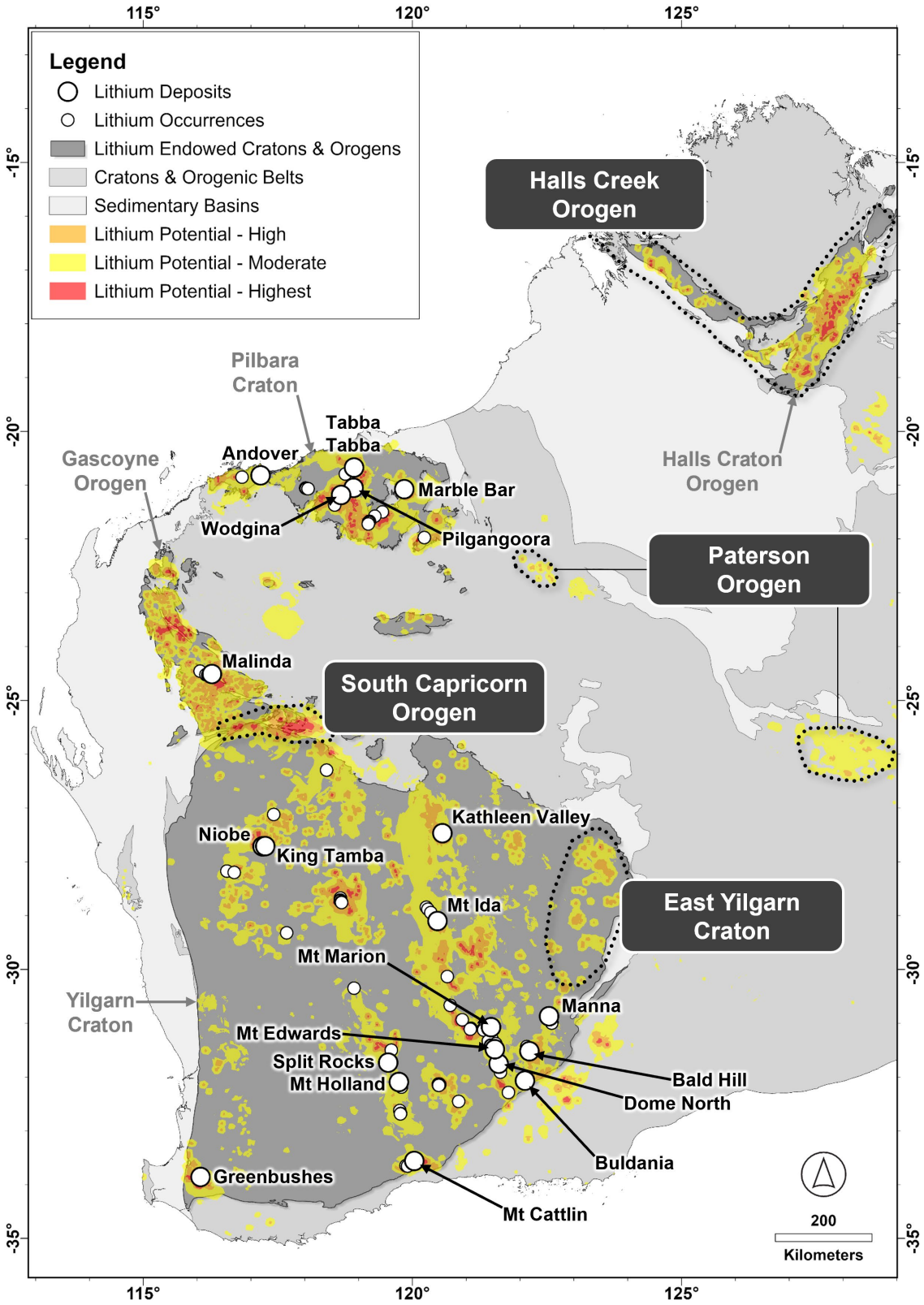

Figure 12. Map of the moderate to highest lithium potential of Western Australia (RF model), also illustrating newly identified lithium prospective domains in the eastern Archean Yilgarn Craton and the Proterozoic southern Capricorn, Halls Creek, and Paterson orogens. Coordinate system: GDA 2020.

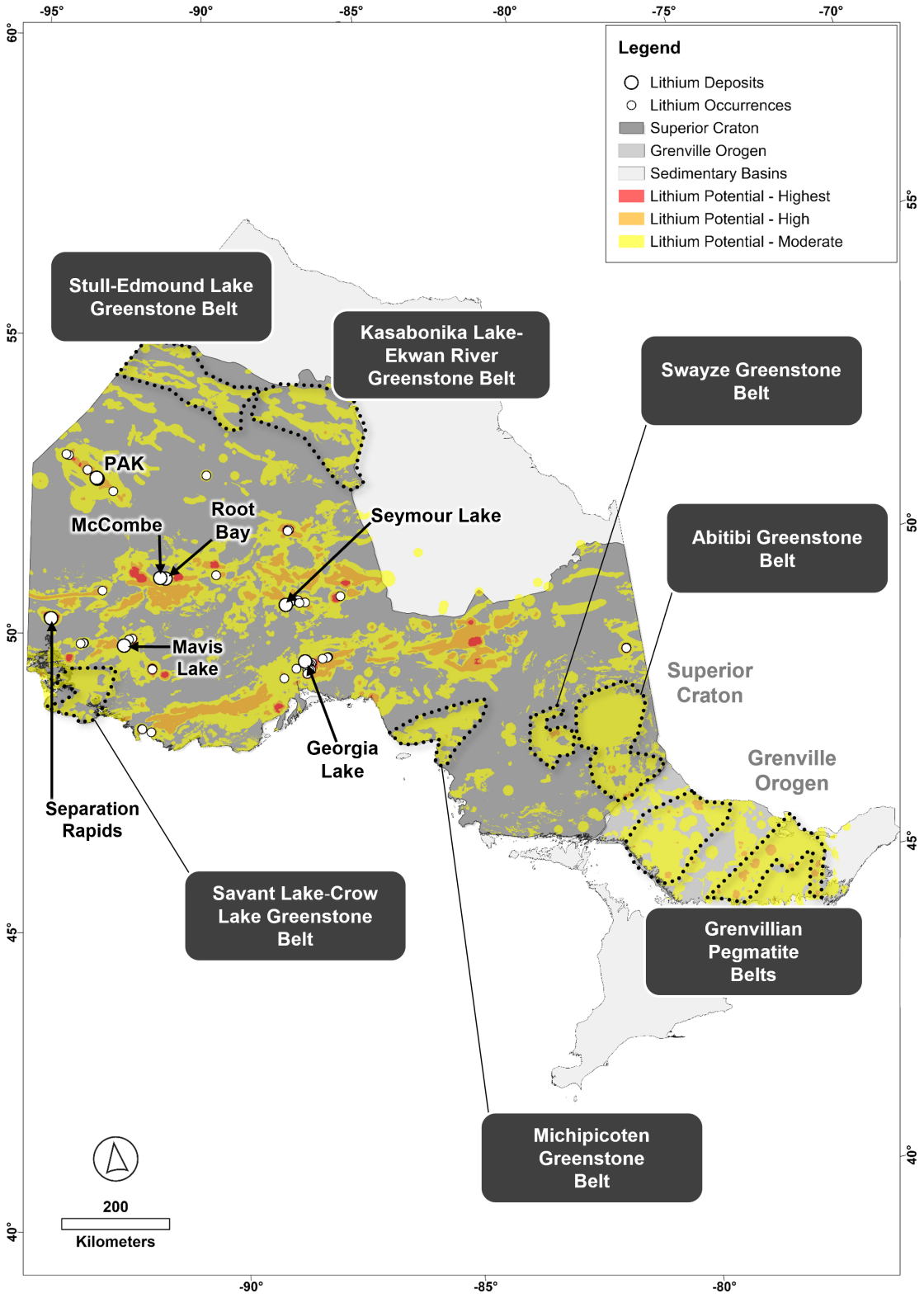

Figure 13. Map of the moderate to highest lithium potential of Ontario (RF model), also illustrating newly identified lithium prospective greenstone belts in the Archean Superior Craton and the Proterozoic Grenville Orogen. Coordinate system: WGS 1984 UTM Zone 15N.

Other aspects to consider here are the differences in geological information collected from and available for Western Australia and Ontario (Table 3). For example, the bedrock geology of Ontario, compiled at a scale of 1:250,000, includes a unit named 'muscovite-bearing granitic rocks', which captures all known Archean two-mica granites, many of

which are recognized as parental lithium source intrusions, and many more are likely lithium pegmatite sources. The Western Australian bedrock geology, on the other hand, is delivered at a scale of 1:500,000 and lacks a breakdown of Archean and Proterozoic granitoids according to their fractionation state. Hence, compiling a map of granitoids that may have lithium source potential is not a straightforward exercise. Having said that, Western Australia offers a pegmatite database and much more detailed structural and geophysical data than Ontario. These differences are reflected in the underlying MPM predictor maps, which differ somewhat between Western Australia and Ontario, given that certain spatial proxies are better supported by either the Western Australian or Ontarian datasets and, thus, more effective if backed by better quality data (Tables 9 and 10).

5.3. Mineral Exploration Implications

5.3.1. Exploration Search Space Concept

Given that lithium was a niche market up to the 2010s [146], most geoscientists have never had the opportunity to work in lithium exploration, and only a few resource companies had owned and operated lithium assets prior to this time. Hence, until recently, there has been a general lack of practical and theoretical know-how amongst explorationists when it comes to LCT pegmatites as well as a lack of modern systematic exploration of this mineral deposit type. As such, the lithium exploration booms of the late 2010s and early 2020s opened an entirely new search space [147] because only very few districts worldwide had ever recorded any noteworthy lithium exploration. Even belts that had received significant previous exploration and, thus, were relatively mature with regards to other metals, became highly attractive, as lithium had never constituted a valid exploration target and, consequently, had been ignored, or the mineralization not been recognized. The worldwide search efforts triggered by the recent lithium price booms of the late 2010s and early 2020s resulted in a 'golden period of discovery', with numerous new and globally significant hardrock lithium deposits (re-)discovered in short succession (e.g., Shaakichiuwaanaan, Quebec; Andover and Tabba Tabba, Western Australia; Ewoyaa, Ghana). A great example to illustrate the above is that of the world-class Mt Holland lithium deposit, which underlies the former Earl Grey gold mine and, locally, truncates the gold mineralization. Prior to its discovery in 2016, the Mt Holland pegmatite system was not understood to be spodumene-bearing and, thus, was never assayed for lithium. A review of the historical drill core eventually confirmed the lithium potential, as demonstrated by pegmatite occurrences with a combined strike length of >25 km, true widths of up to 50 m, and interval grades of up to 2.6% Li_2O. Subsequent drilling programs delivered one of the largest lithium hardrock resources in Australia [87,148].

5.3.2. Exploration Maturity and Potential

Whilst both Western Australia and Ontario may both still be considered exploration frontiers in the search for LCT pegmatite-hosted lithium deposits (see Section 5.3.1 above), Western Australia has, by and large, seen much more exploration drilling than Ontario, in particular when it comes to the highly lithium-fertile and endowed Archean greenstone belts. In contrast to Western Australia, many of northern Ontario's greenstone belts remain significantly underexplored.

For example, in the >300 km-long Southern Cross Greenstone Belt, Yilgarn Craton, Western Australia, which hosts Mount Holland, one of the world's largest hard rock lithium deposits, there are >66,000 publicly recorded drillholes (Figure 14). In comparison, there are only <610 publicly recorded drillholes in the >230 km-long Favorable Lake Greenstone Belt of the Superior Craton of Ontario and neighboring Manitoba (Figure 15). Large segments, up to 45 km long, of the Favorable Lake Greenstone Belt have never been

drilled. This is despite the Favorable Lake Greenstone Belt hosting the PAK deposit cluster, one of the largest and highest-grade hardrock lithium resources in North America. LCT pegmatites have been identified in over ~110 km-long sections of both the Southern Cross and Favorable Lake greenstone belts.

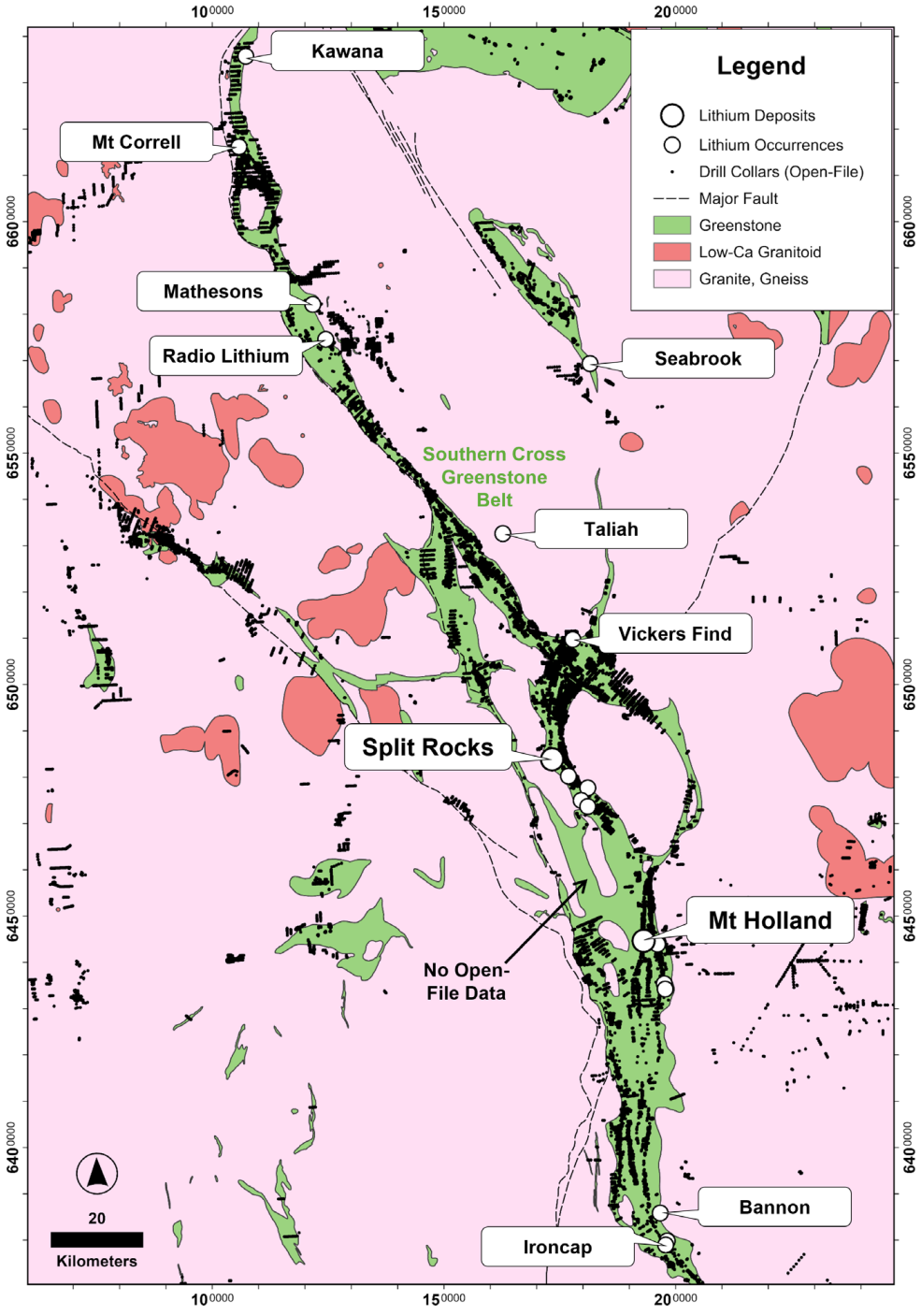

Figure 14. Simplified map of part of the >300 km-long Southern Cross Greenstone Belt, Archean Yilgarn Craton, showing LCT pegmatite occurrences and deposits as well as >66,000 publicly recorded drillholes completed in the area. The globally significant Mt Holland lithium deposit was only discovered in 2016, postdating most of the prior drilling. However, this drilling helped to quickly evaluate the deposit and district potential. The data sources used in the drafting of this map are listed in Table 3. Coordinate system: GDA 2020 MGA Zone 51.

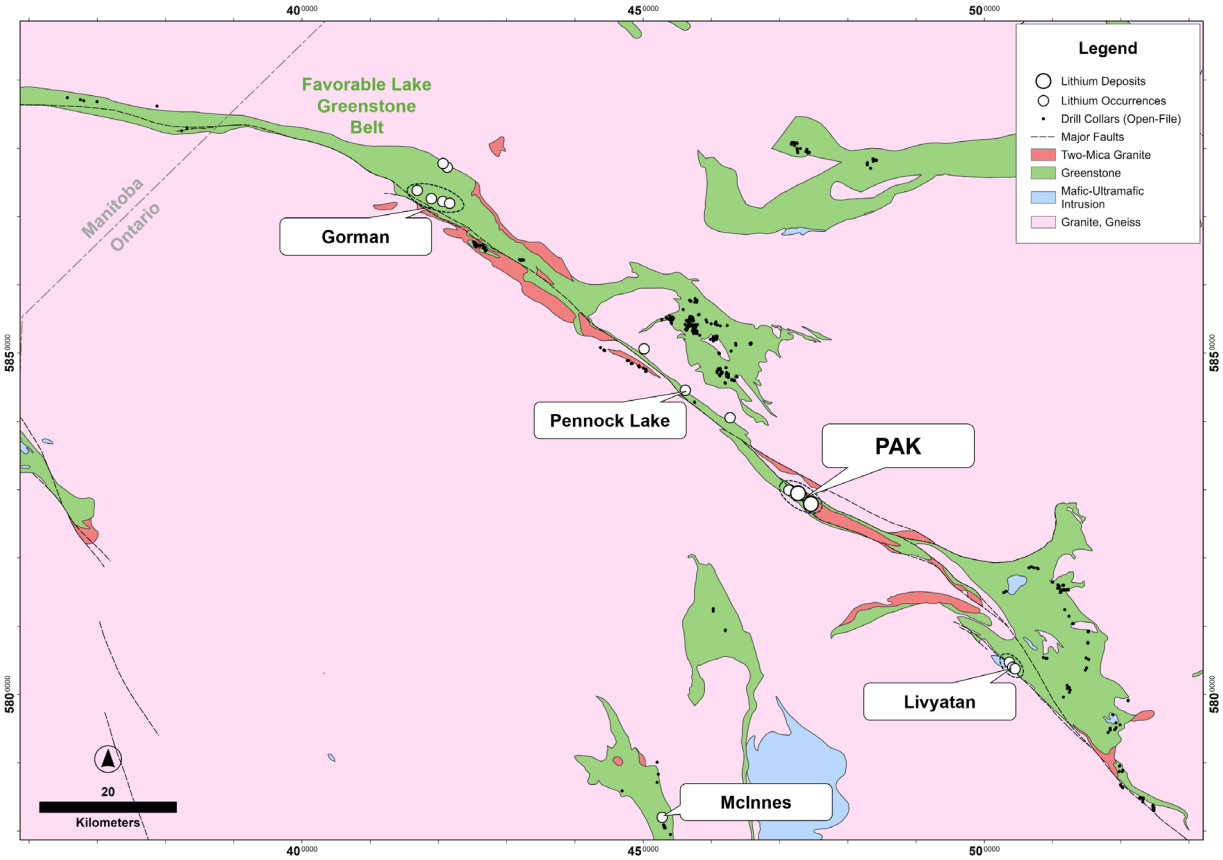

Figure 15. Simplified map of part of the >230 km-long Favorable Lake Greenstone Belt, Archean Superior Craton, showing LCT pegmatite occurrences and deposits as well as the <610 publicly recorded drillholes. Large segments, up to 45 km long, of the Favorable Lake Greenstone Belt have never been drilled. This is despite the Favorable Lake Greenstone Belt hosting the PAK deposit cluster, one of the largest and highest-grade hardrock lithium resources in North America. The data sources used in the drafting of this map are listed in Table 3. Coordinate system: WGS 1984 UTM Zone 15N.

While the PAK (or Pakeagama Lake) pegmatite was discovered in 1999 and has been subject to decades of intermittent lithium exploration, only <100 publicly recorded drillholes have been completed since the maiden drilling program in 2013 [110]. The adjacent Spark and Bolt lithium pegmatites were discovered in 2018 and 2020, respectively [110], while the Gorman and Livyatan lithium pegmatite clusters, ~70 km northwest and ~40 km southeast of PAK, respectively, were only located in 2023 [149,150]. Conducting exploration programs and developing mining operations in the Favorable Lake Greenstone Belt are challenged, amongst other things, by the remote nature of the area, lack of infrastructure, and long and harsh winters, all of which combine to create a high-cost environment. Added challenges are presented by widespread transported till cover, which may conceal the geochemical signals of the prospective bedrock, and thick brush, which may hide outcrops and make it difficult to get around other than by helicopter.

The lithium mineralized Bounty and Earl Grey pegmatites at Mt Holland, on the other hand, were brought into production in 2024, only eight years after their discovery, largely due to the existing gold mine infrastructure, a granted mining lease, and access to an existing mining workforce. Another important aspect was the rapid conversion of the 2016 lithium pegmatite discovery to a world-class lithium resource in under five months [151], aided by the availability of hundreds of previous gold-focused drillholes (<600 publicly

recorded) that had intersected the pegmatites but had not been assayed for lithium and related pathfinder elements.

Overall, given the (i) results of our MPM, (ii) large size of the Superior Craton in Ontario compared to the Western Australian cratons (Superior Craton: ~595,000 km^2; Yilgarn Craton: ~609,000 km^2; Pilbara Craton: ~57,000 km^2), (iii) occurrence of globally significant hardrock lithium deposits across the Canadian Superior Craton (e.g., Tanco in Manitoba, PAK in Ontario, and Shaakichiuwaanaan in Quebec), and (iv) underexplored nature of the Ontarian greenstone belts, in particular those in northern Ontario, the province should be able to deliver additional lithium pegmatite discoveries in the future, as should Western Australia.

5.3.3. Western Australian Target Example

The following example of a target generated by this lithium MPM, the Pinderi Hills area in Western Australia (Figure 16), also serves to provide a more detailed assessment of the modeling results and how MPM can facilitate the rapid recognition of areas of high potential that lack any known mineral occurrences of the targeted type; in this case, that of potential lithium mineralized LCT pegmatites.

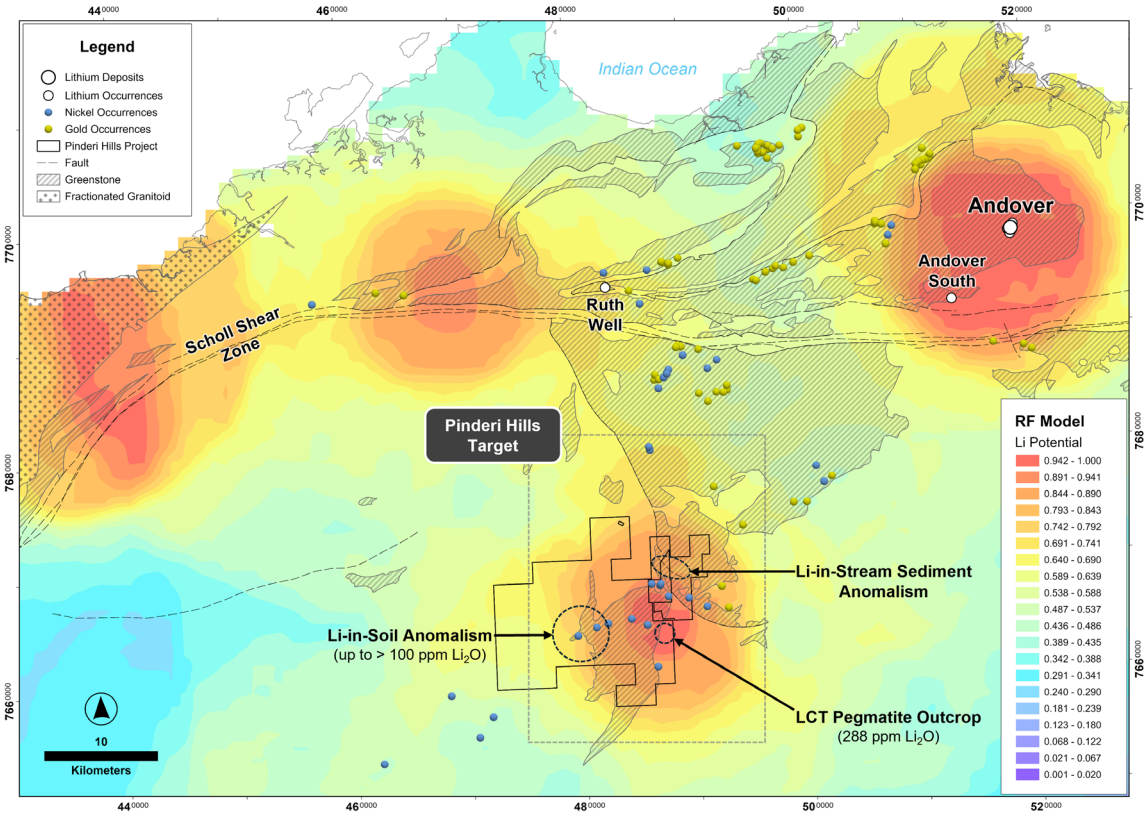

Figure 16. Example of an MPM (RF model)-generated target in the Archean Pilbara Craton, referred to as Pinderi Hills [152]. At the time of modeling, no LCT pegmatites were known to exist at Pinderi Hills, which is only ~32 km southwest of the globally significant Andover lithium deposit. Recent exploration work at Pinderi Hills has identified lithium and associated cesium, tantalum, and niobium anomalism in rock chips, soil, and stream sediments over large areas, which may point to the presence of a poorly outcropped LCT pegmatite swarm. Andover South is a recent LCT pegmatite discovery that postdates our MPM but falls within a domain of highest lithium potential. Coordinate system: GDA 2020 MGA Zone 51.

The Pinderi Hills target is located in the western part of the Archean Pilbara Craton, ~40 km southwest of the globally significant Andover lithium deposit and ~32 km southwest

of the recent Andover South discovery. The east–west-striking Scholl Shear Zone lies 17 km to the north, while the north-northwest–east-southeast-striking Maitland Shear Zone runs straight through the target area. The project geology is dominated by the Munni Munni and Maitland intrusions, two adjoining mafic–ultramafic complexes, and felsic to mafic volcanic rocks of the Whundo Group. The mineral exploration tenure over Pinderi Hills is subject to an earn-in joint venture between Errawarra Resources and Alien Metals announced in April 2024 [152]. Exploration is at a very early stage. Nevertheless, work undertaken by Errawarra Resources to date delivered the following encouraging results: (i) satellite imagery analysis identified a group of linear geomorphic features interpreted as pegmatites, and (ii) field reconnaissance and surface geochemistry surveys returned anomalous rock chips, including an assay of 288 ppm Li_2O (associated with elevated cesium, tantalum, and niobium) from an outcropping pegmatite, and identified several up to >1 km-long, linear soil anomalies with peak anomalies of up to >100 ppm Li_2O [152]. Further investigation is required to demonstrate the lithium potential of the Pinderi Hills area, but the limited work undertaken to date suggests that the MPM generated a valid target.

6. Summary and Conclusions

In this study, we developed the first published predictive models of hardrock lithium potential for two of the world's best-endowed jurisdictions, Western Australia and Ontario. The main conclusions and insights gained from this study can be summarized as follows:

- Western Australia has known resources of ~26 Mt Li_2O contained in 19 lithium-cesium–tantalum (LCT) pegmatite deposit clusters. One of these clusters is in the Gascoyne Complex and is Proterozoic in age. The remainder is hosted by the Yilgarn and Pilbara cratons and was formed during Archean times. Ontario has a much smaller endowment of ~1.5 Mt Li_2O contained in seven LCT pegmatite deposit clusters, all of which are in the Superior Craton and are Archean in age.
- Even the best-endowed lithium pegmatite system in Ontario, PAK, would only rank eighth among the Western Australian lithium pegmatite resources. This size discrepancy may be taken to imply that either the Ontarian LCT pegmatites have lesser endowments than their Western Australian counterparts, or several very substantial pegmatite-hosted lithium resources are yet to be discovered in Ontario or to be fully delineated by further drilling.
- As demonstrated for the Favorable Lake Greenstone Belt of northern Ontario, large tracts of the Archean Superior Craton are significantly underexplored compared to the Archean cratons of Western Australia. Government records indicate that <610 drillholes were completed along the >230 km-long Favorable Lake Greenstone Belt. Despite the presence of the PAK pegmatite cluster, this is one of the largest and highest-grade hardrock lithium resources in North America. In contrast, there are >66,000 publicly recorded drillholes that were completed along the >300 km-long Southern Cross Greenstone Belt, Yilgarn Craton, which hosts one of the world's largest hard rock lithium deposits at Mount Holland. Large segments, up to 45 km long, of the Favorable Lake Greenstone Belt have never been drilled. No such large undrilled search spaces exist near world-class mineralized systems in the Archean Yilgarn and Pilbara cratons of Western Australia.
- In contrast to the Western Australian LCT pegmatites, the Ontarian systems often illustrate clear genetic links to S-type parental granitoids. Terranes that lack S-type granitoids are typically devoid of LCT pegmatites.
- LCT pegmatites in Ontario commonly have steep to subvertical dip angles and lenticular or prolate geometries (e.g., PAK, Separation Rapids), while their Western Australian

counterparts are typically sheet-like and gently dipping to subhorizontal in nature (e.g., Mt Holland, Mt Cattlin, Tabba Tabba).

- Common expressions of LCT pegmatite systems and controls on lithium deposit formation include the following: (i) high degrees of melting of a fertile protolith, typically a sedimentary crustal source (as represented by the S-type, two-mica granitoids of the Superior Craton) or biotite dehydration melting at relatively shallow greenstone-root levels (as potentially represented by the evolved I-type, low-Ca granitoids of the Yilgarn Craton) (in all cases investigated in this study, the crustal melting was spatially associated with convergent margin tectonic settings (Phanerozoic, Proterozoic ± Archean) or continental rift zones marked by greenstone belts (Archean)); (ii) extreme fractionation of the granitic melts that formed the pegmatites; (iii) a high degree of crustal permeability, typically associated with active deformation along first- and second-order fault systems, typically localized along belt margins; and (iv) the presence of mafic to ultramafic rock sequences that have been metamorphosed at greenschist to amphibolite facies grade.
- We adopted a best-practice multi-technique approach to mineral potential mapping (MPM) of the LCT pegmatite system in Western Australia and Ontario, which included the use of five different methods spanning the spectrum between traditional MPM algorithms and artificial intelligence (AI). The best-performing method, the random forest (RF) machine-learning AI technique, achieved excellent overall performance (O_p) metrics (Western Australia: O_p = 0.52; Ontario: O_p = 0.61), bettering all other methods by ~3.05 times for Western Australia and ~2.35 times for Ontario. The validity of the RF model is also demonstrated by most of the known lithium deposits, camps, and districts plotted within areas of elevated to very high lithium favorability, as identified by this modeling approach.
- MPM also identified certain belts that have few to none LCT pegmatite lithium occurrences, but they have moderate to very high lithium potential. In Western Australia, these include, for example, the Proterozoic Halls Creek, southern Capricorn, and Paterson orogens, as well as the eastern Archean Yilgarn Craton. Ontarian examples include the Kasabonika Lake-Ekwan River, Savant Lake-Crow Lake, Stull-Edmound Lake, Swayze, Abitibi, and Michipicoten greenstone belts of the Archean Superior Craton and the pegmatite belts of the Proterozoic Grenville Orogen in southern Ontario. In our opinion, these belts warrant closer investigation as to their LCT pegmatite potential.
- In addition, our modeling revealed a statistically verifiable proximity relationship between lithium, gold, and nickel occurrences. At this stage, the underlying reason for this relationship is speculative, but it seems plausible that the clustering of these different mineral deposit types is linked to their common spatial association with deep-seated faults and mafic–ultramafic rock sequences.

Supplementary Materials: The following supporting information can be downloaded at: https://www.mdpi.com/article/10.3390/min15040397/s1, Figure S1: Receiver operating characteristic curve for the spatial proxies of Western Australia: (a) proximity to fractionated granitic rock units, (b) proximity to metamorphic rocks, (c) domains of greater density of major crustal boundaries, (d) proximity to faults and lineaments, (e) domains of greater density of Bouguer gravity breaks, (f) domains of greater density of RTP magnetic breaks, (g) proximity to pegmatitic or pegmatite-bearing rock units, (h) proximity to mapped pegmatites, (i) proximity to mafic-ultramafic rocks, (j) proximity to LCT pegmatite indicator minerals, (k) proximity to Au occurrences and (l) proximity to Ni occurrences; Figure S2: Receiver operating characteristic curve for the spatial proxies of Ontario: (a) proximity to fractionated granitic rock units, (b) domains of greater density of major crustal boundaries, (c) proximity to Bouguer gravity breaks, (d) proximity to mapped pegmatites, (e) proximity to mafic-ultramafic rocks, (f) proximity to LCT pegmatite indicator minerals, (g) proximity to Au

occurrences and (h) proximity to Ni occurrences; Figure S3: Prediction-area plot for the spatial proxies of Western Australia: (a) proximity to fractionated granitic rock units, (b) proximity to metamorphic rocks, (c) domains of greater density of major crustal boundaries, (d) proximity to faults and lineaments, (e) domains of greater density of Bouguer gravity breaks, (f) domains of greater density of RTP magnetic breaks, (g) proximity to pegmatitic or pegmatite-bearing rock units, (h) proximity to mapped pegmatites, (i) proximity to mafic-ultramafic rocks, (j) proximity to LCT pegmatite indicator minerals, (k) proximity to Au occurrences and (l) proximity to Ni occurrences; Figure S4: Prediction-area plot for the spatial proxies of Ontario: (a) proximity to fractionated granitic rock units, (b) domains of greater density of major crustal boundaries, (c) proximity to Bouguer gravity breaks, (d) proximity to mapped pegmatites, (e) proximity to mafic-ultramafic rocks, (f) proximity to LCT pegmatite indicator minerals, (g) proximity to Au occurrences and (h) proximity to Ni occurrences; Figure S5: (a) Predictor map of proximity to fractionated granitic rock units and (b) continuously-weighted predictor map of proximity to fractionated granitic rock units; Figure S6: (a) Predictor map of proximity to metamorphic rocks and (b) continuously-weighted predictor map of proximity to metamorphic rocks; Figure S7: (a) Predictor map of domains of greater density of major crustal boundaries and (b) continuously-weighted predictor map of domains of greater density of major crustal boundaries; Figure S8: (a) Predictor map of proximity to faults and lineaments and (b) continuously-weighted predictor map of proximity to faults and lineaments; Figure S9: (a) Predictor map of domains of greater density of Bouguer gravity breaks and (b) continuously-weighted predictor map of domains of greater density of Bouguer gravity breaks; Figure S10: (a) Predictor map of domains of greater density of RTP magnetic breaks and (b) continuously-weighted predictor map of domains of greater density of RTP magnetic breaks; Figure S11: (a) Predictor map of proximity to pegmatitic or pegmatite-bearing rock units and (b) continuously-weighted predictor map of proximity to pegmatitic or pegmatite-bearing rock units; Figure S12: (a) Predictor map of proximity to mafic-ultramafic rocks and (b) continuously-weighted predictor map of proximity to mafic-ultramafic rocks; Figure S13: Predictor maps: (a) proximity to Nb occurrences, (b) proximity to Sn occurrences, (c) proximity to Ta occurrences, (d) proximity to mapped tourmaline minerals, (e) proximity to mapped tantalite minerals, (f) proximity to mapped spodumene minerals, (g) proximity to mapped lepidolite minerals, (h) proximity to mapped columbite minerals, (i) proximity to mapped beryl minerals and (j) proximity to mapped cassiterite minerals. (k) The spatial proxy of proximity to LCT pegmatite indicator minerals, which was generated by the combination of predictor maps S13a-S13j using a fuzzy "OR" operator; Figure S14: (a) Predictor map of proximity to mapped pegmatites and (b) continuously-weighted predictor map of proximity to mapped pegmatites; Figure S15: (a) Predictor map of proximity to Au occurrences and (b) continuously-weighted predictor map of proximity to Au occurrences; Figure S16: (a) Predictor map of proximity to Ni occurrences and (b) continuously-weighted predictor map of proximity to Ni occurrences; Figure S17: (a) Predictor map of proximity to fractionated granitic rock units and (b) continuously-weighted predictor map of proximity to fractionated granitic rock units; Figure S18: (a) Predictor map of domains of greater density of major crustal boundaries and (b) continuously-weighted predictor map of domains of greater density of major crustal boundaries; Figure S19: (a) Predictor map of proximity to Bouguer gravity breaks and (b) continuously-weighted predictor map of proximity to Bouguer gravity breaks; Figure S20: (a) Predictor map of proximity to mapped pegmatites and (b) continuously-weighted predictor map of proximity to mapped pegmatites; Figure S21: (a) Predictor map of proximity to mafic-ultramafic rocks and (b) continuously-weighted predictor map of proximity to mafic-ultramafic rocks; Figure S22: Predictor maps: (a) proximity to Nb occurrences, (b) proximity to Sn occurrences, (c) proximity to Ta occurrences, (d) proximity to Be occurrences and (e) proximity to Rb occurrences. (f) The spatial proxy of proximity to LCT pegmatite indicator minerals, which was generated by the combination of predictor maps S22a-S22e using a fuzzy "OR" operator; Figure S23: (a) Predictor map of proximity to Au occurrences and (b) continuously-weighted predictor map of proximity to Au occurrences; Figure S24: (a) Predictor map of proximity to Ni occurrences and (b) continuously-weighted predictor map of proximity to Ni occurrences; Figure S25: Improved prediction-area plot for the spatial proxies of Western Australia: (a) proximity to fractionated granitic rock units, (b)

proximity to metamorphic rocks, (c) domains of greater density of major crustal boundaries, (d) proximity to faults and lineaments, (e) domains of greater density of Bouguer gravity breaks, (f) domains of greater density of RTP magnetic breaks, (g) proximity to pegmatitic or pegmatite-bearing rock units, (h) proximity to mapped pegmatites, (i) proximity to mafic-ultramafic rocks, (j) proximity to LCT pegmatite indicator minerals, (k) proximity to Au occurrences and (l) proximity to Ni occurrences; Figure S26: Improved prediction-area plot for the spatial proxies of Ontario: (a) proximity to fractionated granitic rock units, (b) domains of greater density of major crustal boundaries, (c) proximity to Bouguer gravity breaks, (d) proximity to mapped pegmatites, (e) proximity to mafic-ultramafic rocks, (f) proximity to LCT pegmatite indicator minerals, (g) proximity to Au occurrences and (h) proximity to Ni occurrences; Figure S27: Measure of predictor variable significance derived by RF algorithm: (a) mean decrease in accuracy and (b) mean decrease in Gini impurity index; Figure S28: Evolution of the mean squared error curve for exploration evidential data applied for training the RF potential model; Figure S29: Measure of predictor variable significance derived by RF algorithm: (a) mean decrease in accuracy and (b) mean decrease in Gini impurity index; Figure S30: Evolution of the mean squared error curve for exploration evidential data applied for training the RF potential model; Figure S31: Improved prediction-area plot for the prospectivity models of Western Australia: (a) data-driven index overlay, (b) fuzzy gamma, (c) geometric average, (d) BWM-MARCOS and (e) RF; Figure S32: Improved prediction-area plot for the prospectivity models of Ontario: (a) data-driven index overlay, (b) fuzzy gamma, (c) geometric average, (d) BWM-MARCOS and (e) RF; Table S1: Lithium Occurrence Data, Western Australia, as used in Mineral Potential Modelling; Table S2: Lithium Occurrence Data, Ontario, as used in Mineral Potential Modelling; Table S3: Others-to-worst pairwise comparison vector based on the O_p index; Table S4: Best-to-others pairwise comparison vector based on the O_p index; Table S5: Optimal weights (W^*) derived from the BWM approach; Table S6: Others-to-worst pairwise comparison vector based on the O_p index; Table S7: Best-to-others pairwise comparison vector based on the O_p index; Table S8: Optimal weights (W^*) derived from the BWM approach.

Author Contributions: Conceptualization, O.P.K.; methodology, O.P.K. and B.R.; software, O.P.K. and B.R.; validation, B.R.; formal analysis, O.P.K. and B.R.; investigation, O.P.K. and B.R.; resources, O.P.K. and B.R.; data curation, O.P.K. and B.R.; writing—original draft preparation, O.P.K. and B.R.; writing—review and editing, O.P.K.; visualization, O.P.K. and B.R.; project administration, O.P.K. All authors have read and agreed to the published version of the manuscript.

Funding: This research received no external funding.

Data Availability Statement: Publicly available datasets were analyzed in this study. The data sources are specified in Table 3.

Acknowledgments: The authors would like to thank the five anonymous reviewers whose insightful and constructive comments helped to significantly improve the manuscript. The Assistant Editor is thanked for their expert handling of the manuscript. The governments of Western Australia and Ontario are acknowledged for providing free and unrestricted access to high-quality geoscience and exploration data, without which a regional study like this one would be impossible.

Conflicts of Interest: The authors declare no conflicts of interest.

References

1. Černý, P.; Ercit, T.S. The classification of granitic pegmatites revisited. *Can. Mineral.* **2005**, *43*, 2005–2026. [CrossRef]
2. Bradley, D.C.; Stillings, L.L.; Jaskula, B.W.; Munk, L.; McCauley, A.D. Lithium. In *Critical Mineral Resources of the United States—Economic and Environmental Geology and Prospects for Future Supply*; Professional Paper 1802; Schulz, K.J., DeYoung, J.H., Jr., Seal, R.R., II, Bradley, D.C., Eds.; U.S. Geological Survey: Reston, VA, USA, 2017; pp. K1–K21.
3. Bradley, D.C.; McCauley, A.D.; Stillings, L.M. Mineral-deposit model for lithium-cesium-tantalum pegmatites. In *Mineral Deposit Models for Resource Assessment*; Scientific Investigations Report 2010–5070–O; U.S. Geological Survey: Reston, VA, USA, 2017; pp. 1–48.
4. Bradley, D.C. Tectonic and paleoclimatic controls of lithium-cesium-tantalum (LCT) pegmatite genesis, exhumation, and preservation in the Appalachians. *Can. Mineral.* **2019**, *57*, 715–717. [CrossRef]

5. RCF Ambrian. *Lithium Commodity Market Report, August 2023*; RCF Ambrian: London, UK, 2023; 53p.
6. Geological Survey of Western Australia. *Lithium Investment Opportunities, December 2023*; Government of Western Australia, Department of Energy, Mines, Industry Regulation and Safety: Perth, Australia, 2023; 2p.
7. Hard Rock Lithium Deposits. Available online: https://www.geologyforinvestors.com/hard-rock-lithium-deposits/ (accessed on 14 December 2024).
8. Critical Minerals Analysis, Ontario Mining Association. 2022. Available online: https://oma.on.ca/en/ontario-mining/2022_OMA_Mineral_Profiles.pdf (accessed on 14 December 2024).
9. Ontario Geological Survey. *An Introduction to Ontario's Critical Minerals, with Highlights from the Ontario Mineral Inventory*; Ministry of Northern Development, Mines, Natural Resources and Forestry: Sudbury, ON, Canada, 2022; 69p.
10. Wildcat Resources Limited. Wildcat Delivers Australia's Largest Undeveloped Lithium Resource of 74 Mt @ 1.0% Li_2O at Tabba Tabba, WA. In *Australian Securities Exchange (ASX) Announcement Dated 18 November 2024*; Wildcat Resources Limited: Perth, WA, Australia, 2024; 42p.
11. Global Lithium Resources Limited. GL1 Delivers Transformative 50.7 Mt Lithium Resource Base. In *Australian Securities Exchange (ASX) Announcement Dated 15 December 2022*; Global Lithium Resources Limited: Perth, WA, Australia, 2022; 37p.
12. Azure Minerals Limited. Exploration Target–Andover Lithium Project. In *Australian Securities Exchange (ASX) Announcement Dated 7 August 2023*; Azure Minerals Limited: Perth, WA, Australia, 2023; 19p.
13. Frontier Lithium Inc. Corporate Presentation, 25 November 2024, 20p. Available online: https://www.frontierlithium.com/investors-1/ (accessed on 11 December 2024).
14. Avalon Advanced Materials Inc. Avalon announces a substantive 20% increase in deposit size at its flagship Separation Rapids joint-venture lithium project. In *Toronto Securities Exchange (TSX) Announcement Dated 10 August 2023*; Avalon Advanced Materials Inc.: Toronto, ON, Canada, 2023; 7p.
15. Green Technology Metals Limited. Significant resource and confidence level increase at Root, global resource inventory now at 24.5 Mt. In *Australian Securities Exchange (ASX) Announcement Dated 17 October 2023*; Green Technology Metals Limited: Subiaco, WA, Australia, 2023; 89p.
16. AMC Mining Consultants (Canada) Limited. *Technical Report, Georgia Lake Lithium Project Pre-Feasibility Study*; RockTech Lithium Inc.: Vancouver, BC, Canada, 2022; 350p.
17. Critical Resources Limited. 8.0 Mt at 1.07% Li_2O maiden mineral resource at Mavis Lake. In *Australian Securities Exchange (ASX) Announcement Dated 5 May 2023*; Critical Resources Limited: Perth, WA, Australia, 2023; 25p.
18. Sweetapple, M.T.; Collins, P.L. Genetic framework for the classification and distribution of Archean rare metal pegmatites in the north Pilbara Craton, Western Australia. *Econ. Geol.* **2002**, *97*, 873–895. [CrossRef]
19. Breaks, F.W.; Selway, J.B.; Tindle, A.G. Fertile peraluminous granites and related rare-element mineralization in pegmatites, Superior Province, northwest and northeast Ontario: Operation treasure hunt. *Ont. Geol. Surv. Open File Rep.* **2003**, *6099*, 179.
20. Selway, J.B.; Breaks, F.W.; Tindle, A.G. A review of rare-element (Li-Cs-Ta) pegmatite exploration techniques for the Superior Province, Canada, and large worldwide tantalum deposits. *Explor. Min. Geol.* **2005**, *14*, 1–30. [CrossRef]
21. Sweetapple, M.T. A review of the setting and internal characteristics of lithium pegmatite systems of the Archaean north Pilbara and Yilgarn cratons, Western Australia. In Proceedings of the Extended Abstracts (Australian Institute of Geoscientists Bulletin, 65, 113–117), Granites 2017 Conference, Benalla, VIC, Australia, 25–28 September 2017.
22. Duuring, P. Rare-element pegmatites: A mineral systems analysis. In *Geological Survey of Western Australia Record 2020/7*; Geological Survey of Western Australia: East Perth, Australia, 2020; 6p.
23. Phelps-Barber, Z.; Trench, A.; Groves, D.I. Recent pegmatite-hosted spodumene discoveries in Western Australia: Insights for lithium exploration in Australia and globally. *Appl. Earth Sci.* **2022**, *131*, 100–113. [CrossRef]
24. Wells, M.; Aylmore, M.; McInnes, B. MRIWA Report M532—The geology, mineralogy and geometallurgy of EV materials deposits in Western Australia. *Geol. Surv. West. Aust. Rep.* **2022**, *228*, 187.
25. Sweetapple, M.T.; Vanstone, P.J.; Lumpkin, G.R.; Collins, P.L.F. A review of lithogeochemical dispersion haloes of LCT pegmatites, and their application to rare metal exploration, with special reference to lithium in an Australian context. *Aust. J. Earth Sci.* **2024**, *71*, 1050–1084. [CrossRef]
26. Data WA. Available online: https://www.data.wa.gov.au/ (accessed on 4 March 2025).
27. GeologyOntario. Available online: https://www.hub.geologyontario.mines.gov.on.ca/ (accessed on 4 March 2025).
28. Bruce, M.; Kreuzer, O.P.; Wilde, A.; Buckingham, A.; Butera, K.; Bierlein, F. Unconformity-type uranium systems: A comparative review and predictive modelling of critical genetic factors. *Minerals* **2020**, *10*, 738. [CrossRef]
29. Roshanravan, B.; Kreuzer, O.P.; Buckingham, A.; Keykhay-Hosseinpoor, M.; Keys, E. Mineral potential modelling of orogenic gold systems in the Granites-Tanami Orogen, Northern Territory, Australia: A multi-technique approach. *Ore Geol. Rev.* **2023**, *152*, 105224. [CrossRef]

30. Wyborn, L.A.I.; Heinrich, C.A.; Jaques, A.L. Australian Proterozoic mineral systems: Essential ingredients and mappable criteria. In Proceedings of the 1994 AusIMM Annual Conference: Australian Mining Looks North—The Challenges and Choices, Darwin, NT, Australia, 5–9 August 1994; pp. 109–115.
31. Knox-Robinson, C.M.; Wyborn, L.A.I. Towards a holistic exploration strategy: Using geographic information systems as a tool to enhance exploration. *Aust. J. Earth Sci.* **1997**, *44*, 453–463. [CrossRef]
32. McCuaig, T.C.; Beresford, S.; Hronsky, J. Translating the mineral systems approach into an effective exploration targeting system. *Ore Geol. Rev.* **2010**, *38*, 128–138. [CrossRef]
33. Welcome to DEMIRS Data and Software Centre. Available online: https://dasc.dmirs.wa.gov.au/ (accessed on 4 March 2025).
34. eBookshop. Available online: https://dmpbookshop.eruditetechnologies.com.au/ (accessed on 4 March 2025).
35. OGSEarth. Available online: https://www.geologyontario.mndm.gov.on.ca/ogsearth.html (accessed on 4 March 2025).
36. McCuaig, T.C.; Hronsky, J.M.A. The mineral system concept—The key to exploration targeting. *Soc. Econ. Geol. Spec. Publ.* **2014**, *18*, 153–175. [CrossRef]
37. Hagemann, S.G.; Lisitsin, V.A.; Huston, D.L. Mineral system analysis: Quo vadis. *Ore Geol. Rev.* **2016**, *76*, 504–522. [CrossRef]
38. Kreuzer, O.P.; Etheridge, M.A.; Guj, P.; McMahon, M.E.; Holden, D.J. Linking mineral deposit models to quantitative risk analysis and decision-making in exploration. *Econ. Geol.* **2008**, *103*, 829–850. [CrossRef]
39. Kreuzer, O.P.; Miller, A.V.; Peters, K.J.; Payne, C.; Wildman, C.; Partington, G.A.; Puccioni, E.; McMahon, M.E.; Etheridge, M.A. Comparing prospectivity modelling results and past exploration data: A case study of porphyry Cu–Au mineral systems in the Macquarie Arc, Lachlan Fold Belt, New South Wales. *Ore Geol. Rev.* **2015**, *71*, 516–544. [CrossRef]
40. Kreuzer, O.P.; Buckingham, A.; Mortimer, J.; Walker, G.; Wilde, A.; Appiah, K. An integrated approach to the search for gold in a mature, data-rich brownfields environment: A case study from Sigma-Lamaque, Quebec. *Ore Geol. Rev.* **2019**, *111*, 102977. [CrossRef]
41. Roshanravan, B.; Kreuzer, O.P.; Bruce, M.; Davis, J.; Briggs, M. Modelling gold potential in the Granites-Tanami Orogen, NT, Australia: A comparative study using continuous and data-driven techniques. *Ore Geol. Rev.* **2020**, *125*, 103661. [CrossRef]
42. Kreuzer, O.P.; Yousefi, M.; Nykänen, V. Introduction to the special issue on spatial modelling and analysis of ore-forming processes in mineral exploration targeting. *Ore Geol. Rev.* **2020**, *119*, 103391. [CrossRef]
43. Agterberg, F.P. Computer programs for mineral exploration. *Science* **1989**, *245*, 76–81. [CrossRef]
44. Bonham-Carter, G.F.; Agterberg, F.P.; Wright, D.F. Integration of geological datasets for gold exploration in Nova Scotia. *Digit. Geol. Geogr. Inf. Syst.* **1989**, *10*, 15–23.
45. Carranza, E.J.M. *Geochemical Anomaly and Mineral Prospectivity Mapping in GIS—Handbook of Exploration and Environmental Geochemistry 11*; Elsevier: Amsterdam, The Netherlands, 2008; 351p.
46. Joly, A.; Porwal, A.K.; McCuaig, T.C. Exploration targeting for orogenic gold deposits in the Granites-Tanami Orogen: Mineral system analysis, targeting model and prospectivity analysis. *Ore Geol. Rev.* **2012**, *48*, 349–383. [CrossRef]
47. Porwal, A.K.; Carranza, E.J.M. Introduction to the special issue: GIS-based mineral potential modelling and geological data analyses for mineral exploration. *Ore Geol. Rev.* **2015**, *71*, 477–483. [CrossRef]
48. Roshanravan, B.; Kreuzer, O.P.; Buckingham, A. BWM-MARCOS: A new hybrid MCDM approach for mineral potential modelling. *J. Geochem. Explor.* **2025**, *269*, 107639. [CrossRef]
49. Bonham-Carter, G.F. *Geographic Information Systems for Geoscientists: Modelling with GIS*; Pergamon: Oxford, UK, 1994; 416p.
50. Yousefi, M.; Nykänen, V. Data-driven logistic-based weighting of geochemical and geological evidence layers in mineral prospectivity mapping. *J. Geochem. Explor.* **2016**, *164*, 94–106. [CrossRef]
51. Yousefi, M.; Carranza, E.J.M. Data-driven index overlay and Boolean logic mineral prospectivity modeling in greenfields exploration. *Nat. Resour. Res.* **2016**, *25*, 3–18. [CrossRef]
52. Yousefi, M.; Carranza, E.J.M. Fuzzification of continuous-value spatial evidence for mineral prospectivity mapping. *Comput. Geosci.* **2015**, *74*, 97–109. [CrossRef]
53. Yousefi, M.; Carranza, E.J.M. Geometric average of spatial evidence data layers: A GIS-based multi-criteria decision-making approach to mineral prospectivity mapping. *Comput. Geosci.* **2015**, *83*, 72–79. [CrossRef]
54. Breiman, L. Random forests. *Mach. Learn.* **2001**, *45*, 5–32. [CrossRef]
55. London, D. Rare-element granitic pegmatites. *Rev. Econ. Geol.* **2016**, *18*, 165–193.
56. London, D. Ore-forming processes within granitic pegmatites. *Ore Geol. Rev.* **2018**, *101*, 349–383. [CrossRef]
57. Steiner, B.M. Tools and workflows for grassroots Li-Cs-Ta (LCT) pegmatite exploration. *Minerals* **2019**, *9*, 499. [CrossRef]
58. Černý, P.; London, D.; Novák, M. Granitic pegmatites as reflections of their sources. *Elements* **2012**, *8*, 289–294. [CrossRef]
59. Dittrich, T.; Seifert, T.; Schulz, B.; Hagemann, S.; Gerdes, A.; Pfänder, J. *Archean Rare-Metal Pegmatites in Zimbabwe and Western Australia*; Springer: Cham, Switzerland, 2019; 125p.
60. Nebel, O.; Vandenburg, E.D.; Capitanio, F.A.; Smithies, R.H.; Mulder, J.; Cawood, P.A. Early Earth "subduction": Short-lived, off-craton, shuffle tectonics, and no plate boundaries. *Precambrian Res.* **2024**, *408*, 107431. [CrossRef]

61. Smithies, R.H.; Gessner, K.; Lu, Y.; Kirkland, C.L.; Ivanic, T.; Lowrey, J.R.; Champion, D.C.; Sapkota, J.; Masurel, Q.; Thébaud, N.; et al. Geochemical mapping of lithospheric architecture disproves Archean terrane accretion in the Yilgarn craton. *Geology* **2024**, *52*, 141–146. [CrossRef]
62. Behre Dolbear Australia Pty Limited. *Competent Persons Report, Greenbushes Lithium Mine–Western Australia, Australia, and Cuola Lithium Project–Sichuan, People's Republic of China*; Tianqi Lithium Corporation: North Sydney, NSW, Australia, 2022; 195p.
63. London, D. The origin of primary textures in granitic pegmatites. *Can. Mineral.* **2009**, *47*, 697–724. [CrossRef]
64. Blewett, R.S.; Kennett, B.L.N.; Huston, D.L. Australia in time and space. In *Shaping a Nation: A Geology of Australia*; Blewett, R.S., Ed.; Geoscience Australia and Australian National University (ANU) E Press: Canberra, Australia, 2012; pp. 47–119.
65. Cawood, P.A.; Korsch, R.J. Assembling Australia: Proterozoic building of a continent. *Precambrian Res.* **2008**, *166*, 1–35. [CrossRef]
66. Huston, D.L.; Blewett, R.S.; Champion, D.C. Australia through time: A summary of its tectonic and metallogenic evolution. *Episodes* **2012**, *35*, 23–43. [CrossRef]
67. Johnson, S.P. *The Birth of Supercontinents and the Proterozoic Assembly of Western Australia*; Geological Survey of Western Australia: Perth, Australia, 2013; 78p.
68. Aitken, A.R.A.; Occhipinti, S.A.; Lindsay, M.D.; Joly, A.; Howard, H.M.; Johnson, S.P.; Hollis, J.A.; Spaggiari, C.V.; Tyler, I.M.; McCuaig, T.C.; et al. The tectonics and mineral systems of Proterozoic Western Australia: Relationships with supercontinents and global secular change. *Geosci. Front.* **2018**, *9*, 295–316. [CrossRef]
69. Sweetapple, M.T. Granitic pegmatites as mineral systems: Examples from the Archaean. In Proceedings of the PEG2017—8th International Symposium on Granitic Pegmatites, NGF Abstracts and Proceedings of the Geological Society of Norway, Kristiansand, Norway, 13–15 June 2017; pp. 139–142.
70. GSWA Open Day 2024 | A Li-Pegmatite Paradigm Consistent with Western Australia's Archean Geology. Available online: https://www.youtube.com/watch?v=9pqPLwDUYQA (accessed on 17 January 2025).
71. Champion, D.C.; Sheraton, J.W. Geochemistry and Nd isotope systematics of Archaean granites of the Eastern Goldfields, Yilgarn Craton, Australia: Implications for crustal growth processes. *Precambrian Res.* **1997**, *83*, 109–132. [CrossRef]
72. Kendall-Langley, L.; Kemp, A.I.S.; Grigson, J.L.; Hammerli, J. U-Pb and reconnaissance Lu-Hf isotope analysis of cassiterite and columbite group minerals from Archean Li-Cs-Ta type pegmatites of Western Australia. *Lithos* **2020**, *352*, 105231. [CrossRef]
73. Champion, D.C.; Cassidy, K.F. An overview of the Yilgarn craton and its crustal evolution. In Proceedings of the Geoconferences (WA) Inc. Kalgoorlie '07 Conference, Kalgoorlie, Australia, 25–27 September 2007; Geoscience Australia Record 2007/14. pp. 8–13.
74. Cassidy, K.F.; Champion, D.C.; McNaughton, N.; Fletcher, I.; Whitaker, A.; Bastrakova, I.; Budd, A. *Characterisation and Metallogenic Significance of Archean Granitoids of the Yilgarn Craton, Western Australia*; Minerals and Energy Research Institute of Western Australia (MERIWA): Perth, Australia, 2002; Report 222; 536p.
75. Witt, W.K. *Heavy-Mineral Characteristics, Structural Setting, and Parental Granites of Pegmatites in Archean Rocks of the Eastern Yilgarn Craton*; Record 1992/10; Geological Survey of Western Australia: Perth, Australia, 1992; 61p.
76. Korhonen, F.J.; Kelsey, D.E.; Ivanic, T.J.; Blereau, E.R.; Smithies, R.H.; De Paoli, M.C.; Fielding, I.O. Radiogenic heat production provides a thermal threshold for Archean cratonization process. *Geology* **2024**, *53*, 222–226. [CrossRef]
77. Partington, G.A. Greenbushes tin, tantalum and lithium deposit. In *Australian Ore Deposits*; Monograph 32; Phillips, N., Ed.; The Australasian Institute of Mining and Metallurgy: Carlton, VIC, Australia, 2017; pp. 153–157.
78. Bettenay, L.F.; Partington, G.A.; Groves, D.I. *Development of Exploration Criteria for Sn-Ta Pegmatites: Use of Host Rock Association and Alteration Haloes*; Report 13; Western Australian Mining & Petroleum Research Institute (WAMPRI): Perth, Australia, 1985; 56p.
79. Partington, G.A. Environment and structural controls on the intrusion of the giant rare metal Greenbushes pegmatite, Western Australia. *Econ. Geol.* **1990**, *85*, 437–456. [CrossRef]
80. Partington, G.A.; McNaughton, N.J.; Williams, I.S. A review of the geology, mineralization, and geochronology of the Greenbushes pegmatite, Western Australia. *Econ. Geol.* **1995**, *90*, 616–635. [CrossRef]
81. Sheppard, S.; Johnson, S.P.; Wingate, M.T.D.; Kirkland, C.L.; Pirajno, F. *Explanatory Notes for the Gascoyne Province*; Geological Survey of Western Australia: Perth, Australia, 2010; 336p.
82. Delta Lithium Limited. Yinnetharra lithium project maiden mineral resource estimate. In *Australian Securities Exchange (ASX) Announcement Dated 27 December 2023*; Delta Lithium Limited: West Perth, WA, Australia, 2023; 28p.
83. Holmes, J. *Discovery and Geology of the Pilgangoora Li-Ta Pegmatite Deposit, Western Australia*; Centre for Exploration Targeting (CET) Members Day: Perth, Australia, 2022.
84. Tabba Tabba Pegmatite (Tabba Tabba Tantalum Mine), East Pilbara Shire, Western Australia, Australia. Available online: https://www.mindat.org/loc-12495.html/ (accessed on 10 January 2025).
85. Global Lithium Resources Limited. Prospectus. In *Australian Securities Exchange (ASX) Announcement Dated 4 May 2021*; Global Lithium Resources Limited: Perth, WA, Australia, 2021; 198p.
86. Blockley, J.G. The tin deposits of Western Australia, with special reference to the associated granites. In *Geological Survey of Western Australia Mineral Resources Bulletin*; Geological Survey of Western Australia: East Perth, Australia; Volume 12, 184p.

87. Sociedad Química y Minera de Chile. *Technical Report Summary, Mt Holland Lithium Project*; Sociedad Química y Minera de Chile: Santiago, Chile, 2022; 115p.
88. Kathleen Valley—Kathleens Corner, Mount Mann. Available online: https://portergeo.com.au/database/mineinfo.asp?mineid=mn1781 (accessed on 10 January 2025).
89. Liontown Resources Limited. Kathleen Valley confirmed as a world-class lithium deposit as mineral resource increases to 156Mt @ 1.4% Li_2O. In *Australian Securities Exchange (ASX) Announcement Dated 11 May 2020*; Liontown Resources Limited: West Perth, WA, Australia, 2020; 25p.
90. Ross, J.R.; Smith, B. Mount Marion lithium pegmatite deposit. In *Australian Ore Deposits*; Monograph 32; Phillips, N., Ed.; The Australasian Institute of Mining and Metallurgy: Carlton, VIC, Australia, 2017; pp. 161–162.
91. Mount Marion. Available online: https://portergeo.com.au/database/mineinfo.asp?mineid=mn1543 (accessed on 10 January 2025).
92. Global Lithium Resources Limited. 9.9 million tonnes @ 1.14% Li_2O and 49 ppm Ta_2O_5, maiden Manna project lithium resource. In *Australian Securities Exchange (ASX) Announcement Dated 17 February 2022*; Global Lithium Resources Limited: Perth, WA, Australia, 2022; 17p.
93. Global Lithium Resources Limited. Manna ore sorting trial confirms excellent results across range of ore grades. In *Australian Securities Exchange (ASX) Announcement Dated 4 July 2024*; Global Lithium Resources Limited: Perth, WA, Australia, 2024; 24p.
94. Delta Lithium Limited. Mt Ida lithium project mineral resource estimate upgrade. In *Australian Securities Exchange (ASX) Announcement Dated 3 October 2023*; Delta Lithium Limited: West Perth, WA, Australia, 2023; 23p.
95. Mining Plus Pty. Limited. *SEC Technical Report Summary, Mt. Cattlin Lithium Project*; Allkem Limited: Brisbane, Australia, 2023; 310p.
96. Liontown Resources Limited. Liontown announces maiden mineral resource estimate for its 100%-owned Buldania lithium project, WA. In *Australian Securities Exchange (ASX) Announcement Dated 8 November 2019*; Liontown Resources Limited: West Perth, WA, Australia, 2019; 16p.
97. Develop Global Limited. Updated scoping study shows Pioneer Dome set to generate strong free cashflow. In *Australian Securities Exchange (ASX) Announcement Dated 7 May 2024*; Develop Global Limited: West Leederville, WA, Australia, 2024; 38p.
98. Zenith Minerals Limited. Maiden lithium minerals resource. In *Australian Securities Exchange (ASX) Announcement Dated 28 September 2023*; Zenith Minerals Limited: West Perth, WA, Australia, 2023; 34p.
99. Widgie Nickel Limited. 375% growth in Faraday-Trainline lithium mineral resource. In *Australian Securities Exchange (ASX) Announcement Dated 8 November 2024*; Widgie Nickel Limited: Perth, WA, Australia, 2024; 34p.
100. Mount Farmer Mine (Niobe Prospect), Yalgoo Shire, Western Australia, Australia. Available online: https://www.mindat.org/loc-248995.html (accessed on 10 January 2025).
101. King Tamba Specialty Metals Project. Available online: https://www.ktaresources.com/king-tamba-speciality-metals-project/ (accessed on 10 January 2025).
102. Thurston, P.C. Archean geology of Ontario: Introduction. In *Geology of Ontario*; Thurston, P.C., Williams, H.R., Sutcliffe, R.H., Stott, G.M., Eds.; Ontario Geological Survey, Ministry of Northern Development and Mines: Toronto, ON, Canada, 1991; Volume 4 Pt 1, pp. 73–78.
103. Percival, J.A.; Sanborn-Barrie, M.; Skulski, T.; Stott, G.M.; Helmstaedt, H.; White, D.J. Tectonic evolution of the western Superior Province from NATMAP and Lithoprobe studies. *Can. J. Earth Sci.* **2006**, *43*, 1085–1117. [CrossRef]
104. Percival, J.A. Geology and metallogeny of the Superior Province, Canada. In *Mineral Deposits of Canada: A Synthesis of Major Deposit-Types, District Metallogeny, the Evolution of Geological Provinces, and Exploration Methods*; Goodfellow, W.D., Ed.; Geological Association of Canada, Mineral Deposits Division: St. John's, NL, Canada, 2007; Volume 5, pp. 903–928.
105. Bjorkman, K.E. 4D Crust-Mantle Evolution of the Western Superior Craton: Implications for Archaean Granite-Greenstone Petrogenesis and Geodynamics. Ph.D. Thesis, The University of Western Australia, Perth, Australia, 2017; 313p.
106. Fyon, J.A.; Bennett, G.; Jackson, S.L.; Garland, M.I.; Easton, R.M. Metallogeny of the Proterozoic eon, northern Great Lakes region, Ontario. In *Geology of Ontario*; Thurston, P.C., Williams, H.R., Sutcliffe, R.H., Stott, G.M., Eds.; Ontario Geological Survey, Ministry of Northern Development and Mines: Toronto, ON, Canada, 1991; Volume 4 Pt 2, pp. 1177–1215.
107. Easton, R.M.; Fyon, J.A. Metallogeny of the Grenville Province. In *Geology of Ontario*; Thurston, P.C., Williams, H.R., Sutcliffe, R.H., Stott, G.M., Eds.; Ontario Geological Survey, Ministry of Northern Development and Mines: Toronto, ON, Canada, 1991; Volume 4 Pt 2, pp. 1217–1252.
108. Larbi, Y.; Stevenson, R.; Breaks, F.; Machado, N.; Gariépy, C. Age and isotopic composition of late Archean leucogranites: Implications for continental collision in the western Superior Province. *Can. J. Earth Sci.* **1999**, *36*, 495–510. [CrossRef]
109. Baker, D.R. The escape of pegmatite dikes from granitic plutons; constraints from new models of viscosity and dike propagation. *Can. Mineral.* **1998**, *36*, 255–263.
110. BBA E&C Inc. *NI 43-101 Technical Report, Pre-Feasibility Study for the PAK Project*; Frontier Lithium Inc.: Sudbury, ON, Canada, 2023; 657p.

111. Micon International Limited. *NI 43-101 Technical Report on the Preliminary Economic Assessment of Lithium Hydroxide Production, Separation Rapids Lithium Project, Kenora, Ontario*; Avalon Advanced Materials Inc.: Toronto, ON, Canada, 2016; 262p.
112. Frontier Lithium Inc. Frontier Lithium announces expansion of Spark deposit—18.8 Mt in indicated and 29.7 Mt in inferred categories. In *TSX Venture Exchange (TSXV) Announcement Dated 28 February 2023*; Frontier Lithium Inc.: Sudbury, ON, Canada, 2023; 3p.
113. Green Technology Metals Limited. Prospectus. In *Australian Securities Exchange (ASX) Announcement Dated 8 November 2021*; Green Technology Metals Limited: West Perth, WA, Australia, 2021; 305p.
114. Hronsky, J.M.; Kreuzer, O.P. Applying spatial prospectivity mapping to exploration targeting: Fundamental practical issues and suggested solutions for the future. *Ore Geol. Rev.* **2019**, *107*, 647–653. [CrossRef]
115. Lachaud, A.; Marcus, A.; Vučetić, S.; Mišković, I. Study of the influence of non-deposit locations in data-driven mineral prospectivity mapping: A case study on the Iskut project in northwestern British Columbia, Canada. *Minerals* **2021**, *11*, 597. [CrossRef]
116. Nykänen, V.; Lahti, I.; Niiranen, T.; Korhonen, K. Receiver operating characteristics (ROC) as validation tool for prospectivity models—A magmatic Ni-Cu case study from the central Lapland greenstone belt, northern Finland. *Ore Geol. Rev.* **2015**, *71*, 853–860. [CrossRef]
117. Roshanravan, B.; Agajani, H.; Yousefi, M.; Kreuzer, O.P. Generation of a geochemical model to prospect podiform chromite deposits in North of Iran. In Proceedings of the Generation of a Geochemical Model to Prospect Podiform Chromite Deposits in North of Iran, 80th EAGE Conference and Exhibition, Copenhagen, Denmark, 11–14 June 2018.
118. Roshanravan, B.; Kreuzer, O.P.; Buckingham, A.; Keys, E. On data quality in mineral potential modelling: A case study using random forest and fractal techniques. In Proceedings of the 84th EAGE Annual Conference & Exhibition, Vienna, Austria, 5–8 June 2023.
119. Mihalasky, M.J.; Bonham-Carter, G.F. Lithodiversity and its spatial association with metallic mineral sites, Great Basin of Nevada. *Nat. Resour. Res.* **2001**, *10*, 209–226. [CrossRef]
120. Tsoukalas, L.H.; Uhrig, R.E. *Fuzzy and Neural Approaches in Engineering*; John Wiley & Sons: New York, NY, USA, 1997; 606p.
121. Nykänen, V.; Groves, D.I.; Ojala, V.J.; Eilu, P.; Gardoll, S.J. Reconnaissance-scale conceptual fuzzy-logic prospectivity modelling for iron oxide copper-gold deposits in the northern Fennoscandian Shield, Finland. *Aust. J. Earth Sci.* **2008**, *55*, 25–38. [CrossRef]
122. Karbalaei-Ramezanali, A.; Feizi, F.; Jafarirad, A.; Lotfi, M. Application of best-worst method and additive ratio assessment in mineral prospectivity mapping: A case study of vein-type copper mineralization in the Kuhsiah-e-Urmak Area, Iran. *Ore Geol. Rev.* **2020**, *117*, 103268. [CrossRef]
123. Feizi, F.; Karbalaei-Ramezanali, A.A.; Farhadi, S. FUCOM-MOORA and FUCOM-MOOSRA: New MCDM-based knowledge-driven procedures for mineral potential mapping in greenfields. *SN Appl. Sci.* **2021**, *3*, 358. [CrossRef]
124. Aryafar, A.; Roshanravan, B. BWM-SAW: A new hybrid MCDM technique for modeling of chromite potential in the Birjand district, east of Iran. *J. Geochem. Explor.* **2021**, *231*, 106876. [CrossRef]
125. Riahi, S.; Fathianpour, N.; Tabatabaei, S.H. Improving the accuracy of detecting and ranking favorable porphyry copper prospects in the east of Sarcheshmeh copper mine region using a two-step sequential Fuzzy-Fuzzy TOPSIS integration approach. *J. Asian Earth Sci.* **2023**, *10*, 100166. [CrossRef]
126. Rezaei, J. Best-worst multi-criteria decision-making method. *Omega* **2015**, *53*, 49–57. [CrossRef]
127. Stević, Ž.; Pamučar, D.; Puška, A.; Chatterjee, P. Sustainable supplier selection in healthcare industries using a new MCDM method: Measurement of alternatives and ranking according to COmpromise solution (MARCOS). *Comput. Ind. Eng.* **2020**, *140*, 106231. [CrossRef]
128. Roshanravan, B.; Aghajani, H.; Yousefi, M.; Kreuzer, O.P. An improved prediction-area plot for prospectivity analysis of mineral deposits. *Nat. Resour. Res.* **2019**, *28*, 1089–1105. [CrossRef]
129. Aryafar, A.; Roshanravan, B. Improved index overlay mineral potential modeling in brown- and green-fields exploration using 1324 geochemical, geological and remote sensing data. *Earth Sci. Inform.* **2020**, *13*, 1275–1291. [CrossRef]
130. Carranza, E.J.M.; Laborte, A.G. Random forest predictive modeling of mineral prospectivity with small number of prospects and data with missing values in Abra (Philippines). *Comput. Geosci.* **2015**, *74*, 60–70. [CrossRef]
131. Rodriguez-Galiano, V.F.; Chica-Olmo, M.; Chica-Rivas, M. Predictive modelling of gold potential with the integration of multisource information based on random forest: A case study on the Rodalquilar area, Southern Spain. *Int. J. Geogr. Inf. Sci.* **2014**, *28*, 1336–1354. [CrossRef]
132. Sun, T.; Chen, F.; Zhong, L.; Liu, W.; Wang, Y. GIS-based mineral prospectivity mapping using machine learning methods: A case study from Tongling ore district, eastern China. *Ore Geol. Rev.* **2019**, *109*, 26–49. [CrossRef]
133. Xiang, J.; Xiao, K.; Carranza, E.J.M.; Chen, J.; Li, S. 3D mineral prospectivity mapping with random forests: A case study of Tongling, Anhui, China. *Nat. Resour. Res.* **2020**, *29*, 395–414. [CrossRef]

134. Zhang, S.; Carranza, E.J.M.; Xiao, K.; Wei, H.; Yang, F.; Chen, Z.; Xiang, J. Mineral prospectivity mapping based on isolation forest and random forest: Implication for the existence of spatial signature of mineralization in outliers. *Nat. Resour. Res.* **2022**, *31*, 1981–1999. [CrossRef]
135. Parsa, M. A data augmentation approach to XGboost-based mineral potential mapping: An example of carbonate-hosted ZnPb mineral systems of Western Iran. *J. Geochem. Explor.* **2021**, *228*, 106811. [CrossRef]
136. Bishop, C.M. *Neural Networks for Pattern Recognition*; Oxford University Press: Oxford, UK, 1997.
137. Hronsky, J.M.; Groves, D.I. Science of targeting: Definition, strategies, targeting and performance measurement. *Australian J. Earth Sci.* **2008**, *55*, 3–12. [CrossRef]
138. McCuaig, T.C.; Sherlock, R.L. Exploration targeting. In Proceedings of the Exploration 17: Sixth Decennial International Conference on Mineral Exploration, Toronto, ON, Canada, 22–25 October 2017; pp. 75–82.
139. Yang, F.; Zuo, R.; Kreuzer, O.P. Artificial intelligence for mineral exploration: A review and perspectives on future directions from data science. *Earth-Sci. Rev.* **2024**, *258*, 104941. [CrossRef]
140. Zuo, R.; Yang, F.; Cheng, Q.; Kreuzer, O.P. A novel data-knowledge dual-driven model coupling artificial intelligence with a mineral systems approach for mineral prospectivity mapping. *Geology* **2024**, *53*, 284–288. [CrossRef]
141. Porwal, A.K.; Kreuzer, O.P. Introduction to the special issue: Mineral prospectivity analysis and quantitative resource estimation. *Ore Geol. Rev.* **2010**, *38*, 121–127. [CrossRef]
142. Jaireth, S.; Huston, D. Metal endowment of cratons, terranes and districts: Insights from a quantitative analysis of regions with giant and super-giant deposits. *Ore Geol. Rev.* **2010**, *38*, 288–303. [CrossRef]
143. Kreuzer, O.P.; Porwal, A.K.; Markwitz, V.; McCuaig, T.C. A continent-wide study of Australia's uranium potential. In Proceedings of the Australian Uranium Conference, Fremantle, Australia, 22–23 July 2009.
144. Roshanravan, B.; Kreuzer, O.P.; Mohammadi, S.; Bruce, M.; Davis, J.; Briggs, M. Cuckoo optimization algorithm for support vector regression potential analysis: An example from the Granites-Tanami Orogen, Australia. *J. Geochem. Explor.* **2021**, *230*, 106858. [CrossRef]
145. Wilde, A.; Otto, A.; McCracken, S. Geology of the Goulamina spodumene pegmatite field, Mali. *Ore Geol. Rev.* **2021**, *134*, 104162. [CrossRef]
146. Salakjani, N.K. Extraction of Lithium from Spodumene. Ph.D. Thesis, Murdoch University, Perth, Australia, September 2019.
147. Hronsky, J.M. The exploration search space concept: Key to a successful exploration strategy. *Cent. Explor. Target. (CET) Q. Newsl.* **2009**, *8*, 14–15.
148. Kidman Resources Limited. Review highlights Mt Holland's outstanding lithium potential. In *Australian Securities Exchange (ASX) Announcement Dated 5 July 2016*; Kidman Resources Limited: Melbourne, Australia, 2016; 7p.
149. Patriot Lithium Limited. Exploration update—Rock-chip samples from Gorman LCT pegmatites deliver grades >3% Li_2O in each major outcrop over 5.2km trend. In *Australian Securities Exchange (ASX) Announcement Dated 31 July 2023*; Patriot Lithium Limited: Subiaco, WA, Australia, 2023; 31p.
150. Blaze Minerals Limited. High grade samples returned at North Spirit lithium project. In *Australian Securities Exchange (ASX) Announcement Dated 7 September 2023*; Blaze Minerals Limited: Perth, WA, Australia, 2023; 13p.
151. Kidman Resources Limited. Fast-tracking a world-class lithium resource in Western Australia. In *Australian Securities Exchange (ASX) Announcement Dated 25 May 2017*; Kidman Resources Limited: Melbourne, Australia, 2017; 23p.
152. Errawarra Resources Limited. Quarterly activities report for the period ending 31 December 2024. In *Australian Securities Exchange (ASX) Announcement Dated 30 January 2025*; Errawarra Resources Limited: West Perth, WA, Australia, 2025; 17p.

Disclaimer/Publisher's Note: The statements, opinions and data contained in all publications are solely those of the individual author(s) and contributor(s) and not of MDPI and/or the editor(s). MDPI and/or the editor(s) disclaim responsibility for any injury to people or property resulting from any ideas, methods, instructions or products referred to in the content.